AN ABSTRACT OF THE DISSERTATION OF

Robert E. Kennedy for the degree of Doctor of Philosophy in Forest Science presented on January 26, 2004.

Title: Causes and Consequences of Uncertainty in the Application of a Biogeochemical Model to a Large Geographic Region

Abstract approved:

Signature redacted for privacy.

Warren B. Cohen

Signature redacted for privacy.

David P. Turner

When biogeochemical models are applied to large regions, the values of key model parameters are often unknowable. Through field and modeling studies, I examined the potential impact of such uncertainty on estimates of carbon cycling in western Oregon. I found that variation in key leaf traits could be interpreted ecologically, but that there was little ability to spatially predict leaf traits (Chapter 2). By developing an efficient methodology for spatial extrapolation of model results (Chapter 3), I was able to examine how this uncertainty, along with uncertainty in three other leaf traits, could result in spatially-varying estimates of carbon dynamics (Chapter 4). My results suggest that uncertainty in model parameters is potentially important, and that spatially explicit mapping of this uncertainty would be necessary if carbon dynamics modeling is to improve.

Causes and Consequences of Uncertainty in the Application of a Biogeochemical Model to a Large Geographic Region

by
Robert E. Kennedy

A DISSERTATION

Submitted to
Oregon State University

in partial fulfillment of
the requirements for the
degree of

Doctor of Philosophy

Presented January 26, 2004
Commencement June 2004

Doctor of Philosophy Dissertation of Robert E. Kennedy
presented on January 26, 2004

APPROVED:

Signature redacted for privacy.

Co-Major Professor, representing Forest Science

Signature redacted for privacy.

Co-Major Professor, representing Forest Science

Signature redacted for privacy.

Head of the Department of Forest Science

Signature redacted for privacy.

Dean of the Graduate School

I understand that my dissertation will become part of the permanent collection of Oregon State University libraries. My signature below authorizes release of my dissertation to any reader upon request.

Signature redacted for privacy.

Robert E. Kennedy, Author

ACKNOWLEDGEMENTS

The author wishes to thank Sarah Lobser for assistance in field work and in processing leaf samples; John Campbell, Steve van Tuyl, Osbert Sun, and Colin Edgar for training in field methods; and Bev Law for provision of lab space and expertise to aid in leaf processing. Thanks also to Dave Reed at the Bureau of Land Management, Medford District, for significant aid in locating several study plots.

Further thanks are due to Michael Guzy for extensive support and aid in modeling, including adaptation of his software for the author's modeling studies. Conversations with Dr. Guzy provided the foundation for many strategic modeling and study design decisions. David Turner provided expertise in modeling design, and provided the first seeds of ideas that ultimately led to this project.

The author also wishes to thank the staff of the Forestry Computing Resources group at the College of Forestry for general computer support. Special thanks to Jerry Mohr, Kevin Hudson, Ken West, and Mike Altimus for facilitating the parallel computing that made this project feasible.

Thanks to Warren Cohen for financial support in times of need, psychological support throughout the PhD, and encouragement to embark on the PhD in the first place.

The author thanks the National Aeronautics and Space Administration for support under its Earth System Science and Space Grant programs, and the National Science Foundation for a Doctoral Dissertation Improvement Grant that allowed collection of field data. Through collaboration with Drs. Guzy, Turner, and Law, this project has been supported by a grant from U.S. Environmental Protection Agency's Science to Achieve Results (STAR) Program (Grant # R-82830901-0). Although the research described in the study has been funded wholly or in part by the U.S. Environmental Protection Agency's STAR program, it has not been subjected to any EPA review and therefore does not necessarily reflect the views of the Agency, and no official endorsement should be inferred.

Finally, the author wishes to thank Rebecca Kennedy for her patience, support, and indispensable pep talks. This project would not have been possible without her.

CONTRIBUTION OF AUTHORS

Dr. Michael Guzy assisted in development of modeling software that allowed development of methodologies in Chapter 3 and 4, and provided substantial assistance in modeling design for those chapters.

TABLE OF CONTENTS

TABLE OF CONTENTS (Continued)

Page

LIST OF FIGURES

LIST OF FIGURES (Continued)

LIST OF FIGURES (Continued)

LIST OF TABLES

LIST OF TABLES (Continued)

Causes and Consequences of Uncertainty in the Application of a Biogeochemical Model to a Large Geographic Region

Chapter 1: Introduction

Because of its potential influence on climate, the carbon cycle is under increasing scrutiny at regional and global scales (Schimel 1998). Understanding carbon's dynamics requires that a multi-faceted approach be used, including a suite of measurements both in the lab and in the field (Falkowski et al. 2000). Lab work helps to characterize the important physiological and physical processes that drive the flows of carbon between the atmosphere and the Earth's surface. The net effects of those processes over time lead to accumulation of carbon pools and development of carbon fluxes, both of which can be measured directly in the field. To fully characterize the carbon cycle, such direct measurements would need to be made for every point on the globe. This task is impossible at not only at global but also regional scales (on the order of 10^4 to 10^7 hectares). To extrapolate knowledge to areas where no direct measurements can be made, regional-scale carbon cycling studies require the use of mathematical models.

Biogeochemical models are a common family of mathematical models used to quantify carbon dynamics for large areas (Schimel et al. 1997). These models capture essential biological, hydrological, and edaphic processes that control the flows of carbon, nutrients, and water through an ecosystem. Some important processes that may be modeled at significant detail include photosynthesis, allocation of photosynthate to various plant growth and reproduction tissues, transpiration of

water from leaves, respiration by both plants and their consumers, uptake and release of key nutrients, competition for resources, and both natural and anthropogenic disturbance (Waring and Running 1998, Thornton et al. 2002). To describe these processes, a biogeochemical model requires a large number of controlling parameters. Once parameterized, the model is run under a set of input variables that typically include climate data and soil characteristics. Applying a model over a large area requires that parameters can be defined and input variables calculated.

When models are applied to large geographic areas, at least two important problems emerge. First, computational demands for modeling may exceed available capacity. The biogeochemical models that dominate carbon cycling are computationally intensive. To characterize carbon dynamics over a large landscape, a model must be run in thousands or millions of separate cells. Even with rapidly improving computer technology, the length of time needed to achieve such a task often precludes ready usage. As with any modeling exercise, simplification strategies can be employed (Haefner 1996). Reducing the structural complexity of a model can reduce computational burden, but may eliminate processes that are necessary for robust estimation, especially when subtle climatic changes are to be explored. Decreasing the time step at which the model makes calculations can reduce computational burden, but may mask processes that occur at a finer time step. Similarly, spatial aggregation of processes will reduce computational burden for a given area, but would miss processes acting at fine spatial grains.

A second challenge in regional modeling is building accurate maps of model driving variables and parameters. Input drivers for common biogeochemical models typically include climate and soil data, the spatial patterns of which are difficult to accurately capture (Phillips and Marks 1996). Moreover, these models typically have many parameters whose spatial patterns are poorly characterized, either because of the inherent difficulties of making the necessary measurements, or because the necessary measurements have simply not been measured at a sufficient number of locations to understand spatial patterns.

Uncertainty in these spatial controls on model behavior can cause uncertainty in outputs from the model. Typically, when models of carbon dynamics are run for entire landscapes, the computational burden of modeling over large areas makes efforts to characterize uncertainty rare (White et al. 1998, Williams et al. 2001). This uncertainty may not be trivial: Because carbon dynamics represent the sensitive balance between carbon uptake and release, slight uncertainties can cause a site to move from predicted carbon source to sink. If models are to be useful for researchers, policy-makers, and the public, their predictions must be placed in a context of uncertainties and probabilities.

In the project described in this Dissertation, I used test cases to explore both of the challenges to spatial modeling of carbon dynamics. I focused on BGC 4.1.1 (hereafter "BGC"), a commonly-used model with many parameters, high demand for spatial input variables, and a computationally-intensive design (Running and Coughlan 1988, Thornton 1998). These characteristics made it an excellent test of

methods to cope with computational complexity. To address issues of spatial uncertainty, I limited my investigations to a suite of parameters related to leaves. These parameters have been shown to have potentially strong influence on the behavior of BGC (White et al. 2000). Because information on their geographic distribution is often lacking, the spatial patterns of many model parameters are typically treated simplistically in regional-scale modeling, leaving significant room for uncertainty at any given point in space. Thus, leaf attributes serve as excellent test for exploring questions of spatial uncertainty in model parameters. All of the work was conducted in the forests of Oregon's Cascade Mountains, a region with a strong research history and with a potentially important role to play in regional carbon dynamics (Smithwick et al. 2002). The study was conducted as part of a larger project on regional scaling with field measurements, remote sensing, and modeling (Law et al. in press).

My work is reported in the three following chapters:

- Chapter 2 describes a field study in which I investigated the actual spatial variability of three readily-measured leaf parameters. My goal was to better understand whether hypothesized controls on these parameters would lead to regional-scale spatial patterns in their values. I took advantage of a natural ecotone between Douglas fir and ponderosa pine forests to better separate species-specific and climate-driven effects. These leaf parameters represent attributes whose measurement is relatively straightforward, but whose observation over large spatial areas

has been lacking. The observed range of parameter values was then used later in Chapter 4.

- Chapter 3 reports on a method I developed to reduce the computational burden in modeling over large areas. Rather than running the model at every point in a large landscape, I ran the model only at a sample of points. The points were determined by examining the multidimensional climate space that varies across the landscape, followed by sampling at regular intervals from that space. After sampled points were modeled, the remaining points were estimated by interpolation in the climate space between nearby modeled points. The goal of this chapter was development and testing of a methodology that would facilitate computationally expensive uncertainty analyses that followed in Chapter 4.
- Chapter 4 brings together components of the preceding two chapters to develop spatially-explicit, region-wide estimates of uncertainty in model outputs. In addition to the three leaf parameters that were easily measured in Chapter 2, the modeling analysis included three additional leaf parameters whose measurement in the field is difficult. Together, the six parameters represented the range of uncertainties in parameters typical of most biogeochemical model parameter sets. Model uncertainty analysis occurred in sequential steps. A parameter set specific to the region of interest was identified using both measurements from Chapter 2 and the

literature. A traditional factorial uncertainty analysis identified keystone parameters, which were then examined further. At a small number of points on the landscape, frequency distributions of total variation in carbon metrics was quantified using a dense sampling of parameter space. Then a coarser sampling of parameter space was applied to a large number of points in the landscape sampled using the methods of Chapter 3, and uncertainty frequencies distributed across the landscape. This approach provided a spatially-explicit estimate not only of carbon dynamics, but also of uncertainty in carbon dynamics.

Taken together, the three chapters serve as an investigation into the issues involved when biogeochemical models are applied to large geographic areas. My goal was to identify not only causes and consequences of uncertainties that arise in such an endeavor, but also to establish foundations that might be used to focus further spatial modeling efforts.

Chapter 2: Regional patterns of variation in leaf mass per area, leaf nitrogen, and leaf longevity

Introduction

Because it is the entry point of most carbon into the terrestrial biosphere from the atmosphere, leaf carbon assimilation is a key component of the global carbon cycle. Characterization of the carbon cycle both now and under future climates requires that controls on leaf carbon assimilation be understood over both space and time. In experimental and observational research, three leaf traits have been shown to have high control over carbon assimilation: leaf mass per area (LMA), leaf nitrogen concentration (LN, on mass basis), and leaf longevity (LL) (Field and Mooney 1986, Poorter 1989, Reich et al. 1992, Oren et al. 2001).

Physiologically-based models of carbon dynamics for ecosystems often incorporate one or more of these leaf traits as model parameters (Ollinger et al. 1998, White et al. 2000). By treating the process of leaf carbon assimilation in a physiologically realistic manner, these models have the potential to track changes in carbon assimilation brought about by changes in climate and carbon dioxide levels over time. When such carbon models are applied over large geographic areas, however, spatial variation in those leaf traits may be significant and should be accounted for.

Different species tend towards inherently different combinations of leaf traits (Poorter and Evans 1998). Therefore, given species maps, carbon models can be parameterized with species-specific sets of leaf traits, providing a first-approximation

of the spatial patterns in carbon dynamics. However, this approach ignores potential genetic and phenological variation in these leaf traits within the geographic range of a single species.

Evidence for partial environmental control over these traits is abundant. At a global scale, cross-study comparisons have shown that LMA, LN, and LL are intimately linked through ecological and genetic tradeoffs and cost-benefit strategies (Reich et al. 1997). LMA is thought to respond to average growth irradiance (Rosati et al. 2000, Evans and Poorter 2001, Grassi and Bagnaresi 2001), moisture stress (Mooney et al. 1978, Abrams et al. 1994, Cunningham et al. 1999), and nutrient limitation (Wright et al. 2002). LN has been shown to be related to temperature (Yin 1993) and soil nutrient condition (van den Driessche 1974, Turner and Olson 1976, Wright et al. 2001). LL varies by species or functional group, and it appears to be related to a wide variety of stressors, ranging from temperature to nutrients (Reich et al. 1995), and may be a sensitive integrator of long-term, plant-level production and respiration costs (Walters and Reich 1999).

The abundance of research on these leaf traits poses a problem for understanding their spatial patterns at the regional scale: with so many potential influences and interrelationships identified, it is difficult to predict which set of factors will be important at the regional scale for any given system (on the order of 10^6 to 10^9 ha). This is exacerbated in forested systems by the difficulty of experimental manipulation at appropriate scales and by the long life span of the vegetation.

The conifer forests of Oregon provide a useful natural laboratory that may help in understanding regional patterns in these leaf traits. West of the Cascade Mountains, *Pseudotsuga menziesii* (hereafter PSME) trees dominate forests that experience cool, moist winters and warm, dry summers. East of the Cascades, *Pinus ponderosa* (hereafter PIPO) trees dominate in a climate with similar seasonality but much lower overall precipitation (Franklin and Dyrness 1988). The two species intergrade in an ecotonal region of mixed-conifer forest around the southern portion of the Range (Figure 2.1). By identifying mixed stands where trees of the two species experience essentially identical environmental conditions, and comparing those stands with pure stands of each species in the core zone of its range, greater inference of ecological drivers may be possible.

Here, we describe results from a field study that takes advantage of the geographic convergence of PSME and PIPO to better characterize regional patterns in LMA, LN, and LL. We use our findings to develop a simple conceptual model describing the ecological variation in these leaf traits for the study region, and then discuss how this conceptual model may be applied to carbon modeling.

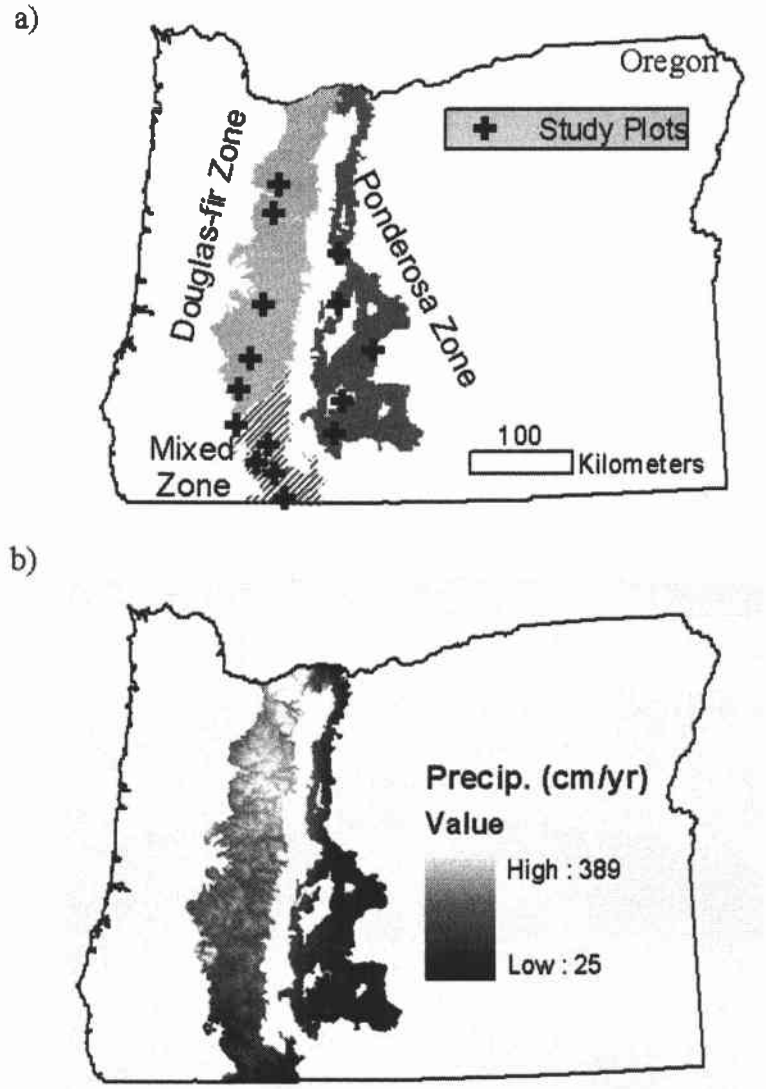

Figure 2.1. a) Study sites (black + symbols) overlaid on a general ecozone mapping showing approximate distributions the western Cascades (light grey), the mixed conifer zone (diagonal hash lines), and the eastern Cascades (dark grey). The white zone in the center of the study area represents crest of the Cascades. b) Precipitation for the region acquired from DAYMET. Note the gradual transition from high precipitation in the northern Douglas-fir zone to low precipitation in the southern Douglas-fir zone, eventually to very low precipitation east of the Cascade crest.

Methods

Overview

Using a variety of spatial datasets and in-field reconnaissance, a set of 15 sample stands were identified that spanned a climatically-driven ecotone between two dominant forest species. Within the core geographic range of each species, five stands were located for leaf sampling. The five remaining stands were located in the transitional zone between the ranges of the two species. After field sampling, needles were processed to obtain LL, LMA, and LN. Statistical investigations sought to characterize relationships between leaf traits and stand attributes and climate, as well as between the traits.

Climate data

Five variables derived from 1km-grain DAYMET data (Thornton et al. 1997, Thornton et al. 2000) were used to characterize the climate of the region, and are listed in Table 2.1. Precipitation and temperature variables were taken directly from aggregated DAYMET data. Vapor pressure deficit (VPD) was derived from minimum and daily temperatures (Thornton et al. 2000). Saturation vapor pressure for calculation of VPD was calculated as 610.79 * (exp(17.269 * T / (237.3 + T)), where T is daily minimum temperature in degrees C (Glassy and Running 1994).

Table 2.1. Definitions of variables used in this study

Variable	Description	Units	Type	Method
YrPrcp	Average annual precipitation between 1980 and 1997	cm	Climate	From DAYMET
SprPrcp	Average precipitation for 15-May to 14-July, 1980 to 1997	cm	Climate	From DAYMET
MaxSprTemp	Average maximum temperature for 15-May to 14-July, 1980 to 1997	°C	Climate	From DAYMET
Temp	Average annual temperature for 1980 to 1997	°C	Climate	From DAYMET
SumrVPD	Calculated vapor pressure deficit for 15-April to 13-August 1980 to 1997	Pa	Climate	See "Climate data" in Methods Section
DBH	Average diameter at breast height (1.37m) for 12 sampled trees	cm	Stand	Direct tape measurement
BA	Average basal area	m^2 / ha	Stand	Prism sweeps
Ht	Average height of the top of 3 to 4 trees in stand	m	Stand	Analog clinometer + laser rangefinder
CrnDpth	Depth (m) of foliated crown of trees on which Ht was measured	m	Stand	Analog clinometer + laser rangefinder

Table 2.1. (continued) Definitions of variables used in this study

Variable	Description	Units	Type	Method
GapFraction	Proportion of sky visible through canopy in stand	Proportion	Stand	Hemispherical digital photo + cite software
Ht/DBH	Average ratio of Ht to DBH for 3-4 trees in stand	m / m	Stand	Mean of tree ratios
Ht/BA	Average ratio of Ht to BA	m / m^2	Stand	Mean of tree ratios
CrnDpth/Ht	Average ratio of CrnDpth to Ht	m / m	Stand	Mean of tree ratios
BranchInc	Average length of yearly growth of needles on shoot	mm	Branch	Direct measurement in lab
FolBranchLngth	Average length of foliated portion of branch (cm) for all sampled trees	mm	Branch	Direct measurement in lab
LMA	Average leaf mass per area (g / cm^2) for target species in stand	kg / m^2	Leaf	See "Leaf Processing" in Methods Section
LN	Average leaf nitrogen (mg N / mg leaf) for target species in stand	mg N / mg leaf	Leaf	See "Leaf Processing" in Methods Section
LL	Leaf longevity (yrs) for target species in stand	years	Leaf	Direct counting of bud scars

Locating sample stands

Digital spatial data sources were used extensively in layout of potential sample plots. These were used to identify a large number of candidate regions for sample stands. Candidate areas were visited in field reconnaissance, and only stands that met certain criteria were chosen for sampling.

A digitized Level IV ecoregion map of Oregon (Thorson et al. 2003) was used to delineate a PSME zone, a MIXED zone, and a PIPO zone. All research was limited to U.S. Government lands: the Willamette and Umpqua National Forests, administered by the US Department of Agriculture's Forest Service, in the PSME zone; the Medford District of the U.S. Department of Interior's Bureau of Land Management (BLM) in the MIXED zone; and the Winema, Fremont, and Deschutes National Forests in the PIPO zone. The goal was to distribute 15 plots along an environmental gradient through these three zones, with 5 plots per zone. SumrVPD (see Table 2.1) was used as a stratifying variable in the PSME zone. Within the PSME zone, potential sites were limited to regions within similar soil parent materials, as recorded by a digital parent material map (Walker and MacLeod 1991). Because the PIPO zone occupies a fundamentally younger geologic type, PIPO stands were necessarily located at sites with different soil parent materials.

Because this study focused on regional-scale patterns, site-level sources of variation were to be avoided. First, only stands on relatively level ground, or, if sloping, east-exposure ground, were chosen, to avoid the microsite climatic effects caused by north, south, or southwest exposures. U.S. Geological Survey 30m-digitial

elevation models (DEM) was used to identify such areas. Natural stands were chosen to avoid potential confusion caused by replanting of different genetic stock, placing a lower age limit on stands at approximately 80 years (before large-scale replanting practices were widespread). Very old stands were also avoided, because of potential leaf-level effects of age-related changes in foliar morphology (Apple et al. 2002). In the PSME zone, an age-map derived from satellite remote sensing (Law et al. In Press) was used to identify areas between 75 and 125 years. In the MIXED zone, the stand-level Forest Operations Inventory (FOI) digital geographic information system (GIS) coverage from the U.S. Department of Interior Bureau of Land Management (BLM, date unknown) was used to identify stands older than 70 years. No appropriate digital age layer was available for the PIPO zone, requiring a lengthy in-field site selection process.

In the field, single-layer canopies were preferred because they avoid competition between canopy layers for light and nutrients. Stands with significant basal area of non-target species (i.e. not PSME or PIPO) were also avoided to minimize competitive effects.

In mixed PSME/PIPO stands, an ideal condition was one where the trees of the two species had experienced essentially identical climates for their entire lifetimes; hence, stands were chosen where both species occupied the dominant canopy layer, where visual traits (bole size, branch condition, size of canopy) suggested similar developmental stages, and where individuals of the two species were interspersed within the stand. To identify stands that might meet this criterion, stands were

considered candidates only where the two species occupied the same size classes in the BLM's FOI coverage. For candidate stands in all three zones, final assessments of canopy complexity and of relative species dominance in the canopy were made in the field during reconnaissance visits; candidate sites not meeting the criteria were eliminated from consideration.

Fifteen stands were chosen, five CORE stands for each of the two species (stands dominated by one species or the other, in that species' core zone), and five MIXED stands where the two species co-occurred (Table 2.2). Total precipitation varied by a factor of five across sites (from 50 to 250 cm per year). Temperature ranges were less variable, although when grouped by ecozone, stands in the PIPO zone were cooler than stands in either the MIXED or PSME zones, in part because of their much higher elevation (Table 2.3). Precipitation in the PSME zone was more than twice that of either the MIXED or PIPO zones.

Table 2.2: Site characteristics of sampled stands

SITE	Species	Longitude [a]	Latitude [a]	Elevation (m)	YrPrcp	SprPrcp	MaxSprTemp	Temp	SumrVPD
Fawn	PSME	-122.38	44.85	575	214.0	27.0	19.9	9.1	1791.1
Quartz Creek	PSME	-122.46	42.27	875	251.7	31.9	17.4	6.7	1639.2
Oak Ridge	PSME	-122.58	43.78	812	168.3	22.3	20.2	8.5	1767.1
Steamboat	PSME	-122.74	43.29	1017	158.0	19.6	20.4	8.4	1448.0
Tiller	PSME	-122.87	43.02	832	133.0	15.5	22.5	9.9	1036.7
Elk Creek	MIXED	-122.90	42.69	675	91.7	10.5	24.6	10.9	1394.7
Butte	MIXED	-122.52	42.53	859	90.1	11.4	24.7	10.1	1801.2
Lake Creek	MIXED	-122.66	42.36	978	89.3	11.4	23.4	9.4	1643.0
Howard	MIXED	-122.45	44.59	1399	103.0	13.0	20.9	7.3	1145.3
Jenny	MIXED	-122.34	42.06	1072	68.6	9.0	24.0	9.2	903.4
Crawford	PIPO	-121.72	42.63	1405	68.3	8.4	22.2	7.2	1304.0
Wildhorse	PIPO	-121.62	42.91	1420	63.2	7.3	22.0	7.0	1192.1
Tar	PIPO	-121.23	43.37	1477	53.0	8.0	21.7	6.5	1630.0
Fall River	PIPO	-121.65	43.79	1356	81.8	9.3	20.6	6.4	1428.7
Sisters	PIPO	-121.64	44.23	1249	120.3	13.7	20.3	6.6	1662.4

[a] Locations in decimal degrees, using datum NAD83 and spheroid GRS1980
Abbreviations and units for all variables are listed in Table 2.1

Table 2.3: Mean site characteristics of sampled stands grouped by zone, with five stands per zone. Standard deviations are shown in parentheses.

Zone	ELEVATION (m)	YrPrcp	SprPrcp	MaxSprTemp	Temp	SumrVPD
PSME[a]	822.4 (159.8)	185.0 (47.5)	23.2 (6.4)	20.1 (1.8)	8.5 (1.2)	1536.4 (310.7)
MIXED[a]	996.7 (269.3)	88.6 (12.5)	11.1 (1.5)	23.5 (1.5)	9.4 (1.3)	1377.5 (363.6)
PIPO[a]	1381.6 (85.9)	77.3 (26.2)	9.3 (2.6)	21.4 (0.9)	6.7 (0.4)	1443.4 (203.4)

[a]PSME: *Pseudotsuga menziesii*; PIPO: *Pinus ponderosa;* MIXED: Mixtures of PSME and PIPO.

Abbreviations and units for site characteristics are listed in Table 2.1

Site sampling

Sampling on the 15 stands occurred during the summer of 2002, chiefly during the one-month period near mid-summer (July) to minimize the effects of within-season variation in leaf traits (Matson et al. 1994).

Based on variability of leaf measurements acquired in a small pilot study conducted in 2001, we estimated the number of branch samples that would be needed per stand to distinguish two stands separated by 10 percent in LMA, with varying alpha and beta levels (Marshall and Jahraus 1987). Depending on significance and power levels, anywhere from 6 to 72 samples would have been needed. To capture conditions across a large region, however, as many stands as possible would need to be sampled, which required fewer samples per stand on a fixed budget. Therefore, 12 trees per stand were sampled in the ten CORE stands; 12 trees per species (for a total of 24) were sampled in the five MIXED stands. A single branch from the middle canopy (vertically) of each tree was shot down with a 12-Gauge shotgun using 00-Buckshot (Matson et al. 1994, Smith and Martin 2001); an average of four to five shells were required before a branch separated and fell clear to the ground. Only branches on the east or west side of the tree were chosen, and only those branches that appeared to represent average light environment (i.e. light gaps in dense canopies were avoided). For the tree from which each branch came, approximate canopy vertical position of the separated branch was noted (based on visual division of vertical canopy into 5 equal-sized quintiles), as well as tree diameter at breast height (DBH; including bark). Across all stands, branches primarily came from the 2nd and 3rd vertical quintiles

of the canopy (data not shown; quintile 1 represents the top 20% of the canopy). For 3 to 4 trees in the stand, height to top of tree and bottom of canopy was estimated using an analog clinometer and laser range finder. At 5 to 7 points in the stand, estimates of canopy basal area were acquired using a BAF 10 ft^2/acre prism, and an upward-looking hemispherical digital photo of the canopy was taken using a Nikon 990 camera (2 megapixel) with a hemispherical lens (Frazer et al. 2001).

Leaf processing

Branches were placed in sealed plastic bags in ice-cooled coolers immediately upon exiting the forest stand. Upon return to the laboratory, branches were stored in 4-5 degree Celsius refrigerators until needle processing.

Needles were stratified by needle age class, as identified by bud scars on the branches. Because sampling occurred during the middle of the growing season when current-year needles are expanding, current-year needles were not used. Needles were plucked from the branches beginning at the prior year, considered year 1, followed by separate plucking for year 2, and grouped plucking of all prior years. Length (in mm) of branch growth for each year grouping was recorded, as well as the total number of years of retained needles on the branch (the leaf longevity, LL).

For PSME needles, a subset of 20 to 40 needles for each age class was separated and used to estimate LMA. Projected leaf area was estimated optically using a Panasonic WV-CD20 Digital Camera and the AgImage digital imaging software (Decagon Instruments, Inc.) on 30 to 45 needles per sample. Projected leaf area was converted to half of all-sided leaf area by assuming that the needles were ellipses; a

handheld micrometer was used on a 1/3 subset of all first-year branch needles to determine an average width and thickness for calculation of the ellipse major and minor axes. In this study, the ratio of half-all-sided leaf area to projected leaf area for PSME needles was calculated to be 1.15.

For 15 PIPO needles per branch, handheld micrometer measurements of needle width (near the center of the needle) and needle length were multiplied to produce a projected area, and that value multiplied by shape correction factor of 1.18 to estimate half of all-sided area.

All needles were placed in envelopes in a drying oven at 70 degrees C for 48 to 72 hours. For needles where leaf area had been calculated, total dry needle mass was recorded using a Denver Instrument Company A-250 balance, with precision to 0.0001 g. LMA was calculated using the dry mass and half of all-sided leaf area.

Chemical analysis was conducted on all year 1 needles, as well as every third tree's year 2 and years 3+ (all remaining years) needles. Analysis was conducted at Oregon State University's Central Analytical Lab for chemical analysis. A Leco CNS-2000 Macro Analyzer instrument was used to measure the percent (by mass) C and N of ground samples. For branches where chemistry for needle years 2 and 3+ was not measured directly, it was estimated based on the species-specific relationship between year 2 or years 3+ needles and year 1 needles of trees where all three sets were analyzed, using the reduced-major-axis form of regression (because of equal errors in both X and Y variables in the regression; Cohen et al. [2003]). Branch-level LMA and leaf N were both estimated using an average of year 1, 2 and 3+ needles, weighted by

relative contribution of each years' branch growth to the total branch growth. Stand-average values for leaf traits were calculated by simple averaging of all 12 branch-level estimates.

Canopy gap fraction estimations

Canopy gap fraction was estimated from the several digital hemispherical photos acquired in each stand. The Gap Light Analyzer (GLA) software (Frazer and Canham, Simon Fraser University; http://www.ecostudies.org/gla/), was used to develop gap fraction estimates. Each photo was individually processed, with separate thresholding values, to account for variation in sky conditions.

Statistical analyses

Statistical tests were used to compare groups and to examine trends.

All PSME trees in PSME stands were considered one group, all PSME trees in MIXED stands a second group, with two parallel groups for PIPO trees. Each of the four groups had 60 individuals. The Kolmogorov-Smirnoff one-sample test for equal distributions suggested that leaf traits across trees in each of the four groups were not normally distributed. Therefore, the non-parametric Kolmogorov-Smirnoff two-sample distribution-matching test was used to compare groups.

Trends in leaf traits across stands were examined using simple regression. For all regressions, the unit of sampling was a single stand-species combination, resulting in 5 samples in the PSME CORE zone, 10 samples in the MIXED zone (5 stands with two species each), and 5 samples in the PIPO CORE zone. Regressions were

conducted with stand-average leaf traits as dependent variables and three groups of variables as independent variables (Table 2.1): climate estimates from DAYMET, stand attributes from field measurement, and the leaf traits themselves.

With only 20 stand-species combinations to use in regression models, only first order linear, exponential, and logarithmic regression models were initially examined. Then, within each variable group (Climate, Stand, and Leaf), the single best predictor of a given leaf trait was identified and Akaike's information criterion was used to evaluate whether a second variable from within the same variable group would significantly improve the model (using the STEP function in SPlus [Insightful Corporation [2002]).

Results

Stand-level traits for all sampled plots are shown in Table 2.4. Tree-specific traits in MIXED zone stands are separated by species. All stand-level traits showed variation among sites, although the relative ranges of variation differed. Gap fraction varied by a factor of eight across species, while DBH varied only by a factor of two. PSME stands were generally taller and had greater basal area than PIPO stands.

Table 2.4. Mean stand attributes for all sampled stands, with trees in MIXED stands separated by species within a stand.

SITE	SPE-CIES	SITE TYPE	GapFrac-tion [a,d]	BA [a,d]	DBH [c]	Ht [b]	CmDpth [b]	CmDpth/Ht [b]	Ht/DBH [b]	Ht/BA [b]	BranchInc [c]	FolBranch Lngth [c]
Fawn	PSME	CORE	5.3	41.3	89.8 (20.3)	59.2 (14.0)	21.3 (9.8)	0.35 (0.09)	74.3 (9.8)	3.3 (0.3)	69.5 (15.5)	362.8 (90.3)
Quartz Creek	PSME	CORE	6.6	65.0	69.1 (11.5)	51.5 (2.4)	21.2 (6.0)	0.41 (0.11)	73.9 (6.0)	1.8 (0.0)	59.0 (19.1)	423.2 (110.9)
Oak Ridge	PSME	CORE	7.4	45.5	79.7 (15.6)	53.5 (2.5)	15.9 (6.7)	0.29 (0.12)	74.8 (6.7)	2.7 (0.1)	57.3 (16.0)	397.5 (130.8)
Steam-boat	PSME	CORE	9.6	49.7	87.8 (13.1)	44.5 (6.4)	12.6 (2.9)	0.29 (0.08)	54.1 (2.9)	2.1 (0.1)	54.1 (10.0)	341.3 (53.4)
Tiller	PSME	CORE	7.9	52.8	69.5 (11.0)	45.0 (3.2)	14.4 (4.1)	0.32 (0.11)	65.3 (4.1)	2.0 (0.1)	74.2 (23.6)	364.0 (87.7)
Elk Creek	PSME	MIXED	11.6	39.7	70.0 (11.4)	38.0 (2.9)	18.0 (5.0)	0.47 (0.11)	61.3 (5.0)	2.2 (0.1)	43.5 (9.7)	294.8 (105.3)
Butte	PSME	MIXED	13.2	31.8	78.6 (13.5)	49.0 (6.0)	26.6 (8.3)	0.55 (0.18)	61.1 (8.3)	3.5 (0.2)	67.5 (19.1)	412.4 (92.9)
Lake Creek	PSME	MIXED	11.5	30.5	71.6 (12.4)	39.7 (13.7)	18.2 (5.2)	0.47 (0.10)	59.2 (5.2)	3.0 (0.5)	52.2 (10.0)	314.2 (79.9)

Table 2.4. (continued) Mean stand attributes for all sampled stands, with trees in MIXED stands separated by species within a stand.

SITE	SPE-CIES	SITE TYPE	GapFrac-tion [a,d]	BA [a,d]	DBH [c]	Ht [b]	CmDpth [b]	CmDpth/Ht [b]	Ht/DBH [b]	Ht/BA [b]	BranchInc [c]	FolBranch Lngth [c]
Howard	PSME	MIXED	16.6	33.3	70.1 (11.3)	35.4 (4.8)	22.7 (2.5)	0.64 (0.02)	48.4 (2.5)	2.4 (0.1)	75.4 (14.7)	427.9 (78.8)
Jenny	PSME	MIXED	17.5	27.5	44.0 (6.3)	25.5 (2.2)	16.6 (3.0)	0.65 (0.12)	54.3 (3.0)	2.1 (0.1)	49.9 (15.2)	299.7 (95.8)
Elk Creek	PIPO	MIXED	11.6	39.7	78.3 (9.8)	56.1 (6.0)	17.3 (9.7)	0.30 (0.14)	68.6 (9.7)	3.2 (0.2)	29.6 (9.9)	71.1 (37.8)
Butte	PIPO	MIXED	13.2	31.8	75.6 (9.3)	48.6 (2.4)	19.8 (1.6)	0.41 (0.04)	65.6 (1.6)	3.5 (0.1)	37.7 (8.8)	112.8 (45.4)
Lake Creek	PIPO	MIXED	11.5	30.5	82.2 (14.4)	39.7 (5.9)	18.0 (3.0)	0.45 (0.02)	49.1 (3.0)	3.0 (0.2)	41.1 (16.4)	114.9 (74.5)
Howard	PIPO	MIXED	16.6	33.3	73.0 (14.6)	39.4 (3.2)	13.3 (3.0)	0.34 (0.08)	56.6 (3.0)	2.7 (0.1)	32.3 (14.0)	125.9 (77.6)
Jenny	PIPO	MIXED	17.5	27.5	47.4 (9.9)	26.3 (3.2)	11.9 (1.8)	0.45 (0.07)	57.3 (1.8)	2.2 (0.1)	45.3 (16.4)	191.3 (88.8)

Table 2.4. (continued) Mean stand attributes for all sampled stands, with trees in MIXED stands separated by species within a stand.

SITE	SPE-CIES	SITE TYPE	GapFrac-tion [a,d]	BA [a,d]	DBH [c]	Ht [b]	CrnDpth [b]	CrnDpth/Ht [b]	Ht/DBH [b]	Ht/BA [b]	BranchInc [c]	FolBranch Lngth [c]
Craw-ford	PIPO	CORE	30.2	18.4	76.3 (10.5)	35.4 (8.4)	26.0 (6.1)	0.74 (0.05)	50.8 (6.1)	4.4 (0.5)	31.8 (6.5)	151.3 (51.4)
Wild-horse	PIPO	CORE	32.6	25.3	67.8 (10.4)	30.6 (3.1)	19.1 (2.9)	0.62 (0.07)	46.8 (2.9)	2.8 (0.1)	29.7 (11.3)	129.6 (64.0)
Tar	PIPO	CORE	39.4	23.0	62.0 (6.1)	26.1 (2.7)	18.8 (4.2)	0.72 (0.12)	43.6 (4.2)	2.6 (0.1)	20.7 (4.9)	103.7 (30.2)
Fall River	PIPO	CORE	28.7	36.7	60.7 (9.4)	34.9 (3.9)	15.8 (4.8)	0.46 (0.17)	58.1 (4.8)	2.2 (0.1)	24.3 (7.8)	134.0 (44.5)
Sisters	PIPO	CORE	24.9	41.3	67.5 (11.9)	30.9 (4.4)	15.9 (3.5)	0.52 (0.12)	46.4 (3.5)	1.7 (0.1)	26.4 (11.6)	124.2 (55.5)

[a] Numbers represent stand-level estimates

[b] Numbers are means of 3 to 5 measurements per stand, with standard deviations in parentheses

[c] Numbers are means of 12 measurements, one for each tree/species combination, in the stand, with standard deviations in parentheses

Units for each measurement variable listed in Table 2.1

Variation in some stand level traits was statistically related to climate. Table 2.5 shows best one-factor linear regression predictors of all stand variables, both for each species separately and across species. Gap fraction, total basal area, and height were all strongly related to climate. Yearly total precipitation (YrPrcp) was a consistent predictor of variation in many traits, both within and across species, although average temperature (Temp) was associated with variation in some PIPO traits.

Trees in MIXED stands differed from trees in CORE stands for most leaf traits. At the tree level, PSME trees in MIXED stands had higher LMA and leaf N values than did PSME trees in CORE stands (Figure 2a, Kolmogorov-Smirnov [K-S] value for comparing two distributions 0.63 and 0.28, respectively). Only LL did not differ (K-S value 0.18). PIPO trees differed significantly between CORE and MIXED stands for all three leaf traits (Figure 2b; K-S values of 0.37, 0.47, and 0.57 for LMA, LN, and LL respectively).

In their CORE zones, PSME trees and PIPO trees also differed in values of LMA and LL (Figure 3a; K-S values of 0.87 and 0.48, respectively). LN did not differ, however (K-S 0.13). When the two species co-existed in the same stands, LL continued to differ (Figure 3b; K-S 0.78), but LMA no longer differed (K-S 0.21). Distributions of LN values were distinct in MIXED stands at the $p=0.1$ but not $p=0.05$ levels (K-S of 0.22), but this represents more differentiation of LN than observed between PSME and PIPO trees in their respective CORE zones.

Table 2.5. Summary of regression models that best relate measured stand attributes to climate variables.

Pseudotsuga menziesii stands

Stand variable	Best Predictor (X)	Equation	r^2	p	n
DBH	log(YrPrcp)	-12.9+17.8X	0.35	0.071	10
GapFraction	log(YrPrcp)	51.5-8.43X	0.75	0.001	10
Ht/BA	---	1.10	0.17	0.239	10
BA	log(YrPrcp)	-69.2+22.9X	0.69	0.003	10
Ht/DBH	SprPrcp	47.4+0.891X	0.55	0.014	10
CrnDpth/Ht	log(YrPrcp)	1.56-0.230X	0.52	0.018	10
CrnDpth	---	17.60	0.14	0.285	10
Ht	log(YrPrcp)	-46.9+18.8X	0.67	0.004	10
BranchInc	exp(Temp)	63.9-0.0003X	0.15	0.270	10
FolBranchLngth	log(Temp)	831-214X	0.39	0.052	10

Pinus ponderosa stands

Stand variable	Best Predictor (X)	Equation	r^2	p	n
DBH	log(YrPrcp)	-2.99+16.4X	0.15	0.262	10
GapFraction	log(Temp)	108-41.02X	0.70	0.003	10
Ht/BA	---	1.30	0.26	0.130	10
BA	log(YrPrcp)	-76.0+24.3X	0.66	0.004	10
Ht/DBH	---	49.10	0.63	0.006	10
CrnDpth/Ht	log(YrPrcp)	2.33-0.416X	0.47	0.028	10
CrnDpth	log(SprPrcp)	33.7-7.01X	0.14	0.278	10
Ht	exp(Temp)	31.8+0.001X	0.71	0.002	10
BranchInc	log(Temp)	-21.1+25.6X	0.46	0.031	10
FolBranchLngth	exp(Temp)	1370X	0.32	0.086	10

All stands

Stand variable	Best Predictor (X)	Equation	r^2	p	n
DBH	log(YrPrcp)	3.01+14.7X	0.28	0.018	20
GapFraction	log(YrPrcp)	95.6-17.10X	0.53	< 0.001	20
Ht/BA	log(MaxSprTemp)	-2.49+1.18X	0.14	0.106	20
BA	log(YrPrcp)	-73.3+23.7X	0.76	< 0.001	20
Ht/DBH	log(YrPrcp)	-15.4+16.0X	0.46	0.001	20
CrnDpth/Ht	log(YrPrcp)	1.53-0.230X	0.44	0.001	20
CrnDpth	---	17.60	0.04	0.420	20
Ht	log(YrPrcp)	-43.0+18.1X	0.53	< 0.001	20
BranchInc	log(SprPrcp)	-17.7+25.2X	0.35	0.006	20
FolBranchLngth	log(SprPrcp)	-263+201X	0.40	0.003	20

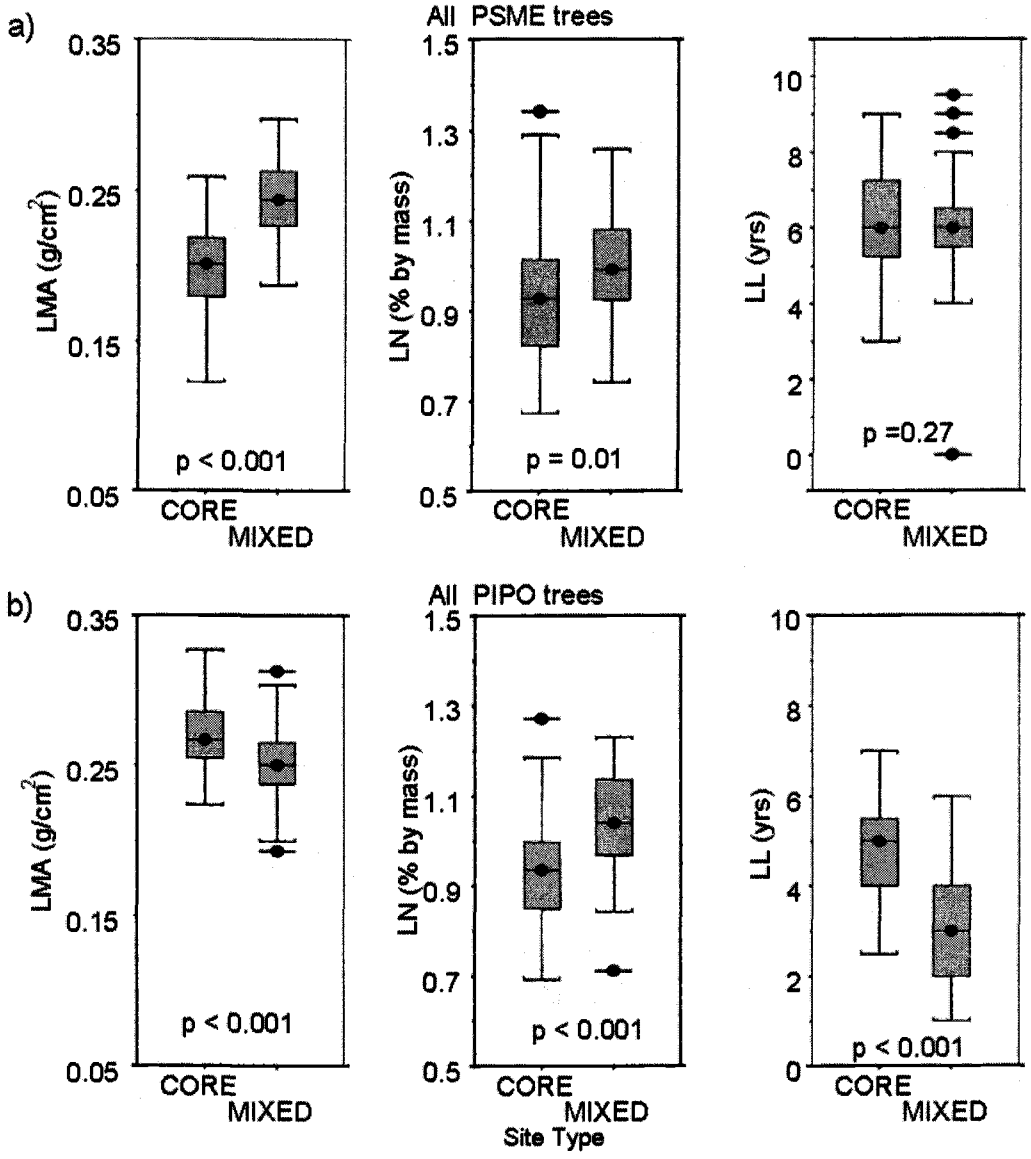

Figure 2.2. Comparisons of leaf traits for all trees in each species. Box plots show first and third quartiles of the distribution of 60 trees, whiskers are placed at 1.5 times interquartile length, and isolated trees outside of whiskers are shown as black lines and solid circles. P-values from Kolmogorov-Smirnov 2-sample tests, with low values suggesting that the distributions of values for the two groups are not the same. a) PSME trees in CORE vs. MIXED stands. b) As in a), but for PIPO trees.

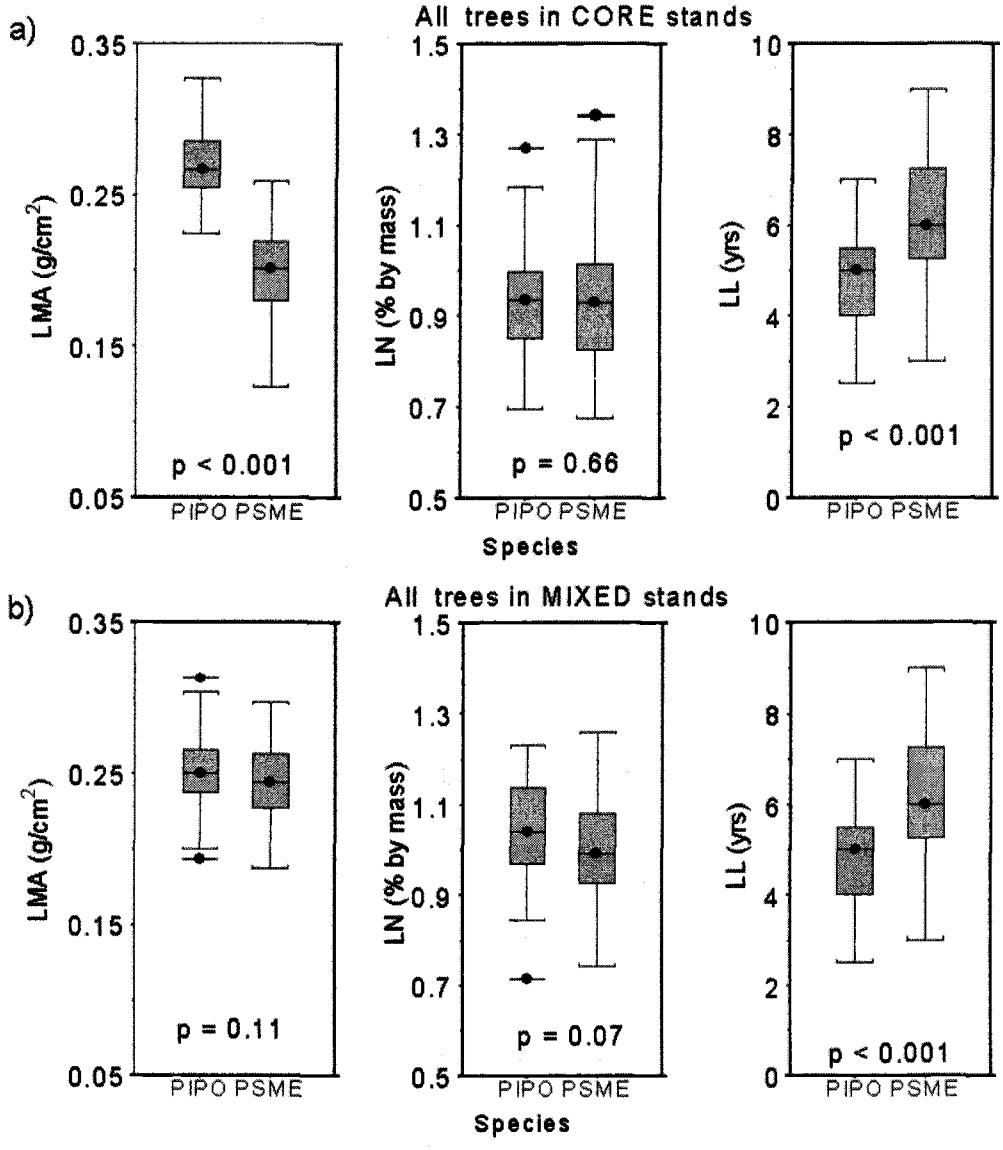

Figure 2.3. Comparisons of leaf traits across species for trees in CORE and MIXED stands. P-values as in Figure 2.2. Box plots symbols as in Figure 2.2. a) PSME vs. PIPO trees in CORE stands and b) in MIXED stands.

When grouped at the stand level, leaf traits varied across stands (Table 2.6). For PSME trees grouped by site across the CORE and MIXED zones, LMA and LN varied by more than 30% of the species-level mean stand values, while LL varied by approximately 15% of the mean. PIPO trees showed similar levels of variation in LMA and leaf nitrogen (between 25 and 30% of means), but much greater variation in LL (more than 80% of the mean).

Variation in climate could explain some of the variation in leaf traits across stands (Table 2.7). For PSME only, LMA was related significantly to climate, but LN and LL were not. For PIPO, on the other hand, climate variation was strongly related to variation in all three traits. Across species, the strongest climate relation was that of LMA, where nearly 70% of observed variation could be explained with a single climate predictor (log(YrPrcp)).

Variation in leaf traits could also be explained by variation in stand- or branch-level attributes (Table 2.8). Across species, approximately 80% of variation in LMA was explained by variation in stand light environment (GapFraction). For PSMES, LN and LL again were not related to stand attributes, but for PIPO, all three leaf traits could be explained by stand attributes.

Examining leaf trait interrelationships, LN and LL were consistently linked, both within and across species (Table 2.9). For both PSME and across species, variation in LMA was not related to the other two leaf traits, but was strongly related to LL for PIPO alone.

Table 2.6. Mean (and standard deviation) of measured leaf traits for all trees in a stand, with trees in MIXED stands separated by species within a stand.

SITE	SPECIES	SITE TYPE	LMA [a,b]	LN [a,b]	LL [a]
Fawn	PSME	CORE	0.18 (0.027)	1.17 (0.12)	5.3 (0.94)
Quartz Creek	PSME	CORE	0.22 (0.025)	0.84 (0.09)	7.3 (0.89)
Oak Ridge	PSME	CORE	0.19 (0.029)	0.89 (0.11)	6.9 (0.91)
Steamboat	PSME	CORE	0.20 (0.020)	0.86 (0.11)	6.4 (1.10)
Tiller	PSME	CORE	0.20 (0.021)	0.98 (0.07)	5.2 (1.34)
Elk Creek	PSME	MIXED	0.23 (0.024)	0.98 (0.14)	6.7 (1.37)
Butte	PSME	MIXED	0.23 (0.032)	0.97 (0.07)	6.3 (1.14)
Lake Creek	PSME	MIXED	0.25 (0.024)	1.06 (0.11)	6.0 (0.93)
Howard	PSME	MIXED	0.26 (0.019)	1.07 (0.10)	5.7 (0.45)
Jenny	PSME	MIXED	0.25 (0.015)	0.90 (0.13)	6.0 (0.39)

Table 2.6. (continued) Mean (and standard deviation) of measured leaf traits for all trees in a stand, with trees in MIXED stands separated by species within a stand.

SITE	SPECIES	SITE TYPE	LMA [a,b]	LN [a,b]	LL [a]
Elk Creek	PIPO	MIXED	0.23 (0.026)	1.07 (0.08)	2.3 (0.69)
Butte	PIPO	MIXED	0.25 (0.009)	1.05 (0.12)	3.0 (0.72)
Lake Creek	PIPO	MIXED	0.25 (0.025)	1.12 (0.06)	2.7 (0.96)
Howard	PIPO	MIXED	0.26 (0.025)	0.98 (0.13)	3.8 (1.39)
Jenny	PIPO	MIXED	0.27 (0.015)	1.00 (0.11)	4.4 (1.35)
Crawford	PIPO	CORE	0.27 (0.020)	0.98 (0.10)	4.7 (1.10)
Wildhorse	PIPO	CORE	0.26 (0.016)	1.00 (0.12)	4.3 (0.72)
Tar	PIPO	CORE	0.29 (0.022)	0.89 (0.10)	5.0 (1.03)
Fall River	PIPO	CORE	0.27 (0.022)	0.94 (0.08)	5.5 (0.95)
Sisters	PIPO	CORE	0.26 (0.016)	0.85 (0.07)	4.8 (1.10)

[a] Numbers are means of 12 measurements, one for each tree/species combination, in the stand, with standard deviations in parentheses

[b] For LMA and LN, each branch's value is the mean of the trait from three different age classes of needle, weighted by the proportion of each age class on the branch.

Units for each measurement variable listed in Table 2.1.

Table 2.7. Summary of regression models that best relate each leaf attribute to either one or two climate variables, for each species separately and across species.

Pseudotsuga menziesii stands

Stand variable	*Best Predictor (X)*	*Equation*	r^2	*p*	*Added variable*[a]	r^2	*p*	*n*
LMA	log(YrPrcp)	0.45-0.047X	0.56	0.013	log(Temp)	0.85	0.001	10
LN	---	0.99	0.20	0.194	---	---	---	10
LL	---	6.0	0.34	0.075	---	---	---	10

Pinus ponderosa stands

Stand variable	*Best Predictor (X)*	*Equation*	r^2	*p*	*Added variable*	r^2	*p*	*n*
LMA	---	0.27	0.66	0.005	---	---	---	10
LN	log(Temp)	0.28+0.34X	0.69	0.003	exp(YrPrcp)	0.82	0.003	10
LL	log(Temp)	14-4.7X	0.78	< 0.001	exp(SumrVPD)	0.85	0.001	10

All stands

Stand variable	*Best Predictor (X)*	*Equation*	r^2	*p*	*Added variable*	r^2	*p*	*n*
LMA	log(YrPrcp)	0.51-0.06X	0.66	< 0.001	log(Temp)	0.85	< 0.001	20
LN	log(Temp)	0.46+0.24X	0.23	0.032	---	---	---	20
LL	log(SumrVPD)	6.4-3.2X	0.21	0.041	---	---	---	20

[a]An added independent variable is listed only if it improves the regression, as suggested by Akaike's information criterion statistic.

Abbreviations for independent and dependent variables are shown in Table 2.1

Table 2.8. Summary of regression models that best relate each leaf attribute to either one or two measured stand variables, for each species separately and across species.

Pseudotsuga menziesii stands

Stand variable	*Best Predictor (X)*	*Equation*	r^2	*p*	*Added variable*[a]	r^2	*p*	*n*
LMA	log(CrnDepth/Ht)	0.29+0.08X	0.83	< 0.001	exp(Ht)	0.93	< 0.001	10
LN	---	0.95	0.43	0.040	---	---	---	10
LL	---	6.0	0.34	0.076	---	---	---	10

Pinus ponderosa stands

Stand variable	*Best Predictor (X)*	*Equation*	r^2	*p*	*Added variable*	r^2	*p*	*n*
LMA	Ht	0.31-0.001X	0.74	0.002	exp(GapFraction)	0.84	0.001	10
LN	log(GapFraction)	1.4-0.14X	0.58	0.011	exp(BA)	0.80	0.004	10
LL	log(GapFraction)	-2.3+2.1X	0.78	< 0.001	DBH	0.87	< 0.001	10

All stands

Stand variable	*Best Predictor (X)*	*Equation*	r^2	*p*	*Added variable*	r^2	*p*	*n*
LMA	log(GapFraction)	0.12+0.05X	0.80	< 0.001	exp(Ht/DBH)	0.83	< 0.001	20
LN	log(Ht/BA)	0.77+0.22X	0.36	0.005	exp(CrnDpth)	0.50	0.003	20
LL	log(FolBranchLngth)	-5.4+2.0X	0.68	< 0.001	log(BranchInc)	0.98	< 0.001	20

[a]An added independent variable is listed only if it improves the regression, as suggested by Akaike's information criterion statistic.

Abbreviations for independent and dependent variables are shown in Table 2.1

Table 2.9. Summary of regression models that best relate each leaf attribute to either one or two of the complementary leaf attributes, for each species separately and across species.

Pseudotsuga menziesii stands

Stand variable	*Best Predictor (X)*	*Equation*	r^2	*p*	*Added variable*	r^2	*p*	*n*
LMA	log(LL)	0.18+0.023X	0.01	0.790	---	---	---	10
LN	LL	1.7-0.11X	0.53	0.016	---	---	---	10
LL	log(N)	6.0-4.8X	0.54	0.015	---	---	---	10

Pinus ponderosa stands

Stand variable	*Best Predictor (X)*	*Equation*	r^2	*p*	*Added variable*	r^2	*p*	
LMA	log(LL)	0.20+0.047X	0.72	0.002	---	---	---	10
LN	LL	1.3-0.065X	0.71	0.002	---	---	---	10
LL	exp(N)	15-4.1X	0.73	0.002	log(LMA)	0.87	< 0.001	10

All stands

Stand variable	*Best Predictor (X)*	*Equation*	r^2	*p*	*Added variable*	r^2	*p*	
LMA	---	0.25	0.20	0.049	---	---	---	20
LN	LL	1.2-0.035X	0.29	0.015	log(LMA)	0.37	0.020	20
LL	log(N)	4.9-8.1X	0.29	0.014	log(LMA)	0.44	0.008	20

[a]An added independent variable is listed only if it improves the regression, as suggested by Akaike's information criterion statistic.

Abbreviations for independent and dependent variables are shown in Table 2.1

Discussion

Variation in leaf traits has been examined extensively at the stand level and at the global level, but for the purposes of running carbon models, it is important to understand causes of variation in these leaf traits at intermediate regional scales. Here, we used a zone of co-occurrence between two dominant tree species to leverage ecological interpretation of regional variation in key leaf traits.

In general, values for the leaf traits we observed were within the range of values reported for these species in other studies (Zinke and Stangenberger 1979, Smith et al. 1981, Gower et al. 1987, Cregg 1994, Pierce and Running 1994, Law et al. 2001b, Apple et al. 2002). If LMA and LL values for PSME and PIPO are compared in their CORE zones, they generally differ (Figure 3a). This is not unexpected, as the two conifers come from different genera and tend to occupy different ecological niches (Burns and Honkala 1990). In the same comparison, the mean values of LN did not differ, however. This is generally consistent with the observation that average leaf nitrogen in evergreens in often stable across species (Körner 1989), but is not consistent with other reports specific to PSME and PIPO that report that PIPO may have slightly lower LN than PSME (Zinke and Stangenberger 1979, Burns and Honkala 1990).

The apparent similarity of mean LN values obscured large variation in LN values within each species (Figure 2.3 and Table 2.6). LMA and LL also showed substantial variation among sites within species. Thus, these three leaf traits cannot be

considered homogeneous across the ranges of the two dominant conifers of the Cascades Mountains in Oregon.

Some of the variation in leaf traits was associated with ecozone. Within each species, trees in the CORE zones were different than those in the MIXED zone in at least two of the three leaf traits (Figure 2.2). Because these leaf traits exert control over carbon accumulation, variation in leaf traits should be considered in efforts to characterize carbon dynamics for the forests of Oregon. This observation, combined with the fact that the two species in their core zones differed from each other in LMA and LL, argues for treating them as separate physiological types in regional carbon modeling efforts.

In MIXED stands, the two species appeared to diverge in LL even more so than in CORE stands, but they converged in LMA (Figure 2.3b). While different species can be considered to have different "inherent" LMAs (Poorter and Evans 1998), convergence of LMA for two conifers from different genera in common stands is notable. While the convergence of LMA values in our study could be coincidental, the smooth progression of LMA values from each CORE zone through the MIXED zone strongly suggests that these two conifers were responding with similar strategies to a common environmental cue.

That cue appears to be related in part to moisture. Higher LMA species are often found in dry sites (Mooney et al. 1978, Cunningham et al. 1999, Wright et al. 2002). Mooney et al. (1978) suggest that the generally thicker mesophyll layers of high LMA leaves may be favored in dry environments because they allow for more

photosynthetic machinery per leaf transpirational area, and hence would confer higher water use efficiency. However, higher LMA is also known to be a response to high light levels (Poorter and Evans 1998, Le Roux et al. 1999), and dry environments tend to favor open stands with higher light levels. Therefore, moisture may control LMA directly or indirectly.

Our results suggest that the control may be indirect. The relationship between LMA and precipitation was strong (Figure 2.4a), but several sites had LMA values

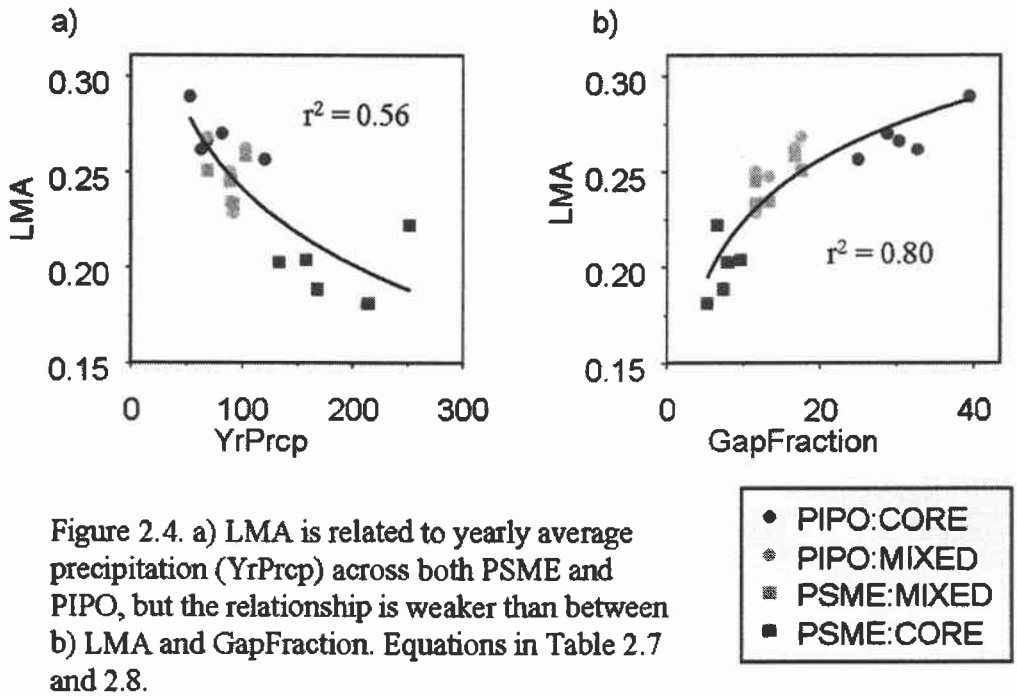

Figure 2.4. a) LMA is related to yearly average precipitation (YrPrcp) across both PSME and PIPO, but the relationship is weaker than between b) LMA and GapFraction. Equations in Table 2.7 and 2.8.

higher than would be expected from the YrPrcp alone. The YrPrcp variable could be inaccurately modeled by the DAYMET algorithm, or LMA may have been responding more directly to other effects. When LMA was related to GapFraction, the relationship

was strong across all sites, and was consistent across species (Figure 2.4b). Local light environment may take precedence over moisture in controlling LMA for the species sampled here. The linkage of LMA to light environment is well-established at the stand-level (Del Rio and Berg 1979, Evans and Poorter 2001, Grassi and Bagnaresi 2001), and precedence of light over moisture stress in controlling LMA has been experimentally shown in at least one case (Frak et al. 2002). The precedence of light over climate in controlling LMA is also supported by forest thinning studies. Both PSME and *Tsuga heterophylla* (western hemlock) stands in Oregon have been shown to have higher LMA after canopy light environment is increased through thinning, even though precipitation regime does not change (Tucker and Emmingham 1977, Smith et al. 1981). Regardless of the proximal cause, these results suggest that LMA was highly plastic at the regional level, an observation supported by the relatively low genetic control over LMA in Douglas-fir in Oregon (St. Clair 1994). More importantly, these results suggest that LMA at the regional scale had a predictable relationship with moisture, whether direct or indirect, across these two species.

Regional patterns of LN and LL, on the other hand, were not common for both species. PIPO showed patterns consistent with prior hypotheses about controls on LN and LL relative both to climate and to LMA. LN was positively related to temperature (Table 2.7), a finding similar to that of (Yin 1993, Castro-Diez et al. 2000). LL was higher for PIPO in CORE stands than in MIXED stands, consistent with the proposition that longer retention of needles is a means of amortizing leaf construction costs in poorer environments (Walters and Reich 1999). The same amortization

argument links higher LMA with longer leaf retention (higher LL) (Kikuzawa 1991, Wright et al. 2002), and this has been observed in other temperate forests (Gower et al. 1993) and across species globally (Reich et al. 1997).

PSME did not appear to follow these expectations. Despite substantial variation among stands, neither PSME LN nor LL were strongly linked to climatic variables (Table 2.7), and neither trait was linked to LMA (Table 2.9; Figure 2.5a illustrates the contrast for PIPO and PSME for LL and LMA). However, LL and LN

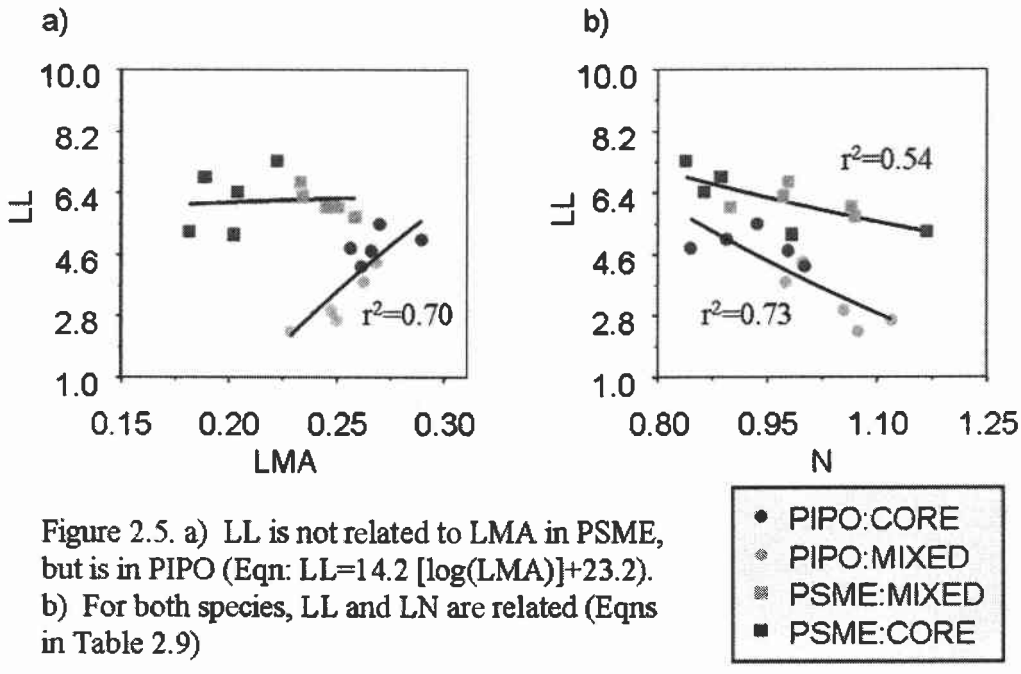

Figure 2.5. a) LL is not related to LMA in PSME, but is in PIPO (Eqn: LL=14.2 [log(LMA)]+23.2). b) For both species, LL and LN are related (Eqns in Table 2.9)

were strongly linked to each other for PSME, as they were for PIPO (Figure 2.5b). These apparently disparate results may be explained if two key propositions are true. The first proposition is that LMA at the stand level is indeed controlled by canopy

light levels, with higher LMA in more open stands, as discussed above. The second proposition is that LN is related to soil nutrient availability. Although this may not be true for tropical systems (Williams et al. 2002), the potential for a link between foliar nutrient levels and availability of nutrients from the soil has long been observed (van den Driessche 1974, Reich et al. 1992). LN increases when trees are fertilized (Powers and Reynolds 1999, Rosati et al. 2000, Turner et al. 2000), and when underburning temporarily increases nutrient availability (Reich et al. 1990). If LN is related to nutrient availability in the soil, then lower LN in the PIPO zone than MIXED zone (Figure 2.2b) would suggest lower soil fertility for the sites in the PIPO zone.

Although soil analyses were not part of our study design, published soil surveys of the PIPO and MIXED zones tended to support this conclusion. Soils in the PIPO zone are derived from relatively recent volcanic parent materials, which are of low fertility (Larsen 1976). The open, single-layer canopies chosen for this study are typically associated with lower fertility sites within the PIPO zone (Dyrness and Youngberg 1966). Plots in the MIXED zone are found on older soils derived from metamorphic or sedimentary parent materials (Johnson 1993) that are expected to be of higher fertility. While only suggestive, this observation is not inconsistent with a linkage between LN and soil nutrition.

Patterns of LN in the MIXED and PSME zones also support this linkage. For the PSME and MIXED zones, sites were restricted to soils derived from similar parent materials (see Methods), and thus there is little reason to suspect zone-wide differences in soil nitrogen availability. Although LN values of PSME trees in the

MIXED zone were slightly higher than in the PSME zone (Figure 2.2a), there was considerable overlap in leaf N between the MIXED and PSME zones at the site level, with both the highest and lowest nitrogen sites found in the PSME zone alone (Figure 2.5b). This is similar to the findings of Bauer et al. (1997) for *Picea abies* in Europe, where local scale variability in LN appeared related to substrate and nitrogen deposition, not to climate.

If these two propositions are true for the forests under study, then a conceptual model of leaf traits for Douglas-fir and ponderosa forests may be envisioned that is consistent both with prior theory and with the observed results:

1. Any factor that improves overall canopy growth will lead to lower light levels within the canopies, which will lower canopy-average LMA.

Because moisture variation is the dominant climatic control across the sites studied, its relationship with LMA across species is strong (Figure 2.4a). However, if nitrogen limits growth of the sampled PIPO stands in their CORE zone, and MIXED stands have higher soil fertility than PIPO CORE stands, then some of the control in canopy light environment for PIPO would be related to nitrogen. For PSME, on the other hand, soil variation was likely minimal and local, and the dominant control on canopy openness in the stands sampled is moisture. Nitrogen would likely show little connection with LMA. Figure 2.6 supports these predictions: as LN increases in PIPO, GapFraction decreases, but PSME show no relationship (Figure 2.6a). Consequently, LMA diminishes as LN increases in PIPO, but shows no relationship for PSME (Figure 2.6b).

The lack of a relationship between LN and LMA in PSME need not be inconsistent with the general global leaf trait model of Reich et al. (1997), which suggests that such a relationship should exist. Our results apply for a relatively small range of LN and LMA values within a limited physiognomic type (evergreen conifers), and may represent noise in an overall global relationship that strongly links LMA and LN. Given that most of the samples of (Reich et al. 1997) lie at LMA values much greater than those observed here, and that the asymptotic relationship between GapFraction and LMA plateaus in our study as GapFraction increases (Figure 2.4b), it is likely that the light-limitation constraint on LMA no longer matters after a critical LMA threshold is surpassed.

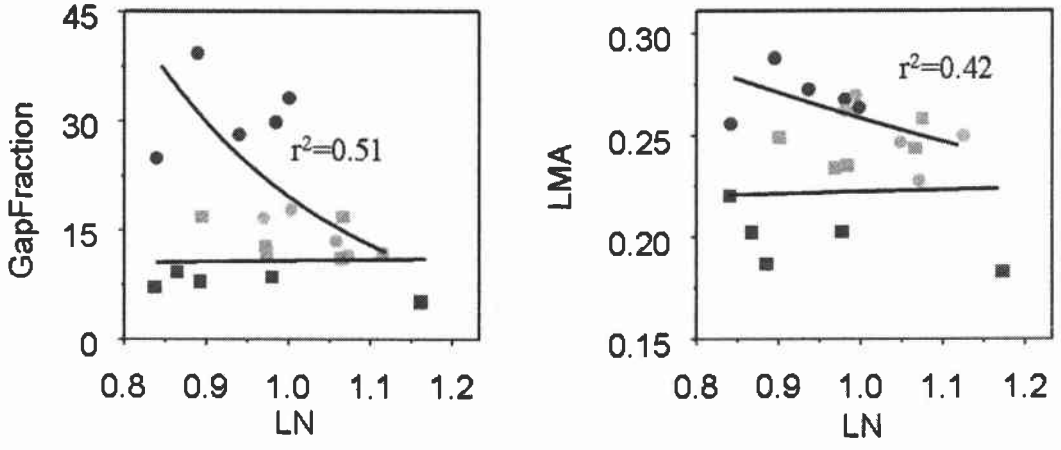

Figure 2.6. a) GapFraction is not related to LN in PSME, but is in PIPO (Eqn: GapFraction = -31.8 [exp(LN)] +108.3) b) Similarly, LMA is not related to LN in PSME but is in PIPO (Eqn: LMA = -0.047[exp(LN)]+0.39).

2. LL is a species-specific tuning mechanism used by leaves in these forest canopies to adjust to changes in soil nutrient availability.

Leaf longevity is frequently viewed as a means by which costs of investment and maintenance in a leaf are balanced with photosynthetic return of the leaf (Kikuzawa 1991, Walters and Reich 1999). Such carbon-gain optimization theory suggests that greater nitrogen availability will lead to faster growth of the canopy, which in turn will lead to faster turnover of leaves to maximize carbon return (Reich et al. 1992). Indeed, our results link higher LN with faster turnover times (Figure 2.5b), consistent with the amortization argument of Kikuzawa (1991).

When PSME and PIPO experience the same climatic and edaphic conditions in MIXED stands, it is LL that diverges the most of the three traits. Thus, although LMA convergence may suggest that the two species are following similar strategies, LL reveals that their overall strategies for managing leaf resources are, in fact, different.

In our model, the link between LN and climate would be indirect, through the long-term effects of climate on soil nitrogen availability. Yin (1993) found that LN in conifers was related to mean January temperature across a continental gradient of many studies. For PIPO in our study, temperature did explain significant variation in LN (Table 2.7), but it is difficult to assess whether this is causal or coincidental. PIPO sites are nearly 400 meters higher than MIXED sites (Table 2.3), and hence are much colder, but they also occupy soils that are younger, and likely less fertile, not because of temperature but because of recent geologic history. To the extent that temperature

at a continental scale is generally related to soil nutrient capacity, our model is consistent with the model of Yin (1993).

These findings have implications for regional modeling of spatial patterns in carbon dynamics. The proposed relationship between stand openness and LMA is encouraging, and supports the suggested use of remote sensing to estimate LMA at regional scales (Pierce and Running 1994, Lymburner et al. 2000). The proposal that LL responds chiefly to LN is also encouraging for regional-scale modeling as it suggests that LL could be derived from LN, once the LL / LN relationship is fully characterized for a species. The problem, then, lies in characterizing the spatial patterns of LN. Reliable soil maps at small grain sizes are difficult to obtain; it may be more feasible to continue efforts to characterize spatial patterns of leaf nitrogen through the use hyperspectral imagery (Martin and Aber 1997, Ollinger et al. 1998).

Conclusions

Our field study of two dominant forest conifers suggests that regional scale patterns in LMA are likely related to factors that control stand-level light environment. Linkage between LMA and LN for these forests may only be indirect through the parallel influence of increased soil fertility on LN and canopy light environment. LL appears to be negatively correlated with LN, and LN itself may be controlled primarily by soil fertility. Taken together, these patterns provide both opportunities and challenges for regional-scale modeling of carbon.

Chapter 3: A method for efficient spatial modeling of biogeochemical models

Introduction

A key challenge to carbon cycle science is characterizing current and future carbon dynamics over large spatial domains. Biogeochemical models offer one means of spatially-explicit carbon modeling, and have been applied for this purpose at regional to continental scales (Aber and Federer 1992, Members 1995, Thornton 1998).

In a standard approach to spatial modeling, the biogeochemical model is run separately at a large number of contiguous grid cells on the landscape. Each cell contains the necessary driving variables (climate, soils, etc.) to run the model. For complex biogeochemical models, computational burden at each cell can be great, even with current computer technology. This reduces the number of model runs feasible over large areas, which diminished the ability to explore fine grain effects, characterize model sensitivity, or investigate alternative climate change scenarios. A more efficient approach to spatial modeling is desirable for some applications.

The core of a more efficient approach lies in an understanding of the controls on model behavior in the spatial realm. Although the derivation of maps of driving variables often must take into account spatial cell-to-cell adjacency effects, biogeochemical models themselves typically do not (Aber and Federer 1992, Running and Hunt 1993, Members 1995, Ollinger et al. 1998, Thornton 1998, Coops and Waring 2001). The model is only affected by the input variables, not by their position, and thus the spatial variation in modeled outputs is constrained only by spatial

variation in input variables. Variation in model outputs over geographic space simply reflects the underlying variability in the multidimensional space of the input variables.

With this understanding, an alternative approach to spatial modeling is possible. Rather than running the model in every cell on the landscape (Figure 3.1, black arrow), we propose that the model be run in the multidimensional space of the model driver variables (Figure 3.1, open arrows). Cells in geographic space are projected into input-variable space, and the model is run only at a sample of points in that space. Because variation in modeled output is solely a function of variation in input-variables, remaining cells can be estimated by interpolation in input-variable space, and then projected back into geographic space to provide a spatially-explicit estimate of model outputs. Below, we describe a detailed implementation of this approach for a common biogeochemical model over an area of mountainous terrain in western Oregon.

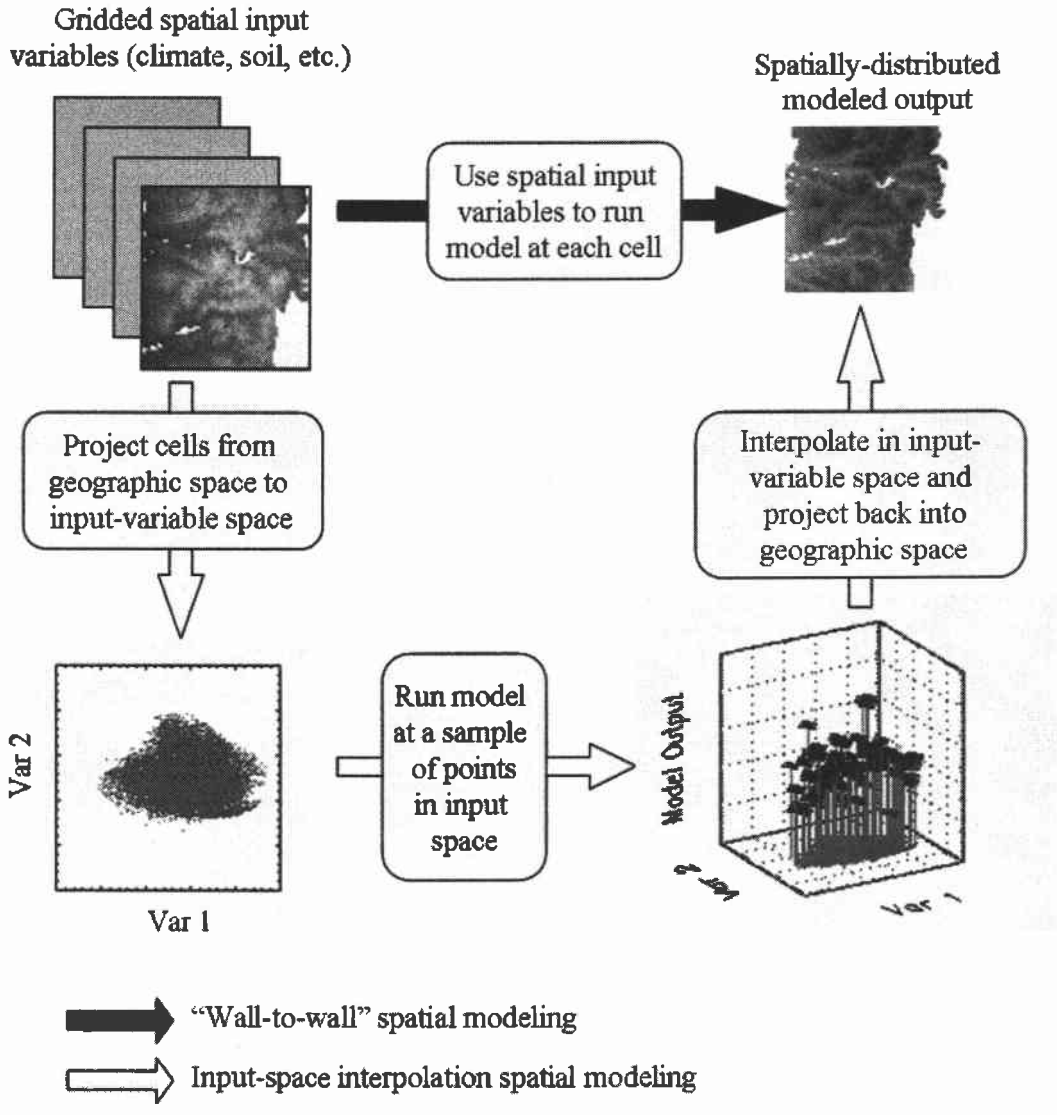

Figure 3.1. Schematic flow of two approaches for spatial modeling with ecosystem models that do not have cell to cell interactions. In "wall-to-wall" modeling (dark arrow), the model is run separately for every cell in the geographic study area. This approach is relatively inefficient, since many cells may have similar driving variables (climate, soils, etc.). The proposed alternative approach moves modeling out of geographic space into the space of the driver variables (the "input space"). Modeling is done only at a sample of grid cells, with the rest of the points being estimated by interpolation in input-space and re-projection into geographic space.

Methods

As a test of the conceptual approach, we compared results from the standard and the alternative approaches to spatial modeling described above and in Figure 3.1. We refer to the standard path as "wall-to-wall" modeling and to the alternative path as "input-space interpolation" modeling.

Wall-to-wall modeling

Ecosystem model

We tested our conceptual approach using the biogeochemical model BGC 4.1.1. (Thornton 1998, Thornton et al. 2002). BGC incorporates many of the general controls on carbon, nitrogen, and water cycling in terrestrial ecosystems. Modeling is conducted for an idealized two-layer canopy of sunlit and shaded leaves. Nitrogen and carbon cycling are linked through photosynthesis in the leaves and decomposition in the soil. Photosynthesis is affected directly or indirectly by incident solar radiation, nitrogen levels in the leaves, air temperature, ambient carbon dioxide concentration, and available moisture for transpiration. Autotrophic respiration is considered primarily a function of temperature and nitrogen levels, while heterotrophic respiration is controlled by temperature, moisture, and character of substrate. Evapotranspiration is calculated by means of the Penman-Monteith equation, which explicitly takes stomatal conductance into account. Low moisture reduces stomatal conductance, which reduces stomatal conductance and limits

transpiration. Soil processes occur in a single vertical layer, with three carbon pools of increasing recalcitrance to decomposition.

Biome-BGC uses an equilibrium-based spin-up approach to develop soil and vegetation pools. The model is run for several thousand years until several carbon and nitrogen pools reach approximate steady state. The model is run for idealized vegetation physiological types, defined by a suite of parameters that describe ecosystem-, canopy-, organism-, and leaf-level attributes for that vegetation type. In this study, the model was run with a parameter set applicable to Douglas-fir (Pseudotsuga menziesii) forests, as detailed in Table 3.1.

Meteorological drivers

BGC requires daily meteorological data on temperature, moisture, and incident radiation. These data were acquired from DAYMET, a model that uses empirical and mechanistic equations to interpolate weather station data from U.S. weather stations (Thornton et al. 1997, Thornton et al. 2000).

DAYMET data are at a grain size of 1km, which defines the grain size for BGC modeling. Each 1km cell has 18 years of daily minimum and maximum temperature, daily total precipitation, and daily incoming radiation estimates. Vapor pressure deficit (VPD) was derived from minimum and daily temperatures (Thornton et al. 2000). Saturation vapor pressure for calculation of VPD was calculated as 610.79 * (exp(17.269 * T / (237.3 + T)), where T is daily minimum temperature in degrees C (Glassy and Running 1994). The 18 year record of daily

meteorological data is cycled through in sequence repeatedly in the same sequence for each model run.

Each 1km^2 model cell is also assigned site constants, which describe the physical properties of the site in terms of elevation and soil type. Soil depth and type were from a dataset described in Kern et al. (1997).

Application to study area

Using meteorological and site constant data described above, the model was run using the Douglas-fir parameter set for a 100km by 260km study area in western Oregon (U.S.A.). Modeling was limited to 1km cells where Douglas-fir was present, as determined by a finer-grained Landsat Thematic Mapper-based landcover map of the area (Law et al. In Press). Study area grid cells are shown in Figure 3.2, along with key meteorological and site constant maps. The model was run in 18395 1 km^2 cells.

Table 3.1. Parameters used in BGC model for Douglas-fir (*Pseudotsuga menziesii*).

Parameter value	Units	Parameter description
0.20	1 / yr	annual leaf and fine root turnover fraction
0.70	1 / yr	annual live wood turnover fraction
0.005	1 / yr	annual whole-plant mortality fraction
0.005	1 / yr	annual fire mortality fraction
1.3	Ratio	new fine root C : new leaf C
2.2	Ratio	new stem C : new leaf C
0.071	Ratio	new live wood C : new total wood C
0.375	Ratio	new croot C : new stem C
0.5	Proportion	current growth proportion
51.0	kg C / kg N	C:N of leaves
93.0	kg C / kg N	C:N of leaf litter after retranslocation
75.0	kg C / kg N	C:N of fine roots
50.0	kg C / kg N	C:N of live wood
729.0	kg C / kg N	C:N of dead wood
0.32	Proportion	leaf litter labile proportion
0.44	Proportion	leaf litter cellulose proportion
0.24	Proportion	leaf litter lignin proportion
0.30	Proportion	fine root labile proportion
0.45	Proportion	fine root cellulose proportion
0.25	Proportion	fine root lignin proportion
0.71	Proportion	dead wood cellulose proportion
0.29	Proportion	dead wood lignin proportion
0.041	1 / LAI / d	canopy water interception coefficient
0.5	Dimensionless	canopy light extinction coefficient
2.6	Ratio	all-sided to projected leaf area ratio
10.0	m^2 / kg C	canopy average specific leaf area (projected area)

Table 3.1. (continued) Parameters used in BGC model for Douglas-fir (*Pseudotsuga menziesii*).

Parameter value	Units	Parameter description
2.0	Ratio	ratio of shaded SLA:sunlit SLA
0.0525	Proportion	fraction of leaf N in Rubisco
.0025	m / s	maximum stomatal conductance (projected area)
.000025	m / s	cuticular conductance (projected area)
0.09	m / s	boundary layer conductance (projected area)
-0.50	MPa	leaf water potential: start of conductance reduction
-2.25	MPa	leaf water potential: complete conductance reduction
600.0	Pa	vapor pressure deficit: start of conductance reduction
2250.0	Pa	vapor pressure deficit: complete conductance reduction

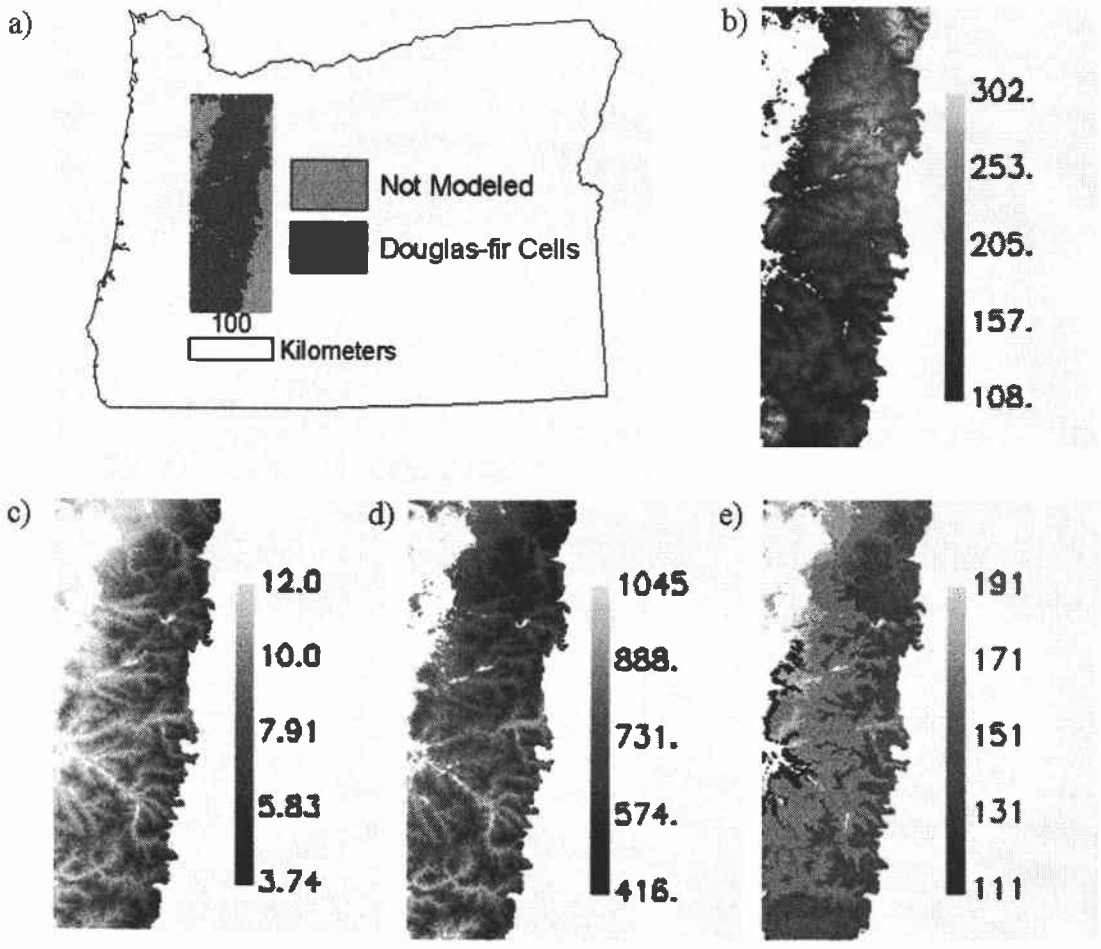

Figure 3.2. The study area, (a) defined as all of the cells within a 100km by 260km area of western Oregon's Cascade Mountains that are likely to support Douglas-fir forests. Shown are (b) average yearly precipitation (cm), (c) temperature (degrees C), and (d) vapor pressure deficit (Pa), as well as (e) estimated soil depth (cm). See Table 3.2 for sources of spatial data.

After spinup equilibrium was reached in each 1 km^2 cell, the forest was "cut" (removal of all live vegetation), leaving 30% of the pre-cut biomass as dead biomass available for decomposition. The model was allowed to regain biomass for 90 years, a second cut was made with the same residual biomass proportion, and finally the model was allowed to run for 200 years. The sequence of spinup and cuts followed the methods of Law et al. (In Press).

The two variables tracked for this study were net primary production (NPP) and net ecosystem production (NEP), both recorded in units of kg C / m^2 yr. NPP is defined as total autotrophic carbon fixation, minus respiration losses due to maintenance and growth within the plant. NEP is the total system balance of carbon, here defined as NPP minus heterotrophic respiration. Both NPP and NEP were tracked for each of the final 200 years of the model runs. The model was run on four 1999 to 2001-era Sun Ultra computers, in a parallel mode made possible using a software structure developed in-house (Dr. Michael Guzy, personal communication) built on the Parallel Virtual Machine (PVM) technology (Version 3.4; Geist et al. 1994). The wall-to-wall run took approximately 12 computer-days.

Because of the cyclic repetition of the DAYMET data, all temporal patterns in output follow a repeated 18-year cycle. Therefore, all resulting NPP and NEP data were aggregated into non-overlapping 18-year bins using simple averaging across all 6570 days in each 18-year cycle. This resulted in 11 temporal slices starting at year 1 and ending at year 198. Each 18-year bin is referred to as an age-class of modeling.

For comparison with the input-space interpolation method described below, the spatial model outputs from the wall-to-wall modeling represent the "truth" set. While the model itself does not capture the truth of the system, the wall-to-wall modeling is a lossless representation of the behavior of the model in every 1km cell across the study area. The goal of the input-space interpolation modeling approach is to efficiently match the behavior of the model over space.

Input-space interpolation modeling

Compression of the spatially-varying inputs

Because the model was run separately for each cell in the wall-to-wall approach, and because there was no stochastic element to the model, any spatial variation in the NEP and NPP truth sets would be caused solely by spatial variation in meteorological and site-constant data (Figure 3.2). The meteorological data have 18 years * 365 days/year, or 6570 data layers per meteorological input variable. Fortunately, the hyperdimensionality of these temporal inputs is not necessarily important for predicting spatial patterns of the model outputs. Rather, it is the *spatial variation of the temporal meteorological data* that causes variation in the modeled outputs over space. Therefore, the spatial variation in the meteorological variables that drive the model may be described with many fewer dimensions.

Compression of spatial input data occurred in several sequential steps, beginning with temporal aggregation. For the meteorological indices listed in Table 3.2, the yearly mean or yearly total (as appropriate for each variable) for each of the

18 years of record was calculated. Thus, for each meteorological index in each cell, 6570 observations of climate data were compressed to 18 observations. The dominant seasonal pattern in the Douglas-fir region is one of spring moisture and summer drought (Waring and Franklin 1979). Therefore, in addition to total precipitation for the year, total precipitation levels for spring and summer were calculated for each of the 18 years. Average values across all 18 years for each of these metrics in the study area are shown in Table 3.2.

Table 3.2. Summaries of spatially-distributed input variables for the study area shown in Figure 3.2.

Variable	Description	Units	Minimum [a]	Maximum [a]	Median [a]	Source
Pr	Average total precipitation (Jan. 1 to Dec. 31)	cm	108.9	302.1	175.5	DAYMET [b]
PrSp	Average spring precipitation (April 1 to June 30)	cm	19.2	60.1	34.8	DAYMET [b]
PrSu	Average summer precipitation (July 1 to Sep. 30)	cm	6.4	22.2	11.6	DAYMET [b]
T	Average daily temperature	° C	3.7	12.1	8.8	DAYMET [b]
Tmn	Average daily minimum temperature	° C	-1.8	6.6	3.0	DAYMET [b]
Sw	Average daily short-wave radiation flux	W/m^2	244.8	330.7	289.0	DAYMET [b]
VPD	Average daily vapor-pressure deficit	Pa	417.0	1045.6	730.1	DAYMET [b] + additional calculation [c]
SDpth	Soil depth	cm	111.0	192.0	163.0	Kern et al. 1997

[a] Minimum, maximum, and median values are for the population of grid cells in the study area; see Figure 3.2.

[b] DAYMET citations: (Thornton and Running 1999, Thornton et al. 2000)

[c] Description of VPD calculation in Methods section of text, under "Wall-to-Wall" modeling

The next step was temporal compression using principal-component analysis (PCA). All meteorological data were approximately normally distributed across the cells in the study area. Before PCA was applied, each 18-year stack of spatial meteorological data was standardized to its global (across all cells and all 18-years) mean and standard deviation. This step preserved inter-year variation within each index, but allowed equal weighting across indices with different units. After principal component analysis, each cell was assigned the PCA scores associated with each of the first several PCA axes. Thus, for each cell, 18 years of aggregated climate data were further reduced to several PCA scores. The result was a stack of several layers (called meteorological "PC" images) representing the spatial variation of each principal component for a given meteorological index. Because the first principal component in a PCA captures the dominant vector through a multi-dimensional space, meteorological PC image #1 represented the dominant spatial pattern of the meteorological index from which it was derived. PC images #2, #3, etc. represented diminishing sources of spatial variation. These meteorological PC images will be referred to as "spatial input variables." In addition to meteorological PC images, normalized soil depth was also calculated and used as a spatial input variable.

In the final step of input-variable compression, spatial input variable images from different meteorological indices were combined and a second PCA calculated on the combined set to derive the final multidimensional input-variable space. This PCA captured dominant patterns of climate across the combination of spatial input

variables. A variety of different combinations was tested. For each spatial input variable used in a given combination, the first PC image (the dominant spatial pattern) was always included. Additionally, a second test was run using both the first and second PC image from each spatial input variable. Soil depth was an exception: as a single layer, no PC images existed, and therefore only the normalized soil depth itself was used. Regardless of the number or type of input PC images in a given test, three output PC images were used, referred to as PC1, PC2, and PC3. Twelve different combinations of spatial input variables were tested, each with one and two layers used in compression, resulting in a total of 24 three-dimensional characterizations of the input space. An effort was made to limit combinations of input variables to those that would be illustrative of controls on the model, not to exhaustively test all possible combinations. Details of spatial input variables and resultant PC images are given in Table 3.3.

Table 3.3. Summary of sets of input variables and principal component analysis weights used to create 24 different three-dimensional PC spaces for input-space interpolation.

Input Variables[a]	# PCs[b]	PC1 Coeff.[c]	Var. PC1[d]	PC2 Coeff.[c]	Var. PC2[d]	PC3 Coeff.[c]	Var. PC3[d]	Sum Var.[e]
Pr+Sw+T	1	0.95, -0.21, -0.87	57	0.16, -0.96, 0.41	37	-0.28, -0.16, -0.27	6	100
Pr+T+Tmn	1	-0.79, 0.98, 0.93	82	-0.61, -0.15, -0.36	18	0.03, 0.10, -0.09	1	100
Pr+T+VPD	1	-0.92, 0.90, 0.97	86	0.36, 0.43, -0.05	11	0.16, -0.11, 0.25	3	100
SDpth+Pr+T	1	0.68, -0.84, 0.90	66	-0.73, -0.42, 0.16	24	-0.11, 0.34, 0.40	10	100
Pr+Sw+T	2	-0.83, 0.81, 0.68, -0.81, 0.44, 0.41	47	-0.42, -0.26, -0.57, -0.28, 0.84, -0.82	34	-0.11, -0.47, 0.00, -0.41, -0.22, 0.12	8	88
Pr+T+Tmn	2	-0.52, -0.09, 0.90, -0.79, 0.94, 0.66	51	-0.74, 0.85, 0.37, 0.57, 0.13, -0.47	33	-0.04, 0.42, -0.16, -0.04, -0.26, 0.56	10	93
Pr+T+VPD	2	-0.87, 0.80, 0.61, 0.28, 0.92, 0.57	50	-0.27, -0.38, 0.75, -0.92, 0.35, -0.80	40	-0.35, -0.44, -0.04, 0.19, -0.02, 0.06	6	96
SDpth+Pr+T	2	-0.64, 0.83, -0.38, -0.92, 0.31	44	0.21, 0.34, -0.83, 0.20, -0.87	33	0.74, 0.20, -0.04, -0.23, 0.25	14	91
PrSu+PrSp+Sw+T	1	-0.96, -0.98, 0.45, 0.69	64	-0.14, 0.07, 0.85, -0.65	29	0.20, 0.15, 0.26, 0.32	6	99
PrSu+PrSp+T+Tmn	1	-0.80, -0.90, 0.92, 0.80	73	-0.59, -0.40, -0.39, -0.60	25	0.12, -0.15, -0.08, 0.03	1	100

Table 3.3. (Continued) Summary of sets of input variables and principal component analysis weights used to create 24 different three-dimensional PC spaces for input-space interpolation.

Input Variables[a]	# PCs[b]	PC1 Coeff.[c]	Var. PC1[d]	PC2 Coeff.[c]	Var. PC2[d]	PC3 Coeff.[c]	Var. PC3[d]	Sum Var.[e]
PrSu+PrSp+T+VPD	1	-0.91, -0.96, 0.81, 0.97	83	-0.39, -0.21, -0.58, -0.09	14	-0.03, 0.19, -0.08, 0.22	2	99
SDpth+PrSu+PrSp+T	1	0.50, -0.88, -0.95, 0.82	65	-0.81, -0.40, -0.27, -0.24	24	-0.29, 0.23, 0.09, 0.52	10	99
PrSu+PrSp+Sw+T	2	-0.91, -0.40, -0.80, 0.77, 0.75, -0.74, 0.31, 0.51	46	-0.31, 0.36, -0.53, -0.51, -0.47, -0.39, 0.86, -0.74	30	-0.17, 0.83, -0.14, 0.06, 0.00, -0.02, -0.30, 0.19	11	87
PrSu+PrSp+T+Tmn	2	-0.16, 0.36, -0.39, -0.58, 0.82, -0.86, 0.90, 0.73	43	-0.94, -0.40, -0.87, 0.69, 0.48, 0.41, 0.24, -0.28	35	-0.26, 0.76, -0.23, 0.17, -0.25, 0.09, -0.31, 0.36	13	91
PrSu+PrSp+T+VPD	2	-0.93, -0.40, -0.82, 0.77, 0.40, 0.48, 0.81, 0.72	48	-0.25, 0.36, -0.48, -0.53, 0.85, -0.81, 0.54, -0.65	35	-0.21, 0.83, -0.18, 0.06, -0.26, 0.18, -0.07, 0.01	11	94
SDpth+PrSu+PrSp+T	2	0.30, -0.97, -0.30, -0.92, 0.62, 0.57, 0.28	39	0.54, -0.01, 0.43, -0.25, -0.72, 0.73, -0.85	33	-0.41, -0.23, 0.79, -0.22, 0.03, -0.16, 0.04	13	86
SDpth+PrSu+PrSp+Sw+T	1	0.44, -0.93, -0.97, 0.35, 0.75	53	-0.64, -0.29, -0.10, 0.83, -0.50	29	-0.63, -0.07, -0.13, -0.36, 0.28	13	95

Table 3.3. (Continued) Summary of sets of input variables and principal component analysis weights used to create 24 different three-dimensional PC spaces for input-space interpolation.

Input Variables[a]	# PCs[b]	PC1 Coeff.[c]	Var. PC1[d]	PC2 Coeff.[c]	Var. PC2[d]	PC3 Coeff.[c]	Var. PC3[d]	Sum Var.[e]
SDpth+PrSu+PrSp+T+Tmn	1	0.55, -0.75, -0.87, 0.93, 0.82	63	-0.51, -0.63, -0.46, -0.25, -0.45	23	-0.67, 0.14, 0.07, 0.27, 0.34	13	99
SDpth+PrSu+PrSp+T+VPD	1	0.45, -0.89, -0.94, 0.83, 0.96	70	0.84, 0.35, 0.22, 0.26, -0.08	19	-0.29, 0.28, 0.15, 0.48, 0.13	9	98
SDpth+Pr+T+Tmn+VPD	1	0.55, -0.83, 0.96, 0.87, 0.90	69	0.74, 0.38, 0.03, 0.19, -0.32	17	0.37, -0.35, -0.27, -0.45, 0.17	11	97
SDpth+PrSu+PrSp+Sw+T	2	0.13, -0.92, -0.39, -0.82, 0.75, 0.72, -0.75, 0.35, 0.48	41	0.58, -0.25, 0.34, -0.48, -0.54, -0.50, -0.34, 0.84, -0.74	30	-0.44, -0.20, 0.78, -0.19, 0.01, -0.02, -0.09, -0.18, 0.05	10	81
SDpth+PrSu+PrSp+T+Tmn	2	0.51, -0.26, 0.29, -0.48, -0.51, 0.87, -0.79, 0.93, 0.66	40	0.19, -0.91, -0.44, -0.81, 0.75, 0.38, 0.52, 0.13, -0.38	32	-0.41, -0.30, 0.67, -0.27, 0.19, -0.18, 0.01, -0.24, 0.43	12	84

Table 3.3. (Continued) Summary of sets of input variables and principal component analysis weights used to create 24 different three-dimensional PC spaces for input-space interpolation.

Input Variables[a]	# PCs[b]	PC1 Coeff.[c]	Var. PC1[d]	PC2 Coeff.[c]	Var. PC2[d]	PC3 Coeff.[c]	Var. PC3[d]	Sum Var.[e]
SDpth+PrSu+PrSp+T+VPD	2	0.21, -0.94, -0.37, -0.85, 0.72, 0.47, 0.41, 0.85, 0.67	43	0.52, -0.16, 0.37, -0.40, -0.60, 0.82, -0.83, 0.47, -0.69	33	0.45, 0.24, -0.76, 0.22, -0.06, 0.17, -0.06, -0.01, 0.05	10	87
SDpth+Pr+T+Tmn+VPD	2	-0.51, 0.58, 0.01, -0.93, 0.72, -0.94, -0.61, -0.69, 0.49	44	-0.14, 0.68, -0.85, -0.27, -0.65, -0.01, 0.51, -0.68, -0.85	35	-0.78, -0.10, 0.21, -0.01, -0.10, -0.07, 0.38, 0.17, 0.00	9	88

[a]Variables defined in Table 3.2

[b]Number of PCA layers used from each meteorological input variable

[c]Eigenvector coefficients used to make compressed PCA image layer. When two layers from meteorological input variables are used, the coefficient for the second layer is listed immediately after the coefficient for the first layer.

[d]Percent of variance captured in this compressed PCA image layer

[e]Total variance captured by the three compressed PCA image layers. Note that when more than three input variables are used, more than three compressed PCA image layers exist, and therefore the total for the three layers used does not equal 100.

Sampling of input variable space

The next step in the method is sampling of the three-dimensional input variable space. A three-dimensional lattice was constructed through the space, with equal spacing between lattice intersections. All cells in the actual landscape were then positioned in that three dimensional space based on their scores in the PC images. The cells closest (using Euclidean distance) to lattice intersections were used as sample points; lattice intersections greater than one cubic hypotenuse length from an actual cell were dropped. At each sampled cell, the model value from the wall-to-wall approach was extracted. In an actual implementation, no such wall-to-wall output would be available, and the model would be run anew in each sample cell.

Interpolation

Cells where the model was not run were estimated by interpolation in input variable space. For each cell to be interpolated, the NEP or NPP value was estimated by weighted averaging of the nearest 8 sampled lattice-intersection cells (in three-dimensional input variable space). Weights were assigned to the 8 nearby points using a linear inverse-distance rule. Once NEP or NPP values were assigned in input-variable space, the cells were mapped back into geographic space to produce a spatial map of estimated model outputs.

Multiple regression

Multiple regression was investigated as a possible alternative to interpolation. Sampling of the input variable space was identical to that used for interpolation. A

multiple linear regression of NEP or NPP values from all sampled points on the three axes of the input space was conducted. The resultant model was then applied to the non-sampled points to produce estimates of NEP or NPP in the input-variable space. As with interpolation, those estimated values were then projected into geographic space to produce a spatial map of modeled outputs.

Variation of sampling density

If the lattice of sample points is sparse, interpolation distance is large and the smoothing properties of interpolation exacerbated. Variation in model output at a scale less than the interpolation distance will be lost. As lattice density increases, the interpolation distance will decrease, and the interpolated surface should conform more and more closely to the actual contours of modeled output.

To investigate this effect, tests were repeated at a range of sample grid densities for NEP outputs only. For each NEP image estimated through interpolation or regression, five target densities ranged from approximately 1% to 15% of the total number of cells in the study area were tested. Actual proportions varied around those targets depending on the character of the 3-d input variable space being tested.

Comparing wall-to-wall with input-space interpolation

Modeled outputs from the input-space interpolation approach were compared on a cell-by-cell basis with all cells in the truth datasets derived using the wall-to-wall approach. Two metrics of comparison were calculated across all cells: a simple correlation and the square root of mean-square error (RMSE). These metrics were

calculated for each of the 11 NEP age-classes, for all lattice-point densities and for all characterizations of the input-variable space.

Developing validation metrics

If the input-space interpolation method is to be useful, its accuracy must be obtainable without the need to run the model in the wall-to-wall approach. An investigation into the use of an independent validation set was conducted.

A small proportion of cells on the landscape were sampled at random, and the model run at these cells. The modeled outputs at these cells were compared to the interpolated estimates for those cells, and the RMSE and correlation metrics calculated. These RMSE and correlation metrics were then compared with the RMSE and correlation metrics calculated for all cells in the study area. Proportions of validation cells at seven levels ranging from 0.5% to 10% were tested.

Results

Figure 3.3 shows a comparison of interpolated and wall-to-wall NEP maps for one age-class at two lattice-point sampling densities. It provides a visual reference for the results presented subsequently.

As expected, the interpolation method works better when more points are sampled for the interpolation. When only 0.4% of the cells are sampled in the input-variable space, the interpolation approach produces a map that captures only the approximate patterns of the wall-to-wall map (Figure 3.3a). The image to image histogram plot shows scatter about the 1:1 line (Figure 3.3b). When the input-space

lattice samples 12% of the cells, the maps match well visually (Figure 3.3c), and the image-to-image histogram plot shows strong attraction to the 1:1 line with relatively little scatter.

The two summary metrics capture these visual patterns. The correlation between the maps provides a quantitative measure of the fit, and is independent from the units of NEP or NPP being estimated. As expected, the poorly-matched map (Figure 3.3a) had a lower correlation than a well-fitted map (Figure 3.3b). The RMSE provides a measure of the potential error in units of NEP or NPP, useful for interpreting the magnitude of the error directly.

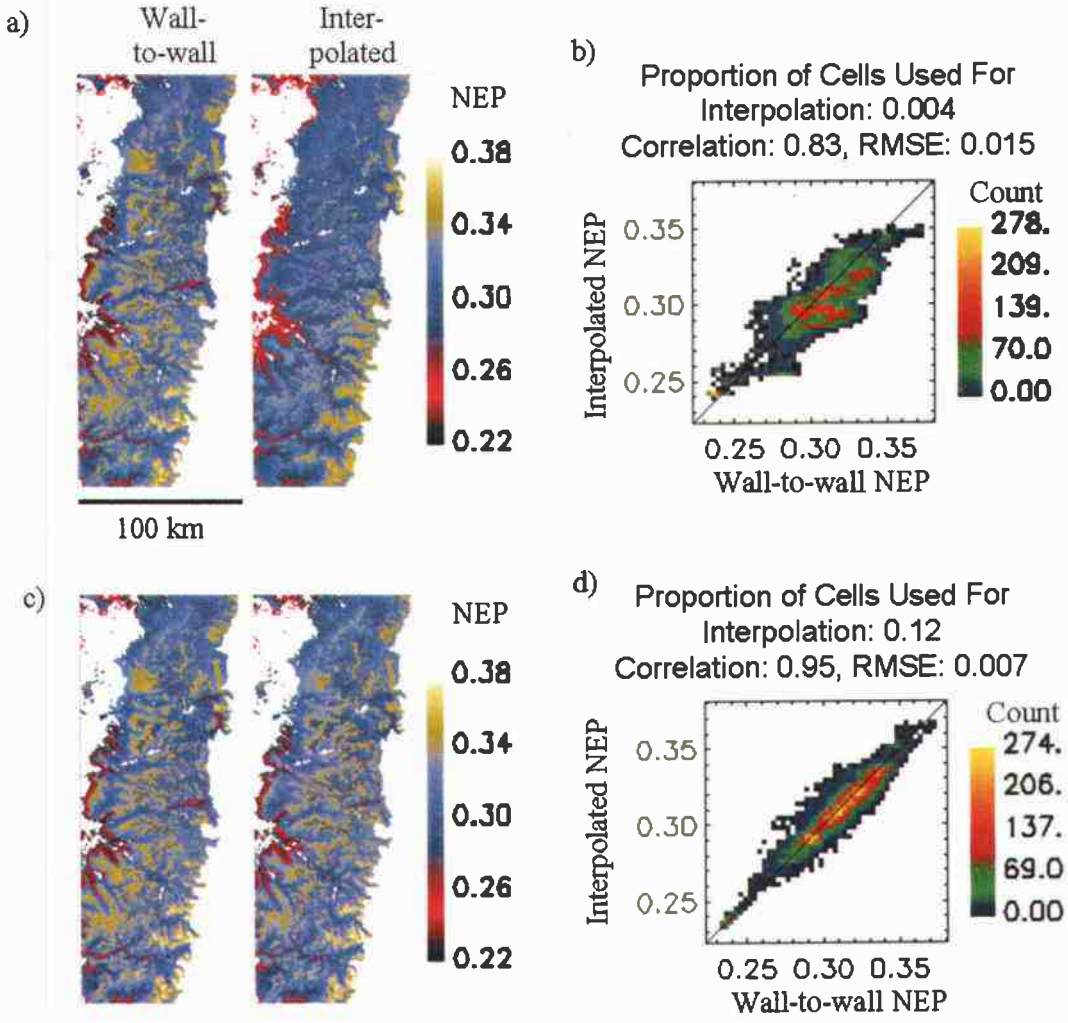

Figure 3.3. Comparing wall-to-wall NEP maps with input-space interpolation NEP maps, at two densities of sampling for interpolation. Each image pair shows the wall-to-wall map on the left and the input-space interpolation map on the right, for the simulation period 73 to 90 years, for sampling proportions of (a) 0.004 and (b) 0.12. NEP units are kg C / m^2yr, with positive values representing uptake by the terrestrial system. Spatial input variables for were soil depth, yearly precipitation, average temperature, average minimum temperature, and average vapor pressure deficit. Plots (c) and (d) show two-dimensional histograms of the interpolated map against the wall-to-wall map, and report the correlation and RMSE of the plots. Higher sampling intensity for interpolation resulted in a better match.

As the sampling lattice density increased, the proportion of cells sampled increased, and the correlation of interpolated maps also increased. Figure 3.4a shows the trajectory of correlation as the proportion of cells increased for the same age-class and input-variable space test as in Figure 3.3. When the NEP map was estimated using a multiple linear regression fit to all sample points, the resultant maps had lower correlations with the wall-to-wall map at all sampling densities. Across all NEP tests conducted for this study, the interpolated maps outperformed their regression-derived counterparts in all but a handful of cases (Figure 3.4b). From here forward, results will be limited to maps built using interpolation.

The correlation of maps reached an asymptotic value as the proportion of cells increased. The level of this asymptote varied depending on the spatial input-variables used to build the input-variable space. Also, the relative ranking of different combinations shifted for different age-classes (examples shown in Figure 3.5). For any given age class, the spatial input-variable combination that provided high correlations tended to reach that asymptote relatively quickly, often before 5% of the cells had been sampled. Spatial input variable combinations that performed poorly approached their asymptotic values more slowly than their better-performing counterparts.

Across age classes, different input variable combinations showed different trajectories of maximum correlation of NEP maps with age-class (Figure 3.6). The 24 input-variable space characterizations could be placed into three broad groups. Group 1 (Figure 3.6a) were those that performed very well for older age-classes, and

moderately well for the younger age-classes. The inclusion of soil-depth as a spatial input-variable was a notable commonality in this group. Group 2 (Figure 3.6b) were those that performed better than Group 1 at young ages, but more poorly at older age classes. Group 3 (Figure 3.6c) performed best at the youngest ages and consistently more poorly as age increased. Absence of soil depth from this group is notable.

Selected details of the runs shown in Figure 3.6 are given in Table 3.4. In addition to correlations, RMSE values for three representative age-classes are reported. The runs are ranked according to the average correlation for young and old age classes.

NPP results were similar to NEP results. For brevity, only one example test from each of the Groups identified in Figure 3.6 is shown in Figure 3.7. The maximum correlations for NPP in Group 1 were slightly lower than for the NEP maps, but were more consistent across age-classes. Groups 2 and 3 were also more stable than for NEP maps, and generally had higher correlations than for NEP.

Looking across all NEP tests, correlations of interpolated and wall-to-wall maps were well-characterized using a sample of validation points. Even at relatively low sampling density (3% of cells), the correlation as estimated by validation points strongly tracked the true correlation (Figure 3.8a). As the proportion of cells used for validation points increased beyond 3%, the match improved slightly (Figure 3.8b). A regression line anchored at zero had a slope near 1 (ideal) for all validation proportions greater than 3%.

Table 3.4. Summary of input-space interpolation results for Douglas-fir NEP for all combinations of input-space indices for selected age classes.

Input Variables [a]	# Pts [b]	Prop. [c]	# PC [d]	Correlation, RMSE [e] for ages: 19 to 36 yr	73 to 90 yr	163 to 180 yr
SDpth+Pr+T+Tmn+VPD	2245	0.12	1	0.87, 0.012	0.95, 0.007	0.98, 0.001
SDpth+PrSu+PrSp+T+VPD	2774	0.15	2	0.89, 0.011	0.86, 0.012	0.85, 0.003
SDpth+PrSu+PrSp+T+VPD	1999	0.11	1	0.85, 0.013	0.95, 0.007	0.98, 0.001
SDpth+PrSu+PrSp+T+Tmn	3240	0.18	2	0.92, 0.010	0.85, 0.013	0.83, 0.003
SDpth+Pr+T+Tmn+VPD	2484	0.14	2	0.84, 0.013	0.93, 0.009	0.96, 0.002
SDpth+PrSu+PrSp+T	2167	0.12	1	0.86, 0.012	0.95, 0.008	0.98, 0.001
PrSu+PrSp+T+Tmn	3156	0.17	2	0.91, 0.010	0.78, 0.015	0.64, 0.004
SDpth+PrSu+PrSp+T	3001	0.16	2	0.89, 0.011	0.84, 0.013	0.85, 0.003
SDpth+PrSu+PrSp+T+Tmn	2494	0.14	1	0.87, 0.012	0.95, 0.008	0.98, 0.001
SDpth+PrSu+PrSp+Sw+T	3464	0.19	2	0.87, 0.012	0.85, 0.013	0.85, 0.003

Table 3.4. (Continued) Summary of input-space interpolation results for Douglas-fir NEP for all combinations of input-space indices for selected age classes.

				Correlation, RMSE [e] for ages:		
Input Variables [a]	# Pts [b]	Prop. [c]	# PC [d]	19 to 36 yr	73 to 90 yr	163 to 180 yr
PrSu+PrSp+T+VPD	2797	0.15	2	0.89, 0.011	0.77, 0.015	0.63, 0.004
SDpth+Pr+T	2297	0.12	1	0.83, 0.014	0.95, 0.008	0.98, 0.001
PrSu+PrSp+Sw+T	3389	0.18	2	0.87, 0.012	0.79, 0.015	0.65, 0.004
SDpth+Pr+T	2121	0.12	2	0.77, 0.015	0.94, 0.008	0.98, 0.001
Pr+T+Tmn	2039	0.11	2	0.88, 0.012	0.77, 0.016	0.60, 0.004
SDpth+PrSu+PrSp+Sw+T	2408	0.13	1	0.72, 0.017	0.93, 0.009	0.97, 0.001
Pr+T+VPD	1695	0.09	1	0.88, 0.012	0.74, 0.016	0.57, 0.005
PrSu+PrSp+T+VPD	1498	0.08	1	0.86, 0.012	0.72, 0.017	0.54, 0.005
PrSu+PrSp+Sw+T	2559	0.14	1	0.86, 0.012	0.71, 0.017	0.56, 0.005

Table 3.4. (Continued) Summary of input-space interpolation results for Douglas-fir NEP for all combinations of input-space indices for selected age classes.

Input Variables [a]	# Pts [b]	Prop. [c]	# PC [d]	Correlation, RMSE [e] for ages: 19 to 36 yr	73 to 90 yr	163 to 180 yr
Pr+Sw+T	2522	0.14	1	0.80, 0.015	0.70, 0.017	0.53, 0.005
Pr+T+VPD	1629	0.09	2	0.71, 0.017	0.72, 0.017	0.54, 0.005
PrSu+PrSp+T+Tmn	1083	0.06	1	0.83, 0.014	0.68, 0.018	0.53, 0.005
Pr+Sw+T	1960	0.11	2	0.69, 0.018	0.70, 0.017	0.55, 0.005
Pr+T+Tmn	762	0.04	1	0.78, 0.016	0.64, 0.019	0.47, 0.005

[a] Combinations of input variables used to define input variable space; see Methods section for details on compression of input variables. Input variables are defined in Table 3.2. Combinations are listed in ranked order, from best to worst, based on combined rank for average correlation score for Ages 1 to 72 and 73 to 198 years. The best runs had high ranks in both young and old age classes.

[b] Number of points in lattice used for interpolation

[c] # Pts / total number of cells in wall-to-wall run

[d] Number of PCA layers used from each meteorological input variable

[e] Correlation and RMSE are for pixel-by-pixel comparison of interpolated maps and wall-to-wall maps

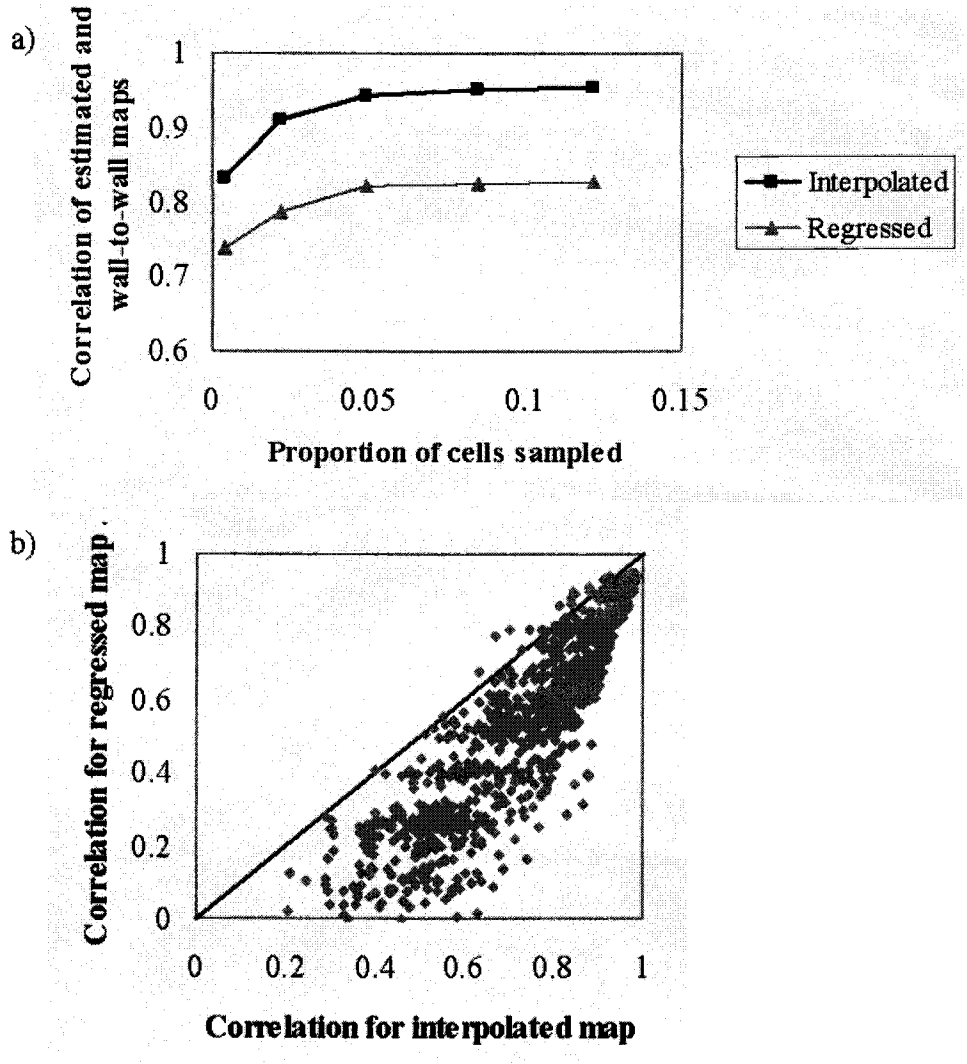

Figure 3.4. Correlation between wall-to-wall and estimated maps. a) Correlation of wall-to-wall NEP map for ages 73 to 90 years with interpolated and regressed maps for the same age. Input variables used to define the input space are the same as in Figure 3.3. As the proportion of cells used for interpolation increases, both estimation procedures improve their match with the wall-to-wall model output, but interpolation attains a better overall match. b) Plots of the correlations for regressed maps against correlations for interpolated maps for 1144 NEP maps spanning a range of input variable combinations and sampling proportions. Maps derived from interpolation of the input space nearly always have a higher correlation than maps derived from regression in the input space.

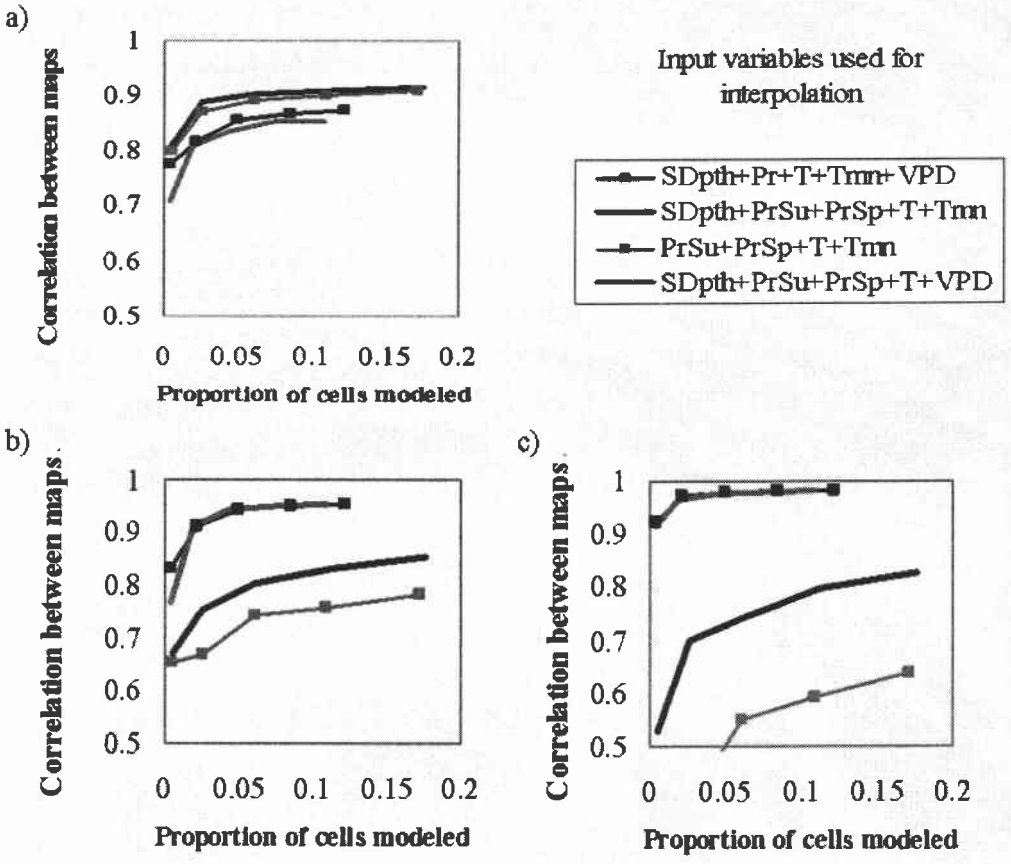

Figure 3.5. Examples of the correlation between wall-to-wall and interpolated maps of NEP for modeled stands at (a) 19 to 36 years, (b) 73 to 90 years, and (c) 163 to 180 years, for four different combinations of input-space drivers for interpolation. Definitions of input-space drivers are given in Table 3.2. In all cases, the correlation of the interpolated map with the wall-to-wall map begin to reach asymptotic values, the value of which depends on the input variables used to build the input-variable space. The relative performance of different input variable combinations varies for different modeled age classes.

Figure 3.6. Correlation between interpolated maps and wall-to-wall maps of NEP for different ages of simulation and different combinations of input variables. All correlations are at the highest sampling density for each combination of input variables; definitions of variables are given in Table 3.2. Numbers in parentheses are the number of PC layers from each meteorological variable used to build the input-variable space. a) Group 1: Input variables that result in better fits at older ages than younger ages. b) Group 2: Input variables that result in better fits at young ages and moderate fits at old ages. c) Group 3: Input variables that fit well at young ages but very poorly at older ages.

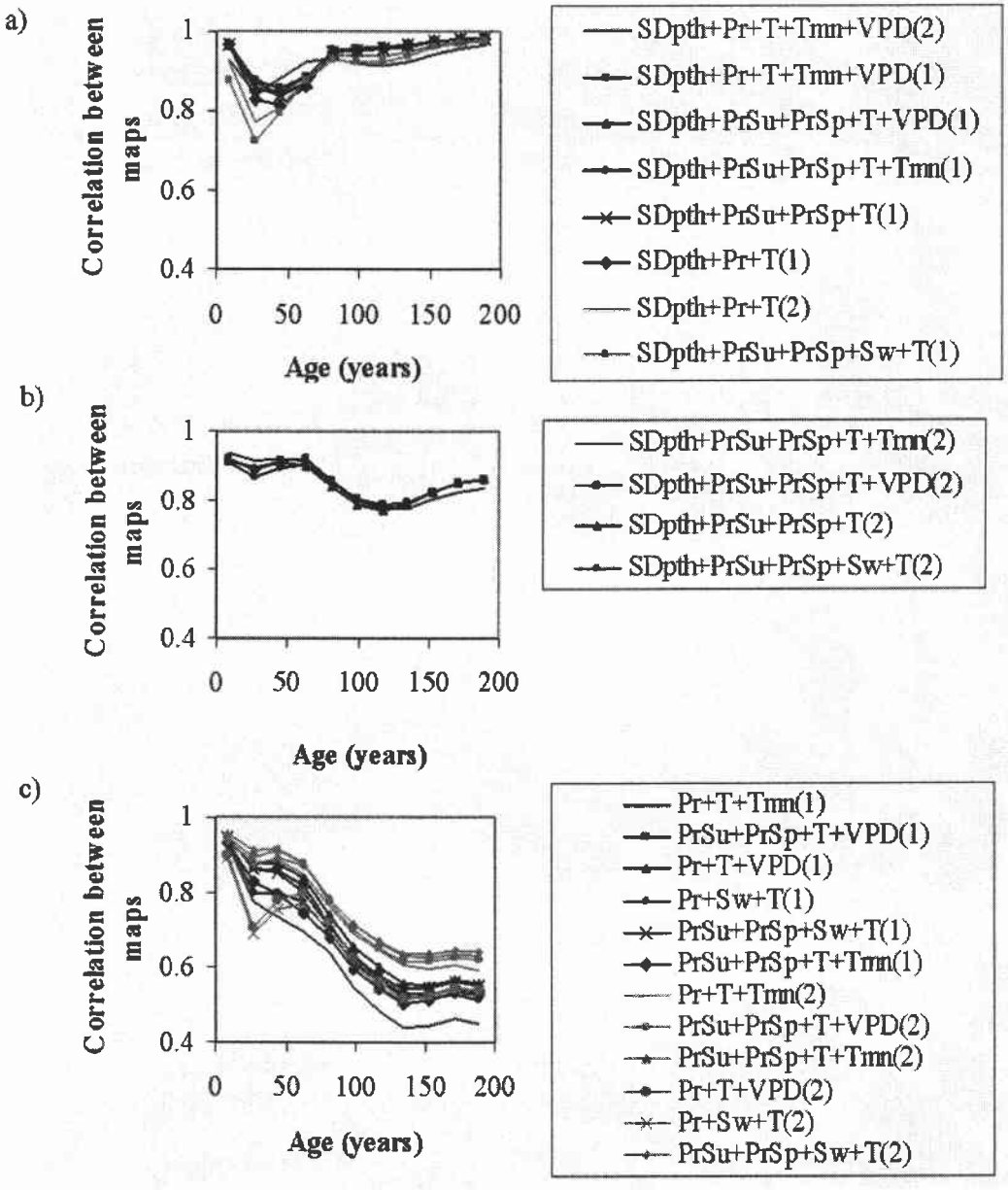
a)
Correlation between maps
1
0.8
0.6
0.4
0
50
100
150
200
Age (years)
SDpth+Pr+T+Tmn+VPD(2)
SDpth+Pr+T+Tmn+VPD(1)
SDpth+PrSu+PrSp+T+VPD(1)
SDpth+PrSu+PrSp+T+Tmn(1)
SDpth+PrSu+PrSp+T(1)
SDpth+Pr+T(1)
SDpth+Pr+T(2)
SDpth+PrSu+PrSp+Sw+T(1)
b)
Correlation between maps
Age (years)
SDpth+PrSu+PrSp+T+Tmn(2)
SDpth+PrSu+PrSp+T+VPD(2)
SDpth+PrSu+PrSp+T(2)
SDpth+PrSu+PrSp+Sw+T(2)
c)
Correlation between maps
Age (years)
Pr+T+Tmn(1)
PrSu+PrSp+T+VPD(1)
Pr+T+VPD(1)
Pr+Sw+T(1)
PrSu+PrSp+Sw+T(1)
PrSu+PrSp+T+Tmn(1)
Pr+T+Tmn(2)
PrSu+PrSp+T+VPD(2)
PrSu+PrSp+T+Tmn(2)
Pr+T+VPD(2)
Pr+Sw+T(2)
PrSu+PrSp+Sw+T(2)

Figure 3.6

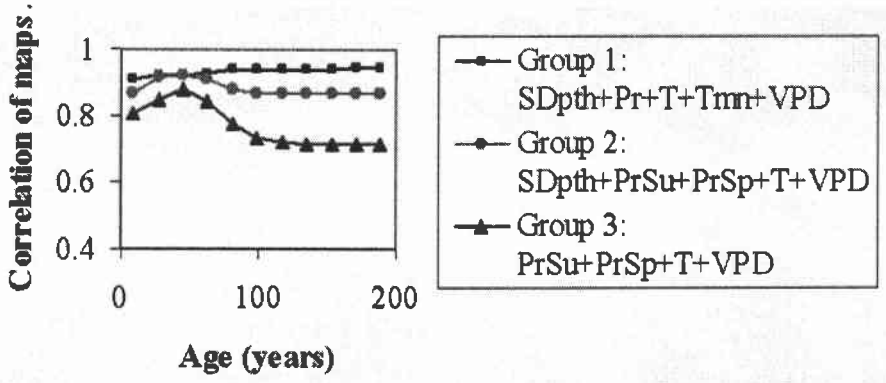

Figure 3.7. As in Figure 3.6, but for NPP rather than NEP maps, and for only one representative combination of input variables from each of the three groups shown in Figure 3.6. Axes are scaled to match Figure 3.6. For NPP, Group 1 performs well across all age classes. Groups 2 and 3 follow similar trajectories with age as they do for NEP, but with generally better correlations at older ages.

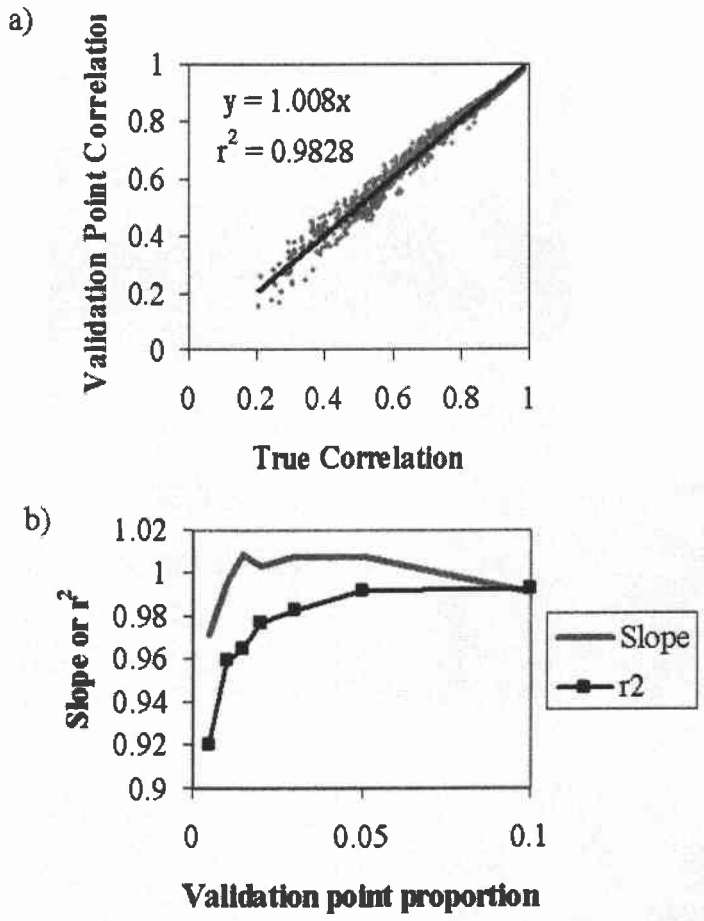

Figure 3.8. Examining whether validation points can be used to estimate the true correlation of interpolated images. True correlation estimates were calculated for all cells in 1144 separate interpolated vs. wall-to-wall NEP maps (including all NEP results presented previously). For each map, random subsets of validation points at varying proportions of the total population were sampled and correlation estimates calculated for the subsets. a) Plot of validation point vs. true correlation for validation point proportion of 0.03, together with equation and fit for simple linear regression. Each point represents one map comparison. b) Slope and r^2 of linear regressions of the type shown in a), for a range of validation point proportions. Reasonable estimates of correlation are achieved with only 3 to 5% of plots used as validation points.

Discussion

When a model lacks cell-to-cell interactions, its behavior across geographic space depends entirely on the spatial patterns of the variables that drive it. Insofar as the driver variables exhibit redundancies across space, wall-to-wall modeling of each cell is inefficient. Here, we described and tested an approach to sample the spatial variation of the input variables, and to infer model results for non-sampled points by interpolation in the space of the input-variables.

Other studies have capitalized on the spatial control of model behavior by input variables. Typically, the input variables are stratified into homogeneous units in geographic space. Using FOREST-BGC, a precursor to the version of BGC tested here, Band et al. (1991) found that such stratification was an efficient means of more efficiently modeling large areas. Franklin (2001), also using an earlier version of BGC, developed a lookup-table approach to modeling, where model runs were conducted only for a sample of levels of landcover type and leaf area index, key drivers in the earlier model. Burke et al. (1991) describe an approach to spatial modeling that identifies key drivers of the CENTURY model (Parton et al. 1987), and then develops a multi-dimensional classification of those drivers. The model is then run only for each unique combination of driver classes. In all of these cases, the input variable space is essentially treated as a categorical rather than a continuous variable.

Treatment of the input-space as a continuous variable has been applied to spatial prediction of forest stand characteristics. Ohmann and Gregory (2002) developed a multivariate statistical approach to characterizing spatial variation in

climate, soils, remote sensing data, and applied it to an extensive field survey of forest stand inventories. Grid cells on the landscape that were not surveyed were assigned inventory attributes of the inventory site closest in input-variable space. In that case, the input variables were considered continuous variables, but the model output was essentially discrete: the nearest inventory plot was assigned in its entirety, with no quantitative modification of attribute values based on characteristics of other nearby plots. In the case of input-space interpolation, the value assigned to a cell is affected by all of its nearest neighbors in input-variable space.

In essence, the input-space interpolation approach develops a site- and input-variable-specific spatial metamodel of the underlying biogeochemical model. A similar approach was tested for a model of NPP (Alexandrov et al. 2002) and for a forest gap model (Acevedo et al. 2001). The metamodel provides a layer of abstraction that captures only the salient variation in a more complex or detailed model (Friedman 1996). Here, the two key abstractions (or simplifications) of the underlying BGC model behavior are 1) compression of the input variable space and 2) interpolation through input variable space. Interpolation appears to be an important part of the methodology, as indicated by its superior performance relative to a multiple regression approach (Figure 3.4b). The multiple regression approach used here was a global model fit to the dataset, and as such cannot capture local variations as well as the interpolation approach. An alternative method would be to use a localized multiple regression, although the simplicity of the interpolation approach is attractive.

As a simplified metamodel of BGC, the input-space interpolation method appears to work well. By sampling only 10 to 15% of the cells in our study area, the approach captured the bulk of the patterns of NEP and NPP produced by the model (Figures 3.3 and 3.4, Table 3.4). More importantly, the error of prediction of model output is generally quite small. Figure 3.9 shows mean RMSE by age-class of NEP predictions for all of the runs in Groups 1 and 2 (of Figure 3.6). Except for the youngest age class, mean error was only 3%. Considering the many uncertainties in model structure and in representation of spatial input variables over space, such low levels of error mean that the method has utility for applications requiring assessment of carbon flux over large areas. The overall success of the approach is notable, especially given that the model used more than 6000 layers of meteorological information, while the interpolated approach compressed those data into three layers.

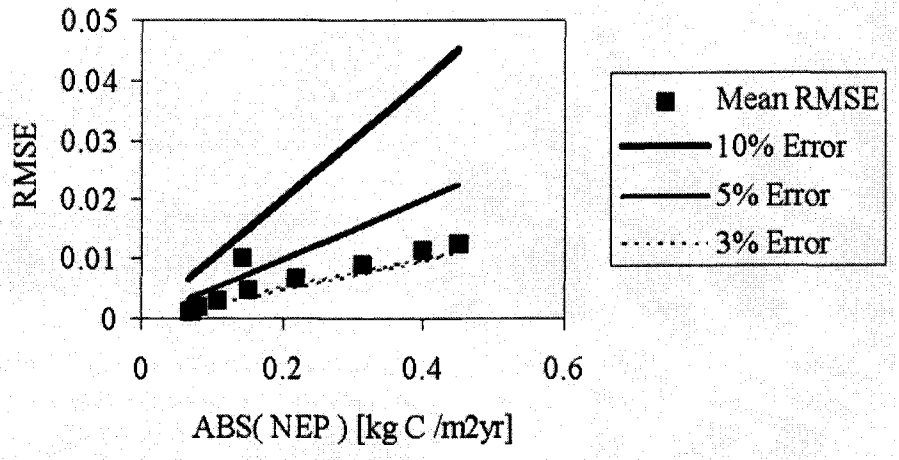

Figure 3.9. Mean RMSE of interpolated NEP as a function of absolute value of true NEP, for all runs in Groups 1 and 2 of Figure 3.6 averaged by age class, with lines indicating gradations of percent error. For most runs, error of interpolation was between 3% and 5% of the true value. The single exception was for age class 1 to 18 years, where RMSE of NEP was more than 5% of the true NEP.

It is this compression of the input-variable space that appears to the set the upper bounds on the accuracy of the interpolated maps. Asymptotic levels of correlation were reached at fairly low sampling intensities (Figures 3.4 and 3.5), suggesting that further increases in sampling density would do little to improve correlation. Rather, correlation was only improved when the correct set of spatial input variables was used to describe the input variable space (Figures 3.6 and 3.7).

Interpreting relative importance of different spatial input variables sheds light on model behavior. When BGC was used to model Douglas-fir dynamics in our study area, soil depth appeared to be a consistently important control on modeled carbon dynamics (both NEP and NPP), especially at older age-classes. All of the input variables in Groups 1 and 2 (the better-fitting Groups) included soil depth as an input variable, and the only difference between some Group 1 and Group 2 combinations was the relative weight given to soil depth in the data compression steps (see coefficients of PC layers in Table 3.3). As modeled by BGC, soil depth controls both the total water content that can be stored in the system and the levels of available nutrients in the soil. Apparently, these controls have high leverage in model behavior, especially over long periods. As a site constant, soil depth was not considered in extensive sensitivity analysis of BGC (White et al. 2000), which makes judging its relative importance difficult. However, it is clear that a better understanding of the effects of soil depth on the behavior of the BGC model will be useful when the model is applied over regional or continental scales.

Although it may aid in understanding model behavior, the input-space interpolation approach is primarily designed to improve computational efficiency. A reasonable approximation of spatial behavior of the BGC model can be achieved using only a fraction of the points on the landscape. Indeed, although the highest-density runs were highlighted in Figures 3.6 and 3.7, the asymptotic behavior seen in Figures 3.4 and 3.5 is typical of the approach, and suggests that only 5 to 10% of cells can be used to capture the bulk of the spatial behavior of the model. The time needed for the interpolation approach itself is minimal: on a 2003-era PC computer, using the software package IDL (Research Systems Inc., Boulder CO), the input-space interpolation approach took anywhere from 5 to 50 minutes, depending on the number of points sampled, while the wall-to-wall run took nearly 12 computer days (using slightly older technology). The order-of-magnitude savings in modeling effort can translate into greater exploration of model behavior and testing, easier development of spatial sensitivity analyses, broader testing of climate change scenarios, or modeling at finer grain sizes. The structure described here could be applied to other common biogeochemical models, including CENTURY (Parton et al. 1987), PnET (Aber and Federer 1992), and others (VEMAP Members 1995). Indeed, any ecological model that does not consider cell-to-cell interactions could use this approach to apply results over space.

The chief drawback of this approach is its sensitivity to the choice of spatial input-variables. Had only input-variable combinations from Group 3 been tested, the results would have been poor. Thus, a certain degree of testing of different variables is

necessary, using an independent set of validation points for establishing error rates. Too much testing counters the computational efficiency of modeling. An understanding of the mechanistic controls within the model should lead to judicious choice of input variables for interpolation.

It is also important to note that the method is designed to function only within categorical modeling units. Many biogeochemical models apply parameter sets according to a categorical land cover type designation within a cell. In these cases, each land cover type would require a separate input-space interpolation process. While this would not appreciably add to the total number of cells sampled on the landscape, it would require additional effort to develop appropriate input-variable combinations.

Conclusions

We have described an approach to spatial modeling that has the potential to improve computational efficiency of modeling by nearly an order of magnitude, while retaining most of the spatial variation in model output. The approach is built on the recognition that variation in many biogeochemical models is solely a function of spatial variation in input drivers, and that modeling in input-variable space is more efficient than in geographic space. By reducing computational burden in spatial modeling, the approach can allow more time for greater exploration of model behavior under different scenarios or conditions.

Chapter 4: Spatially-explicit estimates of uncertainty indicate the potential for significant error in modeled carbon cycle metrics

Introduction

To quantify the net flux of carbon between the terrestrial system and the atmosphere, component fluxes across large spatial regions must be characterized. Because measurement of those component fluxes is costly, direct observations are generally scarce, both regionally and globally. For areas where direct measurements are not available, a suite of indirect methods must be used to estimate carbon cycle dynamics. Process-based models are one powerful indirect method for such estimation of carbon fluxes, and provide a means of predicting carbon dynamics under past, current, and future climates.

A large group of process-based biogeochemical models has been used to model carbon dynamics at regional scales (on the order of 10^6 to 10^9 ha; Parton et al. 1987, Aber and Federer 1992, Cohen et al. 1996, Foley et al. 1996, Friend et al. 1997, Thornton 1998, Coops and Waring 2001). These models vary in temporal and spatial grain and extent, but typically are driven by climate data and are parameter-rich. Because parameter values control the behavior of a model, accurate estimates of parameters are critical for model success. However, there can be significant uncertainty in model parameter values. Some parameters are difficult to measure accurately, even at well characterized sites. Others are relatively easy to measure at research-intensive sites, but have simply not been measured across the geographical extents needed to parameterize a model over a large area.

In either case, the value of a given parameter at a given point in space may be uncertain. When propagated through the model, such uncertainty in parameters results in uncertainty in modeled estimates of carbon dynamics. Although many models of carbon dynamics have been published, few studies have attempted to quantify the potential error in those estimates caused by uncertainty in model parameters (for examples, see White et al. 2000 and Williams et al. 2001). Because net carbon exchange is the small difference between large fluxes of uptake and release, inclusion of error bounds may have important implications for modeled carbon values.

Characterizing the sensitivity of a model to parameter uncertainty has long been recognized as a critical component of model building and evaluation (Haefner 1996). Analyses typically aim to determine the parameters to which the model is particularly sensitive. Parameters are perturbed from an idealized (or base) value by some percentage of the mean or of an estimate of variance (Haefner 1996, White et al. 2000), and a sensitivity metric is calculated that relates magnitude of change in output to magnitude of perturbation in parameters. Parameters whose sensitivity metric is high are said to have high leverage in the model.

When modeling carbon dynamics in a particular study area, the actual impact of uncertainty in a given parameter is not just a function of its leverage in the model. Rather, it also depends on the range of variation that is likely to be encountered in the domain of modeling. A parameter with high leverage may be stable within a given study area, while a lower-leverage parameter may vary considerably. In terms of

actual impact on model outputs for that study area, the lower-leverage parameter may be more important.

Spatial variation in the climate data that drive the biogeochemical model may complicate the uncertainty analysis. Because parameter values control the model's response to the climate driver variables, modeled outputs reflect a sometimes complex set of interactions between parameters and climate. Variation in parameter values therefore interacts with variation in climate, suggesting that parameter uncertainty may have greater impact in some climatic regimes than in others. To the extent that climatic drivers vary over a landscape, the uncertainty caused by variation in parameters may also vary. The total uncertainty in carbon fluxes across the landscape will the thus be the areal integration of spatially-variable uncertainties. Thus, any summary of landscape-wide modeled carbon fluxes will necessarily require spatially-explicit estimates of uncertainties.

Here, we report on a study designed to investigate the potential impact on modeled carbon dynamics of uncertainty in model parameters, and to determine whether spatial patterns in uncertainty are relevant to overall regional estimates of carbon dynamics. We use the biogeochemical model BGC 4.1.1 (Thornton 1998, Thornton et al. 2002), and build on a sensitivity analysis for BGC reported by (White et al. 2000). In that study, a thorough literature search was used to build parameter sets for testing across all major biomes of the globe.

The sensitivity analysis conducted by White et al. (2000) was an important first step, but was limited in two key respects. First, the sensitivity analysis was conducted

only for modeled net primary productivity. Because the model tracks a suite of controls on carbon, this focus on autotrophic inputs of carbon may provide an incomplete view of the model's behavior. By tracking other key model outputs, a greater understanding of the potential impacts of parameter uncertainty may be possible. A second limitation of the sensitivity analysis conducted by White et al. (2000) resulted from its ambitious scope: Because it tracked model sensitivity for the entire globe, the study only examined model sensitivity for ten points in each biome. Regional-scale spatial variation in uncertainty would necessarily be overlooked.

We hypothesized that these two limitations may be important factors in regional scale carbon modeling. Therefore, we designed a set of modeling studies designed to determine if: 1) tracking uncertainties in multiple model outputs allowed better interpretation of model behavior, and 2) model uncertainties varied spatially over a regional landscape. For simplicity of application, we confined our analyses to six parameters associated with the model's handling of leaf physiology and allocation, several of which were found by White et al. (2000) to have relatively large influence on modeled NPP.

Methods

Study area

The study area was an approximately 21,000 km^2 region of the western Cascade Mountains of Oregon, U.S.A., where Douglas-fir (*Pseudotsuga menziesii*) dominates or codominates (Figure 4.1a). Spatial delineation of the study area was

based on Level IV ecoregion maps (Thorson et al. 2003). Ecoregions included the western Cascades lowlands, valleys, and montane highlands, as well as the Umpqua Cascades, southern Cascades, southern Cascade slope, and two small sections of the Siskiyou foothills and Klamath River ridges ecoregions.

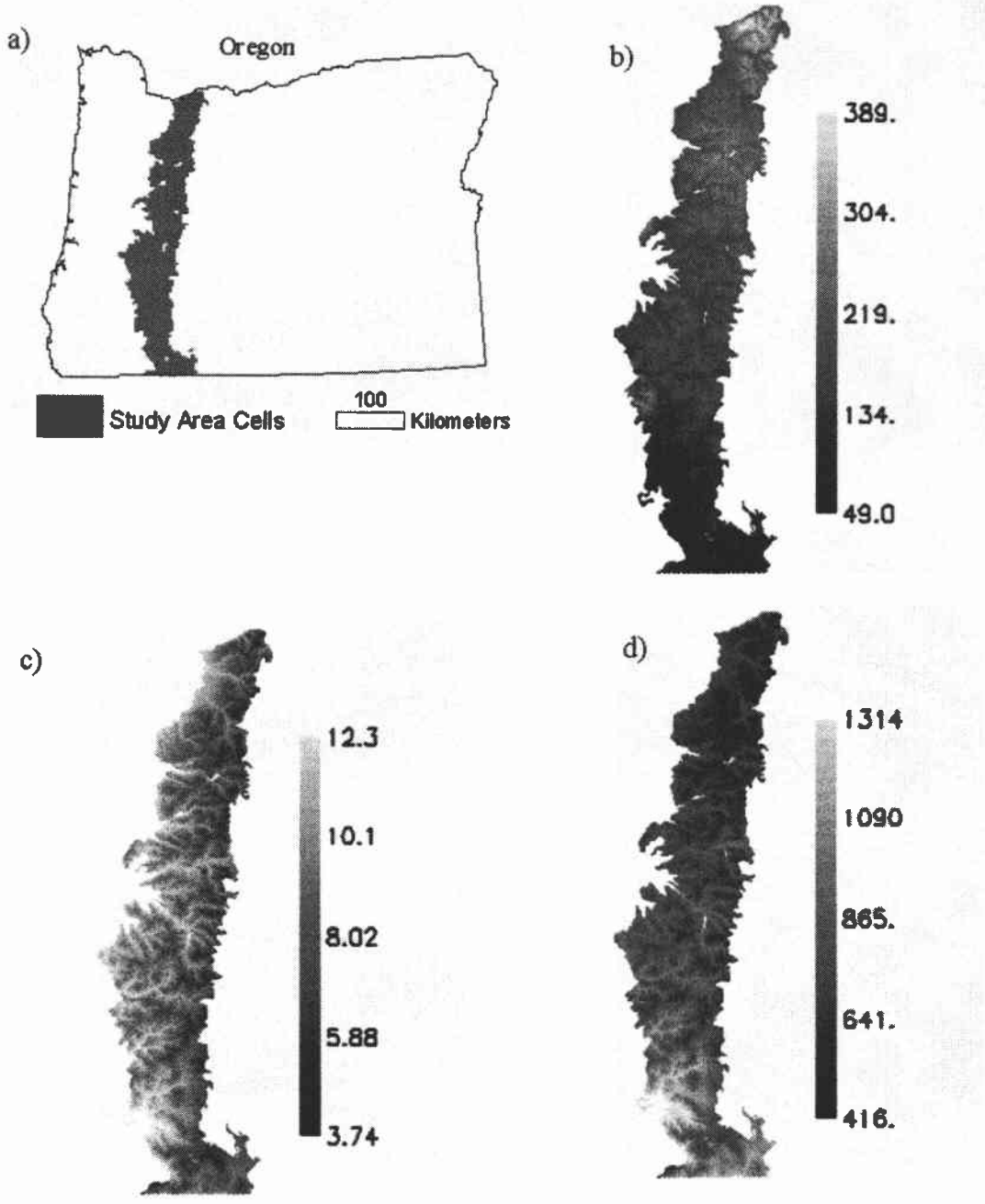

Figure 4.1. a) The study area in Oregon, defined as those Level IV ecoregions near the Cascade Mountains where Douglas-fir dominates or exists as co-dominant in mixed forests. Climate data shown for the study area are (b) average yearly precipitation (cm), (c) temperature (degrees C), and (d) vapor pressure deficit (Pa). See Table 4.1 for sources of climate data.

Climate, especially precipitation, is quite variable across the region (Figure 4.1b-d). Table 4.1 lists climate summaries for the area as estimated by DAYMET, a climate generator that extrapolates daily climate information from observations at distributed weather stations (Thornton et al. 1997, Thornton and Running 1999, Thornton et al. 2000). DAYMET data are at a grain size of 1km, with each cell having 18 years of daily temperature, moisture, and incoming radiation estimates. Vapor pressure deficit (VPD) was derived from minimum and daily temperatures (Thornton et al. 2000). Saturation vapor pressure for calculation of VPD was calculated as 610.79 * (exp(17.269 * T / (237.3 + T)), where T is daily minimum temperature in degrees C (Glassy and Running 1994).

Table 4.1. Summary of climate data the study area shown in Figure 4.1.

Variable	*Description*	*Units*	*Minimum* [a]	*Maximum* [a]	*Median* [a]	*Source*
Pr	Average total precipitation (Jan. 1 to Dec. 31)	cm	55.2	362.6	170.0	DAYMET [b]
PrSp	Average spring precipitation (April 1 to June 30)	cm	10.5	67.3	33.6	DAYMET [b]
PrSu	Average summer precipitation (July 1 to Sep. 30)	cm	4.1	26.7	11.1	DAYMET [b]
T	Average daily temperature (Jan. 1 to Dec. 31)	° C	4.9	11.8	8.5	DAYMET [b]
TmnSp	Average daily minimum temperature (April 1 to June 30)	° C	-0.3	7.1	3.5	DAYMET [b]
Sw	Average daily short-wave radiation flux (Jan. 1 to Dec. 31)	W/m^2	246.6	352.1	295.7	DAYMET [b]
VSu	Average daily vapor-pressure deficit (July 1 to Sep. 30)	Pa	832.7	2456.8	1386.0	DAYMET [b] + additional calculation [c]

[a] Minimum, maximum, and median values are for the population of grid cells in the study area; see Figure 4.1.

[b] DAYMET citations: Thornton et al. 1997, 1999

[c] Description of VPD calculation in Methods section of text

Biogeochemical Modeling

The biogeochemical model BGC 4.1.1 (Thornton 1998, Thornton et al. 2002). incorporates many of the general controls on carbon, nitrogen, and water cycling in terrestrial ecosystems. Modeling is conducted for an idealized two-layer canopy of sunlit and shaded leaves. Nitrogen and carbon cycling are linked through photosynthesis in the leaves and decomposition in the soil. Photosynthesis is affected directly or indirectly by incident solar radiation, nitrogen levels in the leaves, air temperature, ambient carbon dioxide concentration, and available moisture for transpiration. Autotrophic respiration is considered primarily a function of temperature and nitrogen levels, while heterotrophic respiration is controlled by temperature, moisture, and character of substrate. Evapotranspiration is calculated by means of the Penman-Monteith equation, which takes stomatal conductance explicitly into account. Low moisture reduces stomatal conductance, which reduces stomatal conductance and limits transpiration. Soil processes occur in a single vertical layer, with three carbon pools of increasing recalcitrance to decomposition.

Biome-BGC uses an equilibrium-based spin-up approach to develop soil and vegetation pools. DAYMET daily meteorological data (Thornton et al. 1997) are used to drive the model. The model is run for several thousand years until several carbon and nitrogen pools reach approximate steady state.

For the study reported here, the forest was "cut" (removal of all live vegetation) after spinup-equilibrium was reached, leaving 30% of the pre-cut biomass as dead biomass available for decomposition. The model was allowed to regain

biomass for 90 years, a second cut was made with the same residual biomass proportion, and finally the model was allowed to run for 400 years. All runs were conducted at a soil depth of 130cm, a value representative of the region (Kern et al. 1997).

To facilitate sensitivity analysis, we developed a parallel-computer modeling structure (Law et al. in press) based on the Parallel Virtual Machine (PVM) technology (Version 3.4; Geist et al. 1994). Between 12 and 18 Pentium III computers were used for the different model runs reported here.

A parameter set for Douglas-fir (*Pseudotsuga menziesii*) was used for all modeling, and is detailed in Table 4.2. Values generally followed those used by (Thornton et al. 2002) for Douglas-fir in the region. Leaf parameters examined for the uncertainty analysis are shown separately in Table 4.3. For three parameters, the range of values tested had been measured directly at 10 forested stands in the study area (Kennedy et al., Chapter 2). For the two allocation parameters (Root:Leaf and Stem:Leaf; See Abbreviations in Table 4.3), the range of values was assigned as plus or minus 30% of the median value reported for Douglas-fir in White et al. (2000). White et al. (2000) reported relatively few measurements for FracNRubisco, and here a conservative range near the low end of reported values was chosen.

Table 4.2. Parameter values used in this study to represent Douglas-fir (*Pseudotsuga menziesii*) in the biogeochemical model BGC.

Value [a]	*Units*	*Parameter description*
Variable	1 / yr	annual leaf and fine root turnover fraction
0.7	1 / yr	annual live wood turnover fraction
0.005	1 / yr	annual whole-plant mortality fraction
0.0025	1 / yr	annual fire mortality fraction
Variable	Ratio	new fine root C : new leaf C
Variable	Ratio	new stem C : new leaf C
0.07	Ratio	new live wood C : new total wood C
0.3	Ratio	new croot C : new stem C
0.5	Proportion	current growth proportion
Variable	kg C / kg N	C:N of leaves
92	kg C / kg N	C:N of leaf litter after retranslocation
79	kg C / kg N	C:N of fine roots
50	kg C / kg N	C:N of live wood
600	kg C / kg N	C:N of dead wood
0.4	Proportion	leaf litter / fine root labile proportion
0.4	Proportion	leaf litter / fine root cellulose proportion
0.2	Proportion	leaf litter / fine root lignin proportion
0.76	Proportion	dead wood cellulose proportion
0.24	Proportion	dead wood lignin proportion
0.01	1 / LAI / d	canopy water interception coefficient
0.5	Dimensionless	canopy light extinction coefficient
2.3	Ratio	all-sided to projected leaf area ratio

Table 4.2. (Continued) Parameter values used in this study to represent Douglas-fir (*Pseudotsuga menziesii*) in the biogeochemical model BGC.

Value [a]	*Units*	*Parameter description*
Variable	m^2 / kg C	canopy average specific leaf area (projected area)
2	Ratio	ratio of shaded SLA:sunlit SLA
Variable	Proportion	fraction of leaf N in Rubisco
0.003	m / s	maximum stomatal conductance (projected area)
0.00003	m / s	cuticular conductance (projected area)
0.1	m / s	boundary layer conductance (projected area)
-0.6	MPa	leaf water potential: start of conductance reduction
-2.25	MPa	leaf water potential: complete conductance reduction
610	Pa	vapor pressure deficit: start of conductance reduction
3100	Pa	vapor pressure deficit: complete conductance reduction

[a] Parameter values listed as "Variable" were used in uncertainty tests and are detailed further in Table 4.3

Table 4.3. Leaf parameters used for uncertainty tests.

Parameter Description [1]	*Abbreviation*	*Range*[2]	*Source*
annual leaf and fine root turnover fraction	LfTrnovr	0.136 to 0.20	This Study, Chapter 2
new fine root C : new leaf C	Root:Leaf	0.98 to 1.83	White et al. (2000)[3]
new stem C : new leaf C	Stem:Leaf	1.2 to 2.2	White et al. (2000)[3]
C:N of leaves	C:N	45 to 62	This Study, Chapter 2
canopy average specific leaf area (projected area)	SLA	7.5 to 9.5	This Study, Chapter 2
fraction of leaf N in Rubisco	FracNRubisco	0.04 to 0.10	White et al. (2000)[4]

[1] For units, see Table 4.2

[2] Inclusive range of values tested in this study

[3] +/- 30% of median of reported values for *Pseudotsuga menziesii*

[4] With few values reported, the range chosen here spans measurements from non-herbaceous vegetation

Carbon metrics

Variation in leaf parameters could affect any of the hundreds of pools and fluxes tracked by BGC. Here, six carbon-related model outputs or derived variables were examined for uncertainty analysis. Descriptions of and abbreviations for the variables are given in Table 4.4. OLD_LAI, ACC_NEE, and POS_NEE_YR were chosen to provide linkage with studies in the region that reported these values (Gholz et al. 1976, Smithwick et al. 2002, Campbell et al. *In review*). Note that POS_NEE_YR does not take into account the fate of carbon harvested from the stand; because significant carbon is lost to the atmosphere after removal from a site, total carbon accounting would increase the POS_NEE_YR variable, often substantially (Harmon et al. 1996, Harmon 2001). OLD_NPP and OLD_HETR_RESP were included to track net uptake and release by the system near carbon equilibrium, and OLD_DAILY_TRANS was included as a water variable that should be tightly linked to carbon uptake. As a group, these six variables will be referred to as "carbon metrics."

Table 4.4. Definitions of six carbon metrics derived from model runs of BGC for the study area shown in Figure 4.1.

Metric name	*Units*	*Description*
OLD_LAI	m^2 projected leaf area / m^2 ground	Average leaf area index for 18-year period starting at age 370 years
ACC_NEE	kg C / m2	Accumulated net ecosystem exchange (NEE) at the end of 400 years after simulated harvest
NEE_ZERO_YR	yr	The year at which accumulated NEE after disturbance switches from negative (net flux to atmosphere) to positive (net uptake by terrestrial system). Note that this number only considers carbon balance after disturbance, and does not consider the fate of carbon removed at harvest. See Harmon (2001) for a discussion of this issue.
OLD_NPP	kg C / m^2 yr	Average net primary productivity for the 18-year period starting at age 370 years.
OLD_DAILY_TRANS	mm / day	Average daily transpirational losses of water from vegetation
OLD_HETR_RESP	kg C / m^2	Average yearly carbon lost to heterotrophic respiration.

Uncertainty analyses

Overview

Uncertainty analysis proceeded in three phases (Table 4.5). Phase 1 was used to determine which parameters had the largest overall leverage in the model. To keep model run repetitions low, only parameter values at the minimum, maximum, and middle levels of the parameter range (Table 4.3) were modeled. Twelve points across the study area were modeled. The same points were modeled in Phase 2, which focused on the three dominant parameters determined in Phase 1. Here, the goal was to quantify percentile-based distributions of carbon metrics resulting from variation in parameters. This required a dense sampling of the parameter space, with 15 levels tested for each parameter. Finally, Phase 3 brought the uncertainty analysis into the spatial realm, again focusing on the three highest-leverage parameters. The model was run at seven levels per parameter for over 400 points distributed across the study area. Carbon metric maps of the entire study area were built using an interpolation approach developed by Kennedy et al. (Chapter 3), and percentile-based distributions of carbon metric uncertainty across the entire study area produced.

Phase 1

Determining points for modeling

The goal of Phase 1 was general characterization of model uncertainty within the conditions found in the study area. A sparse sample of points in the study area's

climate space was used for modeling. The climate of the study area was characterized using a technique described in detail by Kennedy et al. (Chapter 3). Briefly, daily records of a single climate variable (precipitation, temperature, etc.) were aggregated to yearly averages, which were then compressed, normalized, and joined with other aggregated climate variables in a two-step principal component analysis. The resultant principal component axes described the spatial variation in climate within the study area. Eigenvector coefficients for the final principal component analysis are given in Table 4.6. Increasing values of principal component 1 corresponded with increasing radiation and lower precipitation; increasing values of principal component 2 corresponded with cooler temperatures, higher insolation, and lower vapor pressure deficit.

Points were selected by sampling the climate space along two principal component axes (Figure 4.2a). Twelve points were identified; Figure 4.2b shows their positions in the study area. Details of DAYMET-derived climate for each of the 12 points are shown in Table 4.7.

Evaluating model sensitivity

In Phase 1, 729 combinations of parameter values were modeled for each of the twelve points. For any given focal parameter, there were 243 unique combinations of the other five parameters. For each of those 243 combinations, three output values existed: one for each level of the focal parameter. Variation among those three output values was caused solely by variation in the focal parameter. The maximum absolute difference in the three output values was used as a metric of the effect of that

parameter on the output value, given the single combination of the other five parameters. The median of this metric across all 243 combinations of other parameters represented the first-order effect of the focal parameter on the carbon metric. This process was repeated for all parameters, points, and carbon metrics. In Phase 1, no effort was made to quantify interactions between parameters.

Table 4.5. Summary of the phases of uncertainty analysis used in this study.

Phase	*Number of Points*	*Number of Parameters*	*Number of Levels / Parameter*	*Number of Simulations / Point*	*Purpose*
1	12	6	3	729	Compare relative impact of uncertainty in leaf parameters at a small number of points throughout climate space
2	12	3	15	3375	High-density factorial exploration of parameter space for dominant parameters
3	462	3	7	343	High-density sample of climate space to build interpolated maps of uncertainty in dominant parameters
	118	3	7	343	Validate interpolated maps

Table 4.6. Eigenvector coefficients for two principal component axes of climate used to locate points for Phases 1 and 2.

	Climate Variable [a]					
PC Axis	*PrSu*	*PrSp*	*Sw*	*TmnSp*	*VSu*	*Percent of Variance Explained*
#1	-0.98	-0.98	0.87	0.03	0.93	71%
#2	-0.02	0.07	0.39	-0.99	-0.28	24%

[a] Climate variables are defined in Table 4.1

Table 4.7. DAYMET-estimated climate values for points used in Phases 1 and 2.

	Climate Variable [a]						
POINT	*Pr*	*PrSp*	*PrSu*	*T*	*TMnSp*	*Sw*	*VSu*
1	238	41	15	8.6	4.7	269	1253
2	153	31	11	10.4	5.4	287	1486
3	286	55	22	8.6	4.6	276	1105
4	208	41	14	9.1	4.7	289	1170
5	162	32	11	8.6	3.4	299	1456
6	98	17	6	10.6	4.8	318	2089
7	50	10	4	10.0	4.2	345	2321
8	247	49	18	7.1	3.3	270	982
9	201	41	14	8.3	3.5	287	1265
10	143	28	10	8.3	3.0	310	1403
11	111	21	6	7.3	1.8	330	1660
12	180	33	11	5.3	0.1	322	1155

[a] Climate variables are defined in Table 4.1

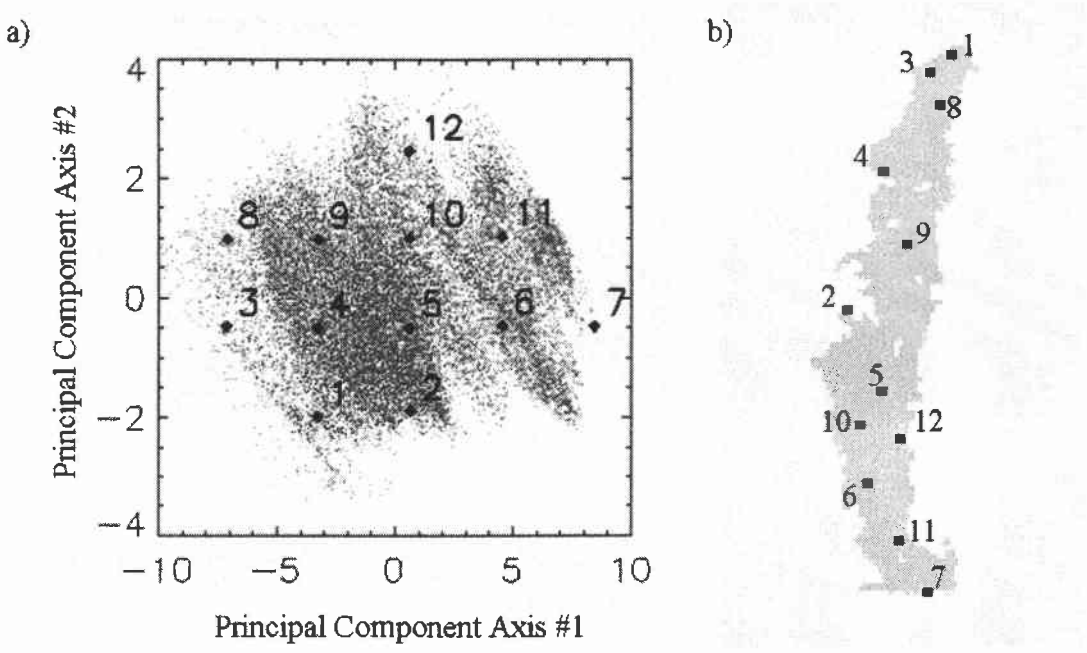

Figure 4.2. Points used for modeling in Phases 1 and 2. A) Points in transformed climate space. Climate space was compressed using principal component analysis of multiple climate data layers (see Table 4.2 for eigenvectors of the Principal Component Axes #1 and #2). High values on Axis #1 correspond to higher moisture stress, while high values on Axis #2 correspond to cool spring temperatures (See Table 4.6). Labeled point numbers are used throughout this study. B) Points positioned in the study area (See Figure 4.1).

The median of absolute difference values was scaled to the median value of the original carbon metrics modeled at each point, producing an estimate of the proportional uncertainty for each carbon metric at each point. This allowed comparison of effects between carbon metrics with different units and among points with different median values of carbon metrics. The median of proportional uncertainty across all 12 points was used as an overall estimate of the variation in each carbon metric caused by the variation in each parameter value. Using this approach, the three parameters with the greatest overall leverage were identified and used for Phases 2 and 3. These parameters will be referred to as "keystone" parameters.

Phase 2

Quantifying total uncertainty

In Phase 2, the full impact of uncertainty in parameters was quantified. At each of the twelve points used in Phase 1, the model was run at 15 levels for each of the three keystone parameters, resulting in 3375 separate model runs for each point. A histogram of the carbon metrics across all of those runs provided an estimate of the frequency distribution of carbon metrics resulting from variation in leaf parameters. The result was an estimate of the frequency distribution of carbon metrics resulting from the tested variation in leaf parameters. Uncertainty could then be stated as the bounds within which a given metric varied a given percentage of the time. By

producing a full distribution of values, this approach would also show whether uncertainty was symmetrical about the mean or skewed toward higher or lower values.

This approach assumed that each of the 15 levels of the parameters would have an equal chance of occurring – i.e. that the frequency of parameter values in the study area followed a uniform distribution. Depending on the form of the relationship between the parameters and the carbon metrics, a different frequency distribution of parameter values could lead to a different distribution of carbon metrics, and hence to a different estimate of uncertainty. To test this, a second histogram of carbon metrics was constructed, this time weighting each of the fifteen parameters according to a normal distribution. Normal weights were distributed such that 5% of the total weight fell on each of the two extreme parameter values.

Phase 3

Determination of modeling points for Phase 3

The goal of Phase 3 was development of maps of carbon metrics and uncertainty in those carbon metrics. Maps were produced using an interpolation method detailed in Kennedy et al. (Chapter 3). Kennedy et al. (Chapter 3) showed that interpolated maps could provide reliable spatial estimates of BGCs modeled outputs when only 10 to 15% the climate space was sampled. To characterize the climate space for Phase 3, yearly averages of DAYMET climate data were aggregated into 3 by 3 km^2 cells using spatial averaging, and the two-step principal-component process described for Phase 1 was applied to the aggregated images. In this case, however,

climate variables included in the principal-component analysis were spring and summer precipitation, spring shortwave-radiation insolation, minimum daily spring temperature, and spring and summer vapor pressure deficits. Climate space was defined using the first three principal component axes of climate variables. Sampling of the climate space followed a regular 3-dimensional lattice, as described by Kennedy et al. (Chapter 3). Using this process, 462 points were located (Figure 4.3a), representing a sample of 19.5% of the study area cells.

Kennedy et al. (Chapter 3) also showed that estimates of error in interpolated maps could be calculated by comparing interpolated values to independently-modeled values at a population of randomly-distributed validation points. Here, 118 validation points were identified and modeled (Figure 4.3b), representing 5% of the study area cells.

Application to the spatial realm

For each of the modeling points for Phase 3, the model was run at seven levels for each of the three keystone parameters, resulting in 343 separate sets of carbon metrics. The input-space interpolation approach of Kennedy et al. (Chapter 3) was used to interpolate carbon metrics for each parameter combination to the remaining 3 km by 3 km grid cells in the study area. This resulted in 343 separate images of each carbon metric for the entire study area. The interpolated value at the 118 validation points was compared against the modeled value; the square root of the mean square error (RMSE) across all 118 validation points was calculated for each of the 343 images for each metric.

Frequency distributions of carbon metrics were then developed for each cell using the parameter weighting and histogram approach described for Phase 2. In this case, only a normal weighting of parameter values was used. The result was a spatially-explicit map of the variability in carbon metrics caused by uncertainties in leaf parameters.

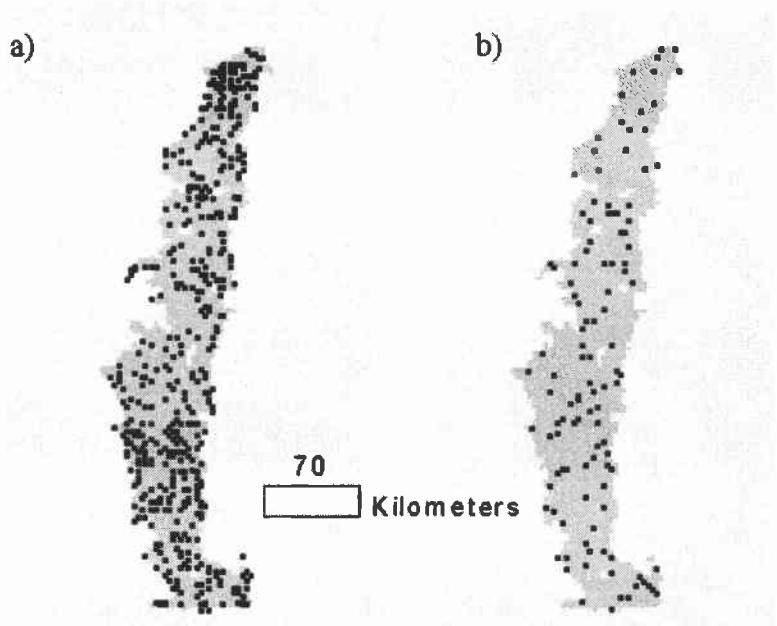

Figure 4.3. Points modeled to develop and test interpolated images of the entire study area. A) 462 points used in Model Run #3 (See Table 4.7), overlaid on an image of the study area. Points were distributed throughout climate space using a method described in detail in Chapter 2. B) 118 points used in Model Run #4. Point positions were chosen using a random-number generator.

Results

Phase 1

Estimates of carbon metrics varied across the 12 points modeled for Phase 1 (Table 4.8), reflecting variation in climate across the study area (Figure 4.1). Point 7 was the driest site modeled (Figure 4.2, Table 4.7) and had the lowest value for all carbon metrics except NEE_ZERO_YR, for which it had the highest value. The most productive site was Point 12, which occupied a cool, moderately moist position in the climate space (Figure 4.2). All other points had carbon metrics intermediate in value between these two points.

Variation in leaf parameters had variable effects on carbon metrics. Table 4.9 shows the median of maximum differences for all six parameters for two selected points. Reported values can be interpreted in units of the carbon metric. For example, ACC_NEE for Point 7 in Table 4.9 had a median value 23 kg C / m^2 yr. Variation in the parameter LfTrnovr from 0.136 to 0.20 (See Table 4.3 for definitions and parameter ranges) caused a median variation in ACC_NEE of 2.98 kg C / m^2 yr. Within a given row of the Table 4.9, the effects of variation in each parameter can be compared directly based on reported values, with larger values indicating a greater effect.

Table 4.8. Median values [a] of carbon metrics derived from model runs of BGC for the 12 points in Phase 1.

	Carbon metric [b]					
Point [c]	*OLD_ LAI*	*ACC_ NEE*	*NEE_ ZERO_ YR*	*OLD_ NPP*	*OLD_ DAILY_ TRANS*	*OLD_ HETR_ RESP*
1	7.5	37.7	22	0.71	1.7	0.66
2	7.5	37.8	22	0.71	1.7	0.66
3	8.1	40.5	23	0.77	1.9	0.72
4	8.0	41.0	22	0.76	1.8	0.71
5	7.4	37.5	22	0.71	1.7	0.66
6	7.1	34.9	22	0.67	1.5	0.63
7	4.8	23.5	26	0.46	1.0	0.42
8	8.2	41.7	23	0.79	1.9	0.74
9	7.9	40.3	22	0.76	1.8	0.71
10	7.7	38.7	22	0.74	1.7	0.69
11	6.9	34.4	22	0.67	1.5	0.62
12	8.4	42.9	24	0.81	2.1	0.76

[a] Values are medians from all 729 model runs of Phase 1 (See Table 4.7)

[b] Carbon metrics are defined in Table 4.4

[c] Points are shown in Figure 4.2

Table 4.9. The median effect on carbon metrics of varying model parameters in Phase 1 for points 7 and 10 in Figure 4.2.

			Median of maximum difference [a] caused by variation in parameter:					
POINT	*Metric [b]*	*Median Value [c]*	LfTrnovr	Root:Leaf	Stem:Leaf	C:N	SLA	FracNRubisco
7	OLD_LAI	4.8	1.07	1.77	0.79	0.32	0.97	1.99
	ACC_NEE	23	2.98	8.49	10.04	1.52	0.75	9.66
	NEE_ZERO_YR	26	4.00	3.00	2.00	2.00	2.00	10.00
	OLD_NPP	0.46	0.067	0.079	0.052	0.032	0.016	0.19
	OLD_DAILY_TRANS	1.0	0.02	0.03	0.01	0.01	0.02	0.05
	OLD_HETR_RESP	0.42	0.07	0.07	0.05	0.03	0.02	0.18
10	OLD_LAI	7.7	1.82	2.16	1.78	0.31	1.60	2.30
	ACC_NEE	39	4.90	10.76	14.67	1.44	1.21	11.83
	NEE_ZERO_YR	22	4.00	2.00	4.00	3.00	1.00	9.00
	OLD_NPP	0.74	0.099	0.057	0.040	0.029	0.026	0.22
	OLD_DAILY_TRANS	1.7	0.07	0.08	0.06	0.01	0.06	0.11
	OLD_HETR_RESP	0.69	0.10	0.05	0.03	0.03	0.03	0.21

[a] In Phase 1, each parameter was varied in the range indicated in Table 4.3, holding all other parameters constant, and the maximum difference in resulting carbon metrics noted. This was repeated across all possible combinations of other parameter values tested. The median of the maximum differences is reported. Units are the same as for the median value reported for each metric.

[b] Carbon metrics are defined in Table 4.4

[c] The median value of the carbon metric across all 729 combinations of parameter values in Phase 1. Units for metrics are described in Table 4.4.

When pooled across all 12 points, variation among metrics and parameters was more evident (Table 4.10). LfTrnovr and FracNRubisco had relatively large effects on all metrics except OLD_DAILY_TRANS, which appeared relatively insensitive to variability in the leaf parameters tested. C:N and SLA had relatively low impacts on most carbon metrics. The two allocation metrics (Root:Leaf and Stem:Leaf) had minor impacts on OLD_NPP, OLD_DAILY_TRANS, and OLD_HETR_RESP, but large impacts on OLD_LAI and ACC_NEE. FracNRubisco, Stem:Leaf, and LfTrnovr all had a median effect of more than 10%. These three parameters were considered keystone parameters, and used for further analysis in Phases 2 and 3.

Phase 2

The response of carbon metrics to variation in pairs of parameters generally described a smooth surface, but often showed discontinuities ranging from abrupt (Figure 4a) to relatively subtle (Figure4b). The surfaces shown in Figure 4.4 are for one of 15 values of Stem:Leaf. As Stem:Leaf was changed, the median value of ACC_NEE changed, but the general shape of the response surfaces (including discontinuities) evolved only slowly (surfaces not shown). The surfaces in Figure 4.4 also show the effect of parameter interactions. Although increases in LfTrnovr and FracNRubisco each resulted in increased ACC_NEE, regardless of the other parameter's value, the highest ACC_NEE values occurred when both parameters were high.

The total uncertainty in most carbon metrics for each point in Phase 2 was relatively large (Figure 4.5). For example, the range of 80% of OLD_LAI values spanned more than 2 units of LAI across most points, representing as much as 30% of the median LAI for some points. Similarly large uncertainties were observed for all other carbon metrics except OLD_DAILY_TRANS, which had relatively low leaf-parameter-related uncertainties for most points. Figure 4.5 also illustrates similarity across points in patterns of median values of OLD_LAI, ACC_NEE, OLD_NPP, and OLD_HETR_RESP carbon metrics.

Phase 3

Carbon metrics were successfully interpolated across the entire study area for all 343 parameter combinations. Table 4.11 lists summary statistics for all 343 images for each carbon metric. Error from interpolation was minor relative to the values of the metrics being interpolated.

Spatial patterns of carbon metrics varied as parameter combinations varied. Figure 4.6 shows four examples of interpolated carbon metric surfaces. In the case of NEE_ZERO_YR, spatial patterns of high and low values varied considerably for the two parameter value combinations shown (Figure 4.6a), even though the ranges of values across the study area were nearly identical. For OLD_LAI, general spatial patterns of high and low values were similar for the two parameter combinations shown, but the range of values was quite different (Figure 4.6b). The values of LAI for the right-hand image of Figure 4.6b are also notable for being very low relative to those expected for the Douglas-fir forests of the region (Gholz et al. 1976).

Uncertainty in carbon metrics showed distinct spatial patterns for the study area (Figure 4.7). The range of values between the 10^{th} and 90^{th} percentiles ("80% Uncertainty Range" images) varied across the landscape by a factor of two or more for all metrics (See image scale bars of 80% Uncertainty Range images). Spatial patterns of proportional uncertainty were similar for ACC_NEE, OLD_NPP, and OLD_HETR_RESP (Figure 4.7b,d, and f), with relatively high uncertainty in the drier, southern portions of the study area. Uncertainty in NEE_ZERO_YR and OLD_DAILY_TRANS (Figure 4.7c) appeared to be greatest near the eastern edges of the southern half of the study area, areas characterized by cooler temperatures and relatively low precipitation (Figure 4.1b and c). Proportional uncertainties in OLD_LAI and OLD_DAILY_TRANS also appeared to correspond with areas of lower temperatures (Figure 4.1c).

Proportional uncertainties varied considerably across the carbon metrics (Figure 4.7, right-most columns). Greatest uncertainties were calculated for ACC_NEE, where uncertainty was greater than 25% for the entire study area, reaching 40% in the south (Figure 4.7b). Proportional uncertainty was lowest for OLD_DAILY_TRANS (Figure 4.7e), consistent with results observed in Phase 2. The remaining four metrics showed uncertainties from 10 to 34% of the median values.

Table 4.10. Median proportional effect[a] on six carbon-cycle indicator metrics of varying model parameters across all 12 points in Phase 1 of the uncertainty analysis.

	Parameter varied [b]						
METRIC [c]	LfTrnovr	Root:Leaf	Stem:Leaf	C:N	SLA	FracNRubisco	Median effect by Metric
OLD_LAI	0.24	0.26	0.23	0.03	0.21	0.25	**0.23**
ACC_NEE	0.13	0.26	0.36	0.03	0.03	0.26	**0.19**
NEE_ZERO_YR	0.14	0.09	0.18	0.09	0.05	0.32	**0.11**
OLD_NPP	0.14	0.07	0.06	0.03	0.03	0.25	**0.06**
OLD_DAILY_TRANS	0.04	0.05	0.04	0.01	0.04	0.05	**0.04**
OLD_HETR_RESP	0.14	0.06	0.05	0.03	0.03	0.25	**0.06**
Median effect by Parameter	**0.14**	**0.08**	**0.12**	**0.03**	**0.03**	**0.25**	

[a] Absolute median differences for each point (as in Table 4.9) were scaled to the median value for that point; the median of that proportional effect across all 12 points is reported here. A proportional effect of 0.10 indicates that varying the parameter in the range indicated in Table 4.3 caused the carbon metric to vary by 10% of its median value.

[b] See Tables 4.2 and 4.3 for definitions of parameters and range of values tested for each parameter.

[c] See Table 4.4 for definitions of carbon metrics.

Table 4.11. Average values and estimates of error in interpolated images of modeled carbon metrics.

Carbon metric[1]	Metric value[2]	Mean RMSE[3]
OLD_LAI	7.7 (5.0, 10.3)	0.19 (0.12, 0.31)
ACC_NEE	39 (24, 52)	1.00 (0.84, 1.2)
NEE_ZERO_YR	22 (14, 29)	0.56 (0.26, 1.5)
OLD_NPP	0.72 (0.54, 0.85)	0.018 (0.015, 0.021)
OLD_DAILY_TRANS	1.7 (1.5, 1.8)	0.063 (0.035, 0.089)
OLD_HETR_RESP	0.67 (0.50, 0.80)	0.017 (0.014, 0.020)

[1] Carbon metric definitions are given in Table 4.4

[2] Reported values are mean (minimum, maximum) across all 343 images resulting from Phase 3 (See Table 4.7 for definitions of Phases);

[3] RMSE is square root of mean square error across all grid cells in a given interpolated image, estimated using validation points from Phase 3 (shown in Figure 4.3). Values reported here are summaries (mean, minimum, and maximum) of RMSE values across 343 images in Phase 3.

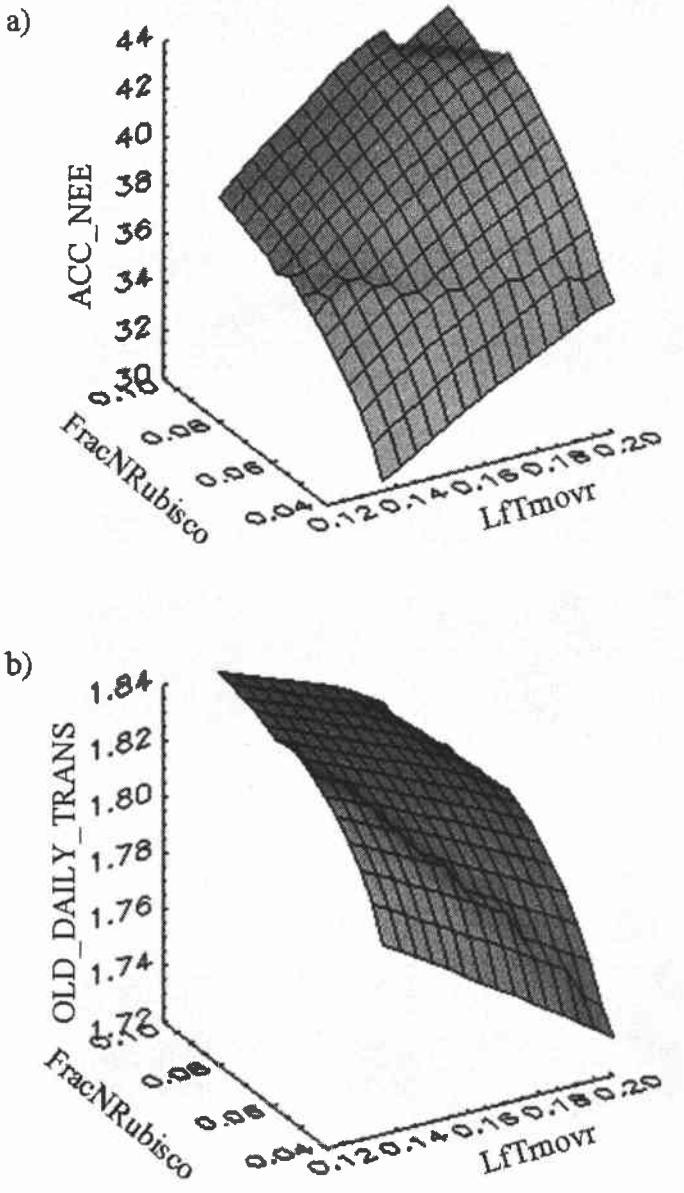

Figure 4.4. Typical examples from Model Run #2 showing how carbon metrics a) ACC_NEE and b) OLD_DAILY_TRANS varied as FracNRubisco and LfTmovr parameters changed. Shown are surfaces for Point #4 (See Figure 4.2 and Table 4.6 for more information) at the Stem:Leaf parameter value of 1.41. These are two of 90 such surfaces for each of the 12 points, one for each of 15 levels of Stem:Leaf for all six carbon metrics. Most surfaces showed subtle discontinuities as seen here, although generally not as abrupt as that seen at the upper ranges of part a).

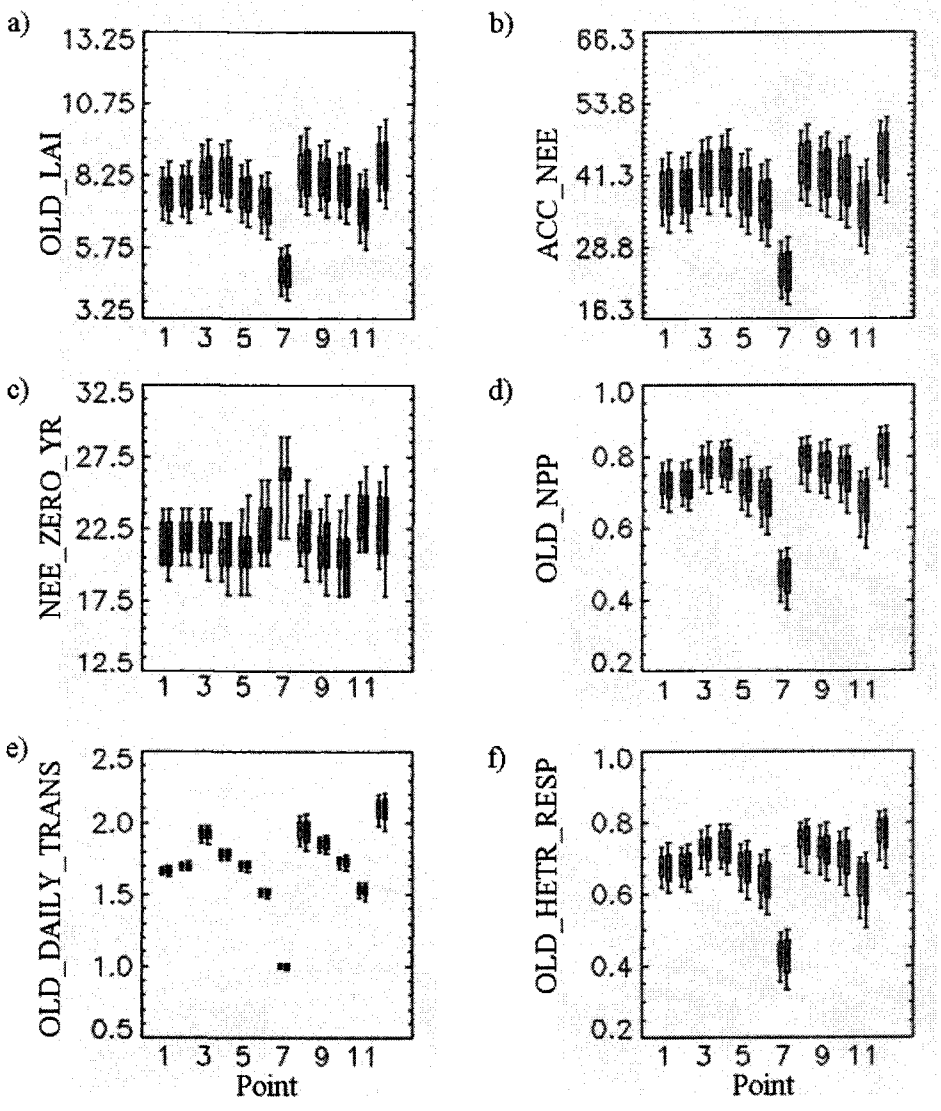

Figure 4.5. Uncertainty in a) OLD_LAI, b) ACC_NEE, c) NEE_ZERO_YR, d) OLD_NPP e) OLD_DAILY_TRANS, and f) OLD_HETR_RESP for the 12 points of Model Run #2. For each point, a pair of box plots is shown. Carbon metric distributions resulting from a normal distribution weighting (left-hand, non-shaded box in each point's box-pair) and a uniform distribution weighting (right-hand, shaded box) of the three input parameters LfTrnovr, Stem:Leaf, and FracNRubisco are shown. Boxed area spans the 25th to 75th percentiles, with the median value noted with a black dot. Outer whiskers indicate the 10th and 90th percentiles.

Figure 4.6. Spatial patterns of a) NEE_ZERO_YR, and b) OLD_LAI for two combinations of the LfTrnovr, Stem:Leaf, and FracNRubisco parameters. Parameter values are given under each image; parameter definitions are given in Tables 4.2 and 4.3. Images on the left and right are, respectively, most and least like the mean spatial pattern for each metric across all 343 different parameter combinations. Each image was created by interpolation through climate space of 462 points in Phase 3 (See Methods).

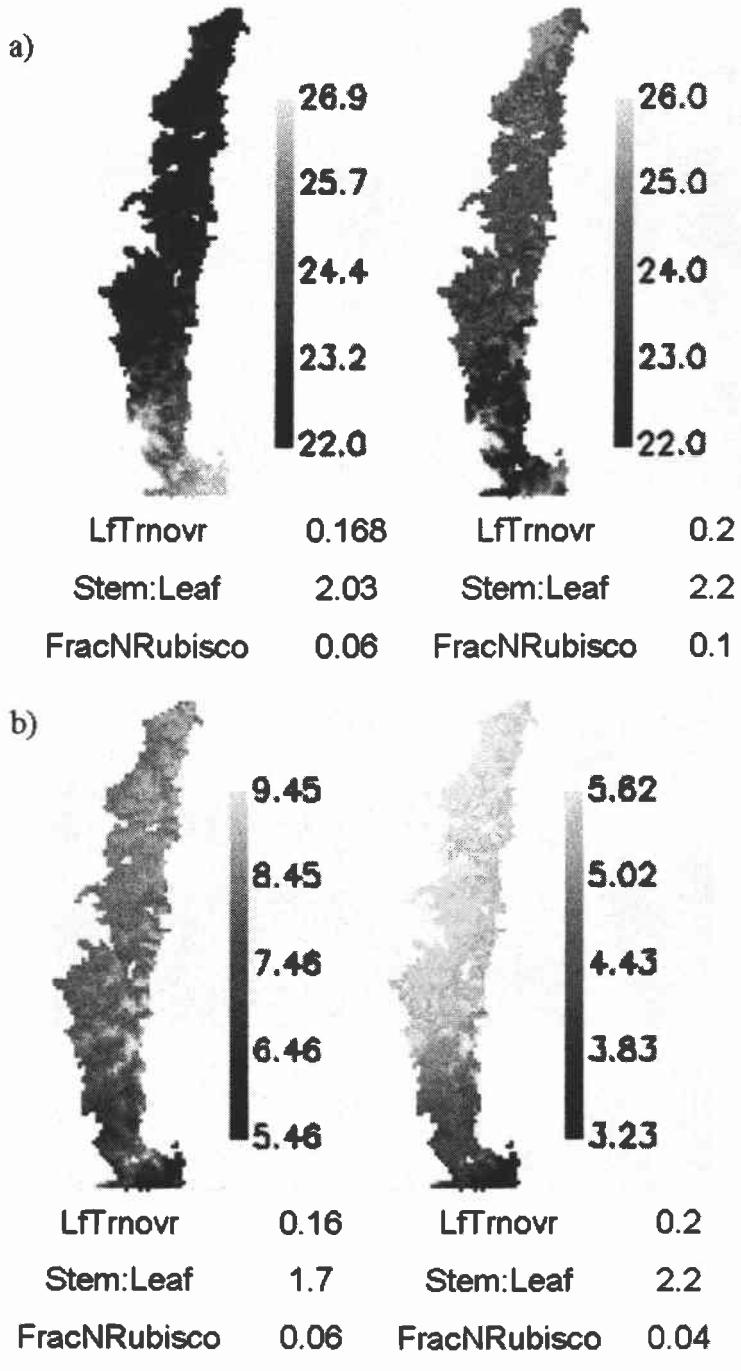
a)
26.9
25.7
24.4
23.2
22.0
LfTrnovr 0.168
Stem:Leaf 2.03
FracNRubisco 0.06
26.0
25.0
24.0
23.0
22.0
LfTrnovr 0.2
Stem:Leaf 2.2
FracNRubisco 0.1
b)
9.45
8.45
7.46
6.46
5.46
LfTrnovr 0.16
Stem:Leaf 1.7
FracNRubisco 0.06
5.62
5.02
4.43
3.83
3.23
LfTrnovr 0.2
Stem:Leaf 2.2
FracNRubisco 0.04

Figure 4.6

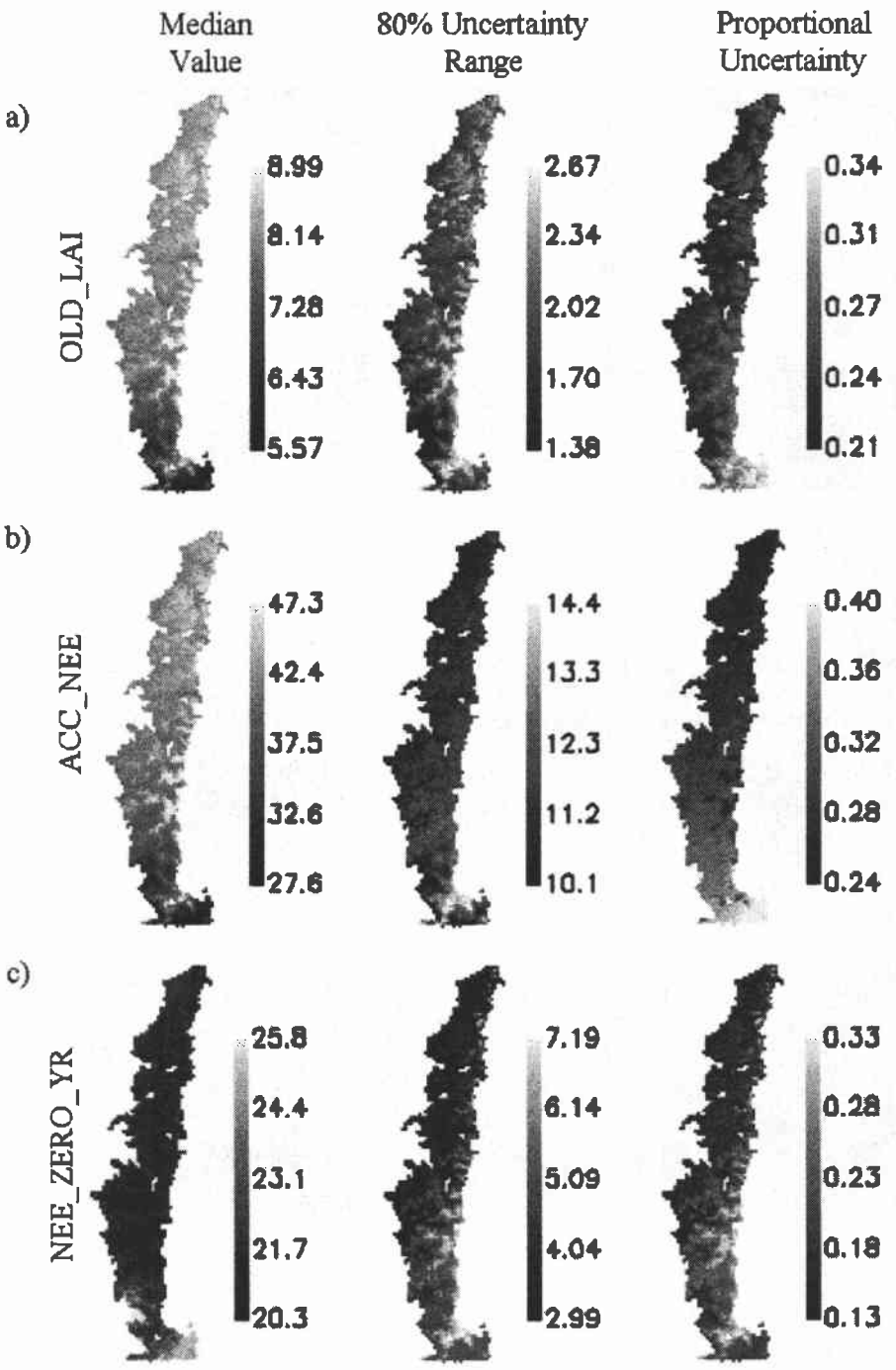

Figure 4.7. Median value and uncertainty surfaces for carbon metrics a) OLD_LAI, b) ACC_NEE, c) NEE_ZERO_YR, d) OLD_NPP, e) OLD_DAILY_TRAN, and f) OLD_HETR_RESP. Percentile values for each of the 2360 grid cells in the study area were calculated as in Figure 4.5, except here they were for Phase 3, and used only a normal distribution for weighting parameter values. Maps of 80% uncertainty

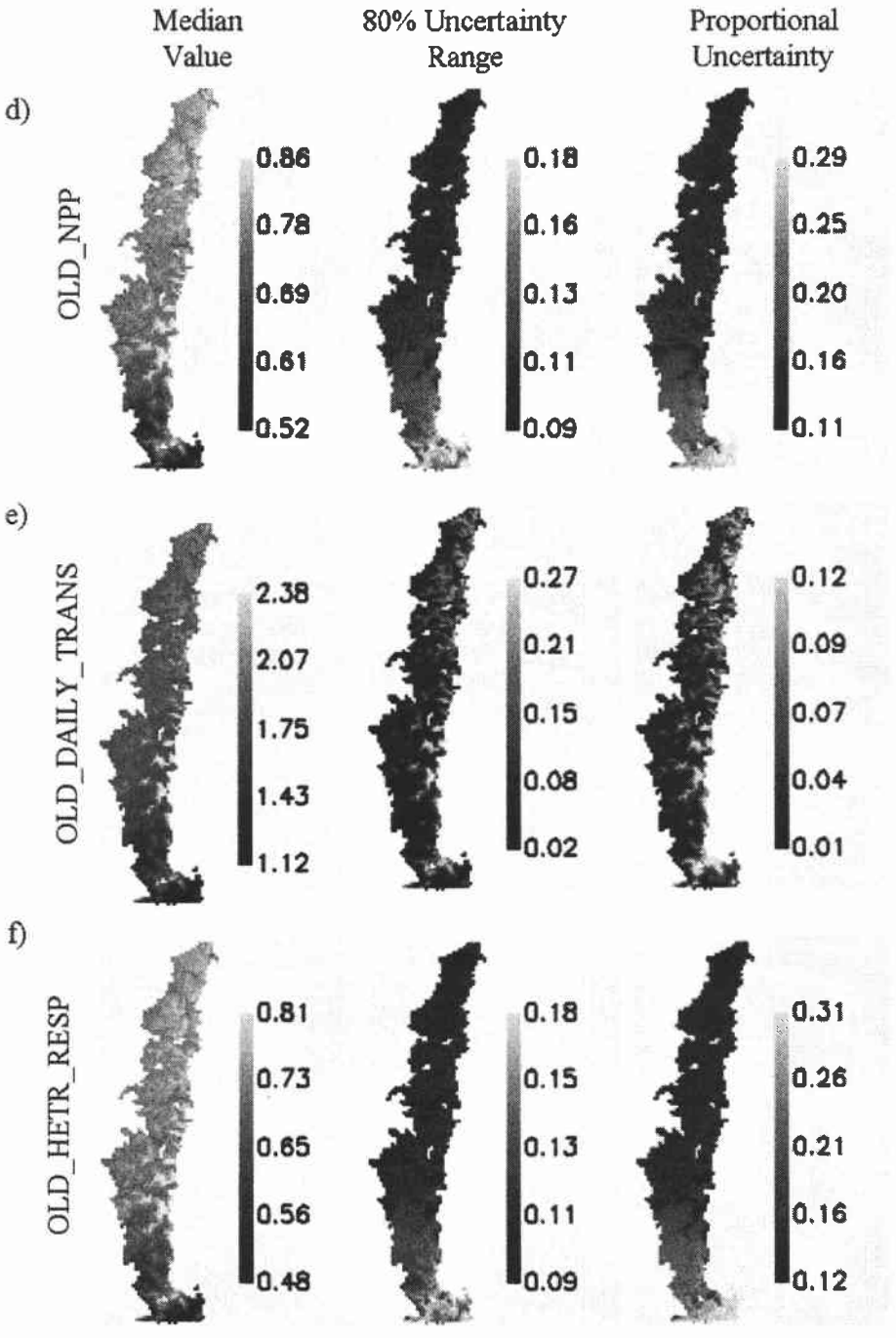

Figure 4.7. (Continued) represent the range of carbon metric values between the 10th and 90th percentiles. Proportional uncertainty maps are calculated as the range of 80% uncertainty divided by the median value. Because the range of parameter values tested was the same for each cell in the study area, any spatial variation in uncertainty arises from the interaction of the parameter uncertainty with climate.

Discussion

If biogeochemical models are to be used to provide regional scale estimates of carbon dynamics, uncertainties in model outputs caused by variation in model parameters must be quantified. Using the popular model BGC (Thornton 1998), we explored two key issues in uncertainty analysis at the regional scale. First, we examined whether it was important to track model uncertainty in a suite of model outputs rather than a single output. Second, we examined whether the interactions between climate and parameter variability would lead to meaningful spatial variation in model uncertainty.

By tracking multiple modeled carbon metrics, it was possible to assess whether model behavior followed expectations on several fronts. Generally, spatial patterns in all carbon metrics estimated with the biogeochemical model BGC followed expectations at a regional scale (Figure 4.7, Median Values). Long-term site productivity (OLD_NPP, ACC_NEE) increased from south to north (Figure 4.7b and d), mirroring regional-scale patterns in moisture (Figure 4.1b). Total carbon accumulations were on the lower end of the range of potential carbon stores estimated for the region by Smithwick et al. (2002), and LAI values were slightly lower than have been reported from direct measurements (Waring et al. 1978). Because leaf area index controls the amount of photosynthetic surface available for primary production, the similar spatial patterns of OLD_LAI and OLD_NPP follow expectations for the model. Transpirational losses of water were within the range of values expected for

forests in the region (Waring and Running 1998). Spatial patterns in heterotrophic respiration closely match patterns in productivity (comparing Figures 4.7f with 4.7b and 4.7d). Over the short term, heterotrophic respiration and photosynthesis are not necessarily coupled. In BGC, photosynthesis is affected primarily by radiation levels, transpirational constraints, and the availability of nitrogen in the leaves, while heterotrophic respiration is directly affected by temperature and moisture in the soil. The observed similarity in spatial patterns between respiration and productivity suggests that the long-term control on heterotrophic respiration is availability of vegetative inputs into decomposition pools, which is controlled by vegetative productivity. Similarly, vegetative productivity is partially controlled by availability of nitrogen in the soil, which is controlled by the rate of decomposition by heterotrophs. Over the long term, these two processes become coupled. This observation underscores the need to track multiple carbon metrics when examining model behavior at the regional scale.

One aspect of observed spatial patterns did not appear to match expectations. For all carbon metrics except NEE_ZERO_YR, modeled estimates suggest that the greatest productivity sites were found along the eastern border of the midsection of the study area (Figures 4.7a,b,d-f). This spatial pattern is not likely an artifact of the interpolation approach, since RMSE values for interpolation were small relative to the range of carbon metric values in question (comparing RMSE values in Table 4.11 with spatial patterns in Figure 4.7). Moreover, modeled estimates of carbon metrics for individual points in Phase 2 corroborate this pattern in the modeled carbon metrics.

The point lying in the apparent high-productivity region (Point 12) had the highest carbon metric values (Figure 4.5).

The region of apparent high-productivity corresponds to higher elevation areas (elevation maps not shown), where actual productivity is likely to be constrained by lower temperatures and shortened growing seasons. This should result in lower -- not higher -- productivity than in mid-elevation forests to the north and west. The apparent discrepancy may be caused by a structural error in the model, whereby temperature constraints are not adequately characterized, or by errors in the climate drivers, whereby spatial patterns of temperature or moisture are simply incorrect. Another possible source of the error was the use of uniform soil characteristics for the entire study area. Soil characteristics reflect long-term interactions between soil parent material and climate, and cool, moist, high-elevation sites in the study area would be expected to have poorer soil conditions for growth than mid-elevation sites (Schlesinger 1991). By running the model under uniform soil conditions, the potential for such variation was removed.

The choice to use uniform soil characteristics was deliberate. In the course of developing this and a separate study (Kennedy, Chapter 3), soil depth was implicated as a potentially dominant control on the carbon dynamics modeled by BGC for this study area. Initial investigations (data not shown) suggest that soil depth's control on carbon dynamics in the model may be far greater than expected in theory; a separate study of the influence of site factors on carbon dynamics has thus been initiated. However, until soil depth's role in modeled outputs is validated, the conservative

approach dictated that its influence be held constant for the current study. When spatial variation in soil depth is eventually incorporated, the difficulty in obtaining reliable, spatially-explicit maps of soil depth at a fine grain size (3 by 3 km^2) will mean that uncertainties in model outputs are likely to increase relative to those reported here.

Even without soil depth varying, uncertainties in leaf parameters caused significant variability in carbon metrics (Figures 4.5 and 4.7). This variability would have significant implications for carbon-based management of forests, especially if biogeochemical models were used to predict forest carbon dynamics under future climates. Modeled estimates of total accumulated carbon (ACC_NEE) typically varied by nearly one third of the median value, while estimates of the recovery of carbon dynamics after disturbance (NEE_ZERO_YR) varied by one fifth of the median value.

By focusing on only six parameters, the uncertainties examined here represent only a small portion of the total uncertainty that is encountered when biogeochemical modeling is conducted over large spatial extents. Uncertainties in climate drivers, in site characteristics (including soil conditions), and in the other model parameters may add to composite uncertainty estimates of carbon dynamics. Estimates of total uncertainty could follow the general approach described here, but could be expanded to include all sources of potential error.

Once uncertainties in carbon metrics are quantified, further modeling research can focus on reducing the largest uncertainties. Parameters that cause large variation within a given study area can be targeted for better direct measurement in the field. Of

the parameters studied here, C:N, SLA, and LfTrnovr are all straightforward to measure in the field with single visits to a site. Given C:N and SLA, FracNRubisco can be estimated if additional physiological measurements are taken (Law et al. 2001a), but this variable is relatively uncommonly reported (White et al. 2000). Estimating allocation parameters (Root:Leaf and Stem:Leaf) typically requires more extensive research at a site (White et al. 2000). Future research would need to balance cost for acquisition of each parameter with its potential impact on modeled output.

Field studies can be aided by the development of spatially-explicit maps of uncertainty. When designing sampling schemes for field study, greater weight can be given to areas where the penalty for parameter uncertainty is larger. Better constraint of the model in these locations provides a greater return on investment than if areas were sampled where uncertainty is low.

A key step toward improving uncertainty is the characterization of the covariance structure of model parameters. In this study, lack of information on covariance between keystone parameters required that parameters be uncorrelated. In nature, however, certain combinations of traits are unlikely to occur. Without a means of eliminating unlikely parameter combinations, some modeled outputs may be highly unlikely, as evidenced by the anomalously low LAI values in Figure 4.6b. If estimates of the likely distributions of carbon metrics can be created, however, Bayesian approaches may provide a means of reducing uncertainty in likely parameter combinations (Gelman et al. 1995, Raftery et al. 1995). Although Bayesian approaches may hold significant promise for improving uncertainty bounds, their potential utility

depends on defining carbon metrics that lends themselves to estimation of frequency distributions, with, at the least, estimates of the minimum and maximum likely values.

Regardless of the potential for future narrowing of uncertainty bounds, the results shown here suggest that the spatial pattern of uncertainty is indeed important (Figure 4.7). Uncertainty in carbon metrics varied over space, and that variation was itself variable among metrics. A single estimate of uncertainty for any given carbon metric would be insufficient for describing the actual uncertainty likely to be encountered across the entire study area. Thus, we would propose that regional scale modeling should include some effort to examine spatial variability in the uncertainties of modeled carbon dynamics.

Derivation of spatially-explicit maps of uncertainty was facilitated by the input-space interpolation approach (Kennedy et al. Chapter 3). By reducing the computational burden by a factor of four, parameter space could be explored more thoroughly, which allowed better characterization of uncertainties in modeled outputs. The importance of thorough sampling of the parameter space is underscored by the observation of discontinuities in the response surfaces of carbon metrics to variation in parameters (Figure 4.4). Without the adequate sampling of the parameter space facilitated by the methodology developed by Kennedy et al. (Chapter 3), such model behavior would be lost.

Spatially-explicit mapping of model uncertainties is possible for many of the biogeochemical models used to characterize the carbon cycle (Aber and Federer 1992, Members 1995, McGuire et al. 1997, Ollinger et al. 1998, Thornton et al. 2002).

Comparing spatial patterns in uncertainties among models may provide greater insight into the relative strengths and weaknesses of different approaches to biogeochemical modeling, and may lead to faster improvement in biogeochemical modeling of the carbon cycle.

Conclusions

Using a common biogeochemical model, we showed that uncertainties in several key leaf parameters could lead to substantial variability in a suite of carbon metrics. This uncertainty varied spatially at the regional scale, suggesting that the interaction between spatially-varying climate drivers and uncertainty in model parameters could have important consequences.. Moreover, we showed that patterns of uncertainty varied for carbon metrics representing different underlying physiological processes. This suggests no single carbon metric can represent all of the behavior of a model at the regional scale, and that multiple processes should be tracked if model robustness is to be assessed. Taken together, these results suggest that regional modeling of carbon dynamics will be incomplete without spatially-explicit estimates of uncertainty of a suite of model outputs. Because uncertainties may be large, true reporting of uncertainties may diminish the ability to firmly quantify carbon fluxes. However, it is through focused research on the reducing uncertainties that we feel the greatest improvements in carbon modeling are possible.

Chapter 5: Conclusion

The work reported in this Dissertation explored the potential spatial variability in key parameters of a biogeochemical model, and how variability might affect modeled estimates of key carbon cycle metrics.

In Chapter 2, I measured leaf mass per area (LMA), leaf nitrogen (LN), and leaf longevity (LL) for *Pseudotsuga menziesii (PSME) and Pinus ponderosa* (PIPO) trees, growing both in their core geographic ranges (CORE stands) and in the ecotonal region at the margins of their ranges where the two species co-occur (MIXED stands). The three traits have been shown to be important controls on carbon uptake (Field and Mooney 1986, Poorter 1989, Oren et al. 2001), and have been shown to be linked ecologically (Reich et al. 1992).

My results provided evidence that stand-level light environment largely controlled LMA, consistent with lab experiments and some observational field studies. However, my results further indicated that this relationship followed the same mathematical form across the two species, suggesting a high degree of plasticity in the trait. Moreover, because stand light environment is largely controlled by canopy leaf area, the upper limit of which is related to available moisture, LMA was strongly related to overall moisture patterns.

Across species LL and LN were not strongly related to climatic drivers. Rather, I proposed that LN was more tightly linked to levels of nitrogen in the soil, which likely varied in the study area more as a function of geologic parent material rather than climate. Additionally, I suggested LL served as a species-specific,

physiological tuning mechanism that compensated for the controls on the other two traits.

Regardless of mechanisms controlling variation, my results showed substantial variation (15 to 30% of the mean values) in leaf traits both within and across the two species at the regional scale. Because variation in LMA may have been related to moisture, there is the potential that climate data be used to estimate spatial patterns in LMA. LN and LL could likely not be predicted from spatial climate data alone. A linkage between LN and soil nitrogen would offer some opportunity to predict spatial patterns if reliable maps of soil nitrogen were available. However, the interrelationships between the three leaf parameters would likely complicate the task and require significant additional study, especially if spatial patterns of LL were desired.

Within the context of the larger Dissertation, a key conclusion of the Chapter 2 is that much of the variation in leaf traits is difficult to predict spatially.

Before attempting to quantify the effect of that variation on BGC-derived estimates of spatial patterns in carbon dynamics, I developed an approach to more efficiently bring modeled estimates into the spatial realm. The traditional approach to modeling across a landscape is to partition the landscape into a regular grid, establish climate drivers for each cell in the grid, and run the model for each and every grid cell. Such wall-to-wall modeling can be inefficient if the soil and climate drivers are similar for nearby cells. Indeed, absent cell-to-cell interactions, any spatial variation in modeled outputs is strictly a function of spatial variation in the drivers of the model.

This latter observation allowed development of an approach to subsample the cells at which the model would be run. Climate drivers were compressed using a two-step principal-component analysis process into a simplified three-dimensional climate space. This space was sampled using a regular lattice, and modeled values between sampled points estimated by simple interpolation. I called the approach input-space interpolation. I tested its ability to capture spatial patterns of BGC-derived estimates of net primary productivity (NPP) and net ecosystem productivity (NEP) for a 100 by 260km area in the Douglas-fir zone of my study area.

I found that the method was robust, allowing reasonable prediction of spatial patterns in model output with as few as five to ten percent of the total model runs. The choice of climate data used in the data compression step was important, with some combinations of meteorological data allowing much better approximation of spatial patterns than others. The choice of best predictor variables itself varied with the age at which modeled estimates were desired, reflecting the changing controls on NPP and NEP over time within the model. By using a set of independent validation points, I could provide good estimates of the error introduced by the input-space interpolation approach.

I then applied the input-space interpolation approach to the goal of developing spatially-explicit uncertainty estimates. In addition to the three model parameters measured in Chapter 2, I included estimated uncertainty ranges for three addition leaf parameters: the allocation ratio of new fine root to new leaf carbon (Root:Leaf), the allocation ratio of new stem to new leaf carbon (Stem:Leaf), and the fraction of leaf N

in Rubisco (FracNRubisco). The study area was expanded to include all areas of Oregon's Western Cascades where Douglas-fir was an expected dominant or co-dominant species.

Even though uncertainty analysis was limited to six model parameters, variation in those parameters led to substantial variability in key carbon metrics. For example, total accumulated carbon varied by as much as 40% for some portions of the study area.

Uncertainty in all parameter values was considered to have no spatial component, meaning that uncertainty ranges for parameter values were common across the entire study area. A key question was whether this spatially-uniform uncertainty in parameter values would interact with spatially-varying climate variables to produce variability in spatial uncertainty of carbon metrics. My results suggest that this indeed did occur, and that the variation in uncertainty could be substantial.

Taken together, the results reported here suggest several general conclusions. First, ecological variability in plant attributes may cause substantial variability in the parameters used to describe and constrain a biogeochemical model. Because a long-term goal of biogeochemical modeling is the characterization of controls on carbon fluxes, this variation over space is potentially important not only for modeling, but for fundamental understanding of the ecology of the systems being modeled.

This leads to a second conclusion that is likely applicable to a large class of biogeochemical models: if model parameters are subject to spatial variation, then modeled predictions of carbon cycle dynamics will require a better quantification of

the potential uncertainties arising out of this variation. Chapter 4 shows that this uncertainty is not only important, but that non-spatial estimates of uncertainty could be misleading. Through the interaction with spatially-varying climate data, uncertainties in model parameters may vary spatially, and region-wide estimates of carbon flux would necessarily need to include such variation in estimates.

None of the spatial estimates of uncertainty would have been as feasible were it not for the third major conclusion of this project: for biogeochemical models without cell-to-cell interactions, spatial variation in modeled outputs is solely a function of variation spatially-varying input data (climate, etc.). This observation allowed the development of an efficient approach to developing spatially-explicit model outputs.

The final conclusion summarizes essentially all of the work in this Dissertation: the process of applying a biogeochemical model to a large spatial area carries with it significant challenges that must be addressed before the carbon cycle can adequately be characterized at regional scales. These challenges are not trivial, and the uncertainty introduced by them may rival some of the better-recognized challenges to understanding the carbon cycle at fixed points.

Despite the significant uncertainties that can arise when modeling in the spatial realm, I believe that the issues raised here also provide opportunities. By beginning to recognize and characterize spatial uncertainties, my work provides a means of focusing additional efforts on how to quantifiably reduce them. Research can be focused on understanding covariance relationships among model parameters, both in the lab and in the field. Field sampling may be designed to focus on areas where the

penalty for ignorance is high. Together, these steps could lead to an iterative measuring and modeling structure that would allow faster learning and, potentially, better characterization of carbon fluxes.

Bibliography

Aber, J. D., and C. A. Federer. 1992. A generalized, lumped-parameter model of photosynthesis, evapotranspiration and net primary production in temperate and boreal forest ecosystems. Oecologia **92**:463-474.

Abrams, M. D., M. E. Kubiske, and S. A. Mostoller. 1994. Relating wet and dry year ecophysiology to leaf structure in contrasting temperate tree species. Ecology **75**:123-133.

Acevedo, M. F., S. Pamarti, M. Ablan, D. Urban, and A. Mikler. 2001. Modeling forest landscapes: parameter estimation from gap models over heterogeneous terrain. Simulation **77**:53-68.

Alexandrov, G. A., T. Oikawa, and Y. Yamagata. 2002. The scheme for globalization of a process-based model explaining gradations in terrestrial NPP and its application. Ecological Modelling **148**:293-306.

Apple, M., K. Tiekotter, M. Snow, J. Young, A. Soeldner, D. Phillips, D. Tingey, and B. J. Bond. 2002. Needle anatomy changes with increasing tree age in Douglas-fir. Tree Physiology **22**:129-136.

Band, L. E., D. L. Peterson, S. W. Running, J. Coughlan, R. Lammers, J. Dungan, and R. Nemani. 1991. Forest ecosystem processes at the watershed scale: basis for distributed simulation. Ecological Modelling **56**:171-196.

Bauer, G., E.-D. Schulze, and M. Mund. 1997. Nutrient contents and concentrations in relation to growth of *Picea abies* and *Fagus sylvatica* along a European transect. Tree Physiology **17**:777-786.

Burke, I. C., T. G. F. Kittel, W. K. Lauenroth, P. Snook, C. M. Yonker, and W. J. Parton. 1991. Regional analysis of the central Great Plains. BioScience **41**:685-692.

Burns, R. M., and B. H. Honkala, editors. 1990. Silvics of North America: 1. Conifers; 2. Hardwoods. U.S. Department of Agriculture, Forest Service, Washington, D.C.

Campbell, J. L., O. Sun, and B. E. Law. In review. Disturbance and net ecosystem production across three climatically distinct forest landscapes. Global Biogeochemical Cycles.

Castro-Diez, P., J. P. Puyravaud, and J. H. C. Cornelissen. 2000. Leaf structure and anatomy as related to leaf mass per area variation in seedlings of a wide range of woody plant species and types. Oecologia **124**:476-486.

Cohen, W. B., M. E. Harmon, D. O. Wallin, and M. Fiorella. 1996. Two decades of carbon flux from forests of the Pacific Northwest. BioScience **46**:836-844.

Cohen, W. B., T. K. Maiersperger, S. T. Gower, and D. P. Turner. 2003. An improved strategy for regression of biophysical variables and Landsat ETM+ data. Remote Sensing of Environment **84**:561-571.

Coops, N. C., and R. H. Waring. 2001. Estimating forest productivity in the eastern Siskiyou Mountains of southwestern Oregon using a satellite driven process model, 3-PGS. Canadian Journal of Forest Research **31**:143-154.

Insightful Corporation. 2002. S-Plus v. 6. Seattle, WA.

Cregg, B. M. 1994. Carbon allocation, gas exchange, and needle morphology of Pinusponderosa genotypes known to differ in growth and survival under imposed drought. Tree Physiology **14**:883-898.

Cunningham, S. A., B. Summerhayes, and M. Westoby. 1999. Evolutionary divergences in leaf structure and chemistry, comparing rainfall and soil nutrient gradients. Ecology **69**:569-588.

Del Rio, E., and A. Berg. 1979. Specific leaf area of Douglas-fir reproduction as affected by light and needle age. Forest Science **25**:183-186.

Dyrness, C. T., and C. T. Youngberg. 1966. Soil-vegetation relationships within the ponderosa pine type in the central Oregon pumice region. Ecology **46**.

Evans, J. R., and H. Poorter. 2001. Photosynthetic acclimation of plants to growth irradiance: the relative importance of specific leaf area and nitrogen partitioning in maximizing carbon gain. Plant, Cell, and Environment **24**:755-767.

Falkowski, P., R. J. Scholes, E. Boyle, J. Canadell, D. Canfield, J. Elser, N. Gruber, K. Hibbard, P. Hoegberg, S. Linder, F. T. Mackenzie, B. M. III, T. Pedersen, Y. Rosenthal, S. Seitzinger, V. Smetacek, and W. Steffen. 2000. The global carbon cycle: a test of our knowledge of Earth as a system. Science **290**:291-296.

Field, C., and H. A. Mooney. 1986. The photosynthesis-nitrogen relationship in wild plants. Pages 25-55 *in* T. J. Givnish, editor. On the economy of plant form and function. Cambridge University Press, Cambridge.

Foley, J. A., I. C. Prentice, N. Ramankutty, S. Levis, D. Pollard, S. Sitch, and A. Haxeltine. 1996. An integrated biosphere model of land surface processes, terrestrial carbon balance, and vegetation dynamics. Global Biogeochemical Cycles **10**:603-628.

Frak, E., X. Le Roux, P. Millard, B. Adam, E. Dreyer, C. Escuit, H. Sinoquet, M. Vandame, and C. Varlet-Grancher. 2002. Spatial distribution of leaf nitrogen and photosynthetic capacity within the foliage of individual trees: disentangling the effects of local light quality, leaf irradiance, and transpiration. Journal of Experimental Botany **53**:2207-2216.

Franklin, J. F., and C. T. Dyrness. 1988. Natural vegetation of Oregon and Washington. OSU Press, Corvallis, OR.

Franklin, S. E. 2001. Modeling forest net primary productivity with reduced uncertainty by remote sensing of cover type and leaf area index. Pages 402 *in* C. T. Hunsaker, M. F. Goodchild, M. Friedl, and T. J. Case, editors. Spatial uncertainty in ecology: implications for remote sensing and GIS applications. Springer-Verlag, New York, NY.

Frazer, G. W., R. A. Fournier, J. A. Trofymow, and R. J. Hall. 2001. A comparison of digital and film fisheye photography analysis of forest canopy structure and gap light transmission. Agricultural and Forest Meteorology **109**:249-263.

Friedman, L. W. 1996. The simulation metamodel. Kluwer Academic Publishers, Norwell, Massachusetts.

Friend, A. D., A. K. Stevens, R. G. Knox, and M. G. R. Cannell. 1997. A process-based, terrrestrial biosphere model of ecosystem dynamics (Hybrid v3.0). Ecological Modelling **95**:249-287.

Geist, G. A., A. Beguelin, J. J. Dongarra, W. Jiang, R. Manchek, and V. S. Sunderam. 1994. PVM: Parallel Virtual Machine. MIT Press, Boston, MA.

Gelman, A. B., J. S. Carlin, H. S. Stern, and D. B. Rubin. 1995. Bayesian data analysis. Chapman and Hall, Boca Raton.

Gholz, H. L., F. K. Fitz, and R. H. Waring. 1976. Leaf area differences associated with old-growth forest communities in the western Oregon Cascades. Canadian Journal of Forest Research **6**:49-57.

Glassy, J.M., and S.W. Running. 1994. Validating diurnal climatology logic of MT-CLIM model across a climatic gradient in Oregon. Ecological Applications **4**(2): 248-257.

Gower, S. T., C. C. Grier, D. J. Vogt, and K. A. Vogt. 1987. Allometric relations of deciduous (*Larix occidentalis*) and evergreen conifers (*Pinus contorta* and *Pseudotsuga menziesii*) of the Cascade Mountains in central Washington. Canadian Journal of Forest Research **17**:630-634.

Gower, S. T., P. B. Reich, and Y. Son. 1993. Canopy dynamics and aboveground production of five tree species with different leaf longevities. Tree Physiology **12**:327-345.

Grassi, G., and U. Bagnaresi. 2001. Foliar morphological and physiological plasticity in *Picea abies* and *Abies alba* saplings along a natural light gradient. Tree Physiology **21**:959-967.

Haefner, J. W. 1996. Modeling biological systems. Chapman and Hall, New York, NY.

Harmon, M. E. 2001. Carbon sequestration in forests -- Addressing the scale question. Journal of Forestry **99**:24-29.

Harmon, M. E., J. M. Harmon, W. K. Ferrell, and D. Brooks. 1996. Modeling carbon stores in Oregon and Washington forest products: 1900-1992. Climatic change **33**:521-550.

Johnson, D. R. 1993. Soil survey of Jackson County Area, Oregon. USDA Soil Conservation Service.

Kern, J. S., D. P. Turner, and R. F. Dodson. 1997. Spatial patterns in soil organic carbon pool size in the northwestern United States. Pages 29-43 *in* R. Lal, J. M. Kimbal, R. Follett, and B. A. Stewart, editors. Soil processes and the carbon cycle. CRC Press, Boca Raton.

Kikuzawa, K. 1991. A cost-benefit analysis of leaf habit and leaf longevity of trees and their geographical pattern. American Naturalist **138**:1250-1263.
Körner, C. 1989. The nutritional status of plants from high altitudes. Oecologia **81**:379-391.

Larsen, D. M. 1976. Deschutes National Forest Soils. USDA Pacific Northwest Region.

Law, B., P. Thornton, J. Irvine, S. VanTuyl, and P. Anthoni. 2001a. Carbon storage and fluxes in ponderosa pine forests at different developmental stages. Global Change Biology **7**:755-777.

Law, B. E., D. P. Turner, M. Lefsky, J. Campbell, M. Guzy, O. Sun, S. Van Tuyl, and W. B. Cohen. In Press. Carbon fluxes across regions: observational constaints at multiple scales. *in* J. Wu, H. Jones, H. Li, and O. Loukes, editors. Scaling and uncertainty analysis in ecology: methods and applications. Columbia University Press, New York, USA.

Law, B. E., S. Van Tuyl, A. Cescatti, and D. D. Baldocchi. 2001b. Estimation of leaf area index in open-canopy ponderosa pine forests at different successional stages and management regimes in Oregon. Agricultural and Forest Meteorology **108**:1-14.

Le Roux, X., H. Sinoquet, and M. Vandame. 1999. Spatial distribution of leaf dry weight per area and leaf nitrogen concentration in relation to local radiation regime within an isolated tree crown. Tree Physiology **19**:181-188.

Lymburner, L., P. J. Beggs, and C. R. Jacobson. 2000. Estimation of canopy-average surface-specific leaf area using Landsat TM data. Photogrammetric Engineering & Remote Sensing **66**:183-191.

OR/WA Bureau of Land Management. Unknown date. Forest Cover/Operations Inventory.

Marshall, P. L., and K. Jahraus. 1987. Sample size for foliar analysis of coastal Douglas-fir. Canadian Journal of Forest Research **17**:1240-1245.

Martin, M. E., and J. D. Aber. 1997. High spectral resolution remote sensing of forest canopy lignin, nitrogen, and ecosystem processes. Ecological Applications **7**:431-443.

Matson, P., L. Johnson, C. Billow, J. Miller, and R. Pu. 1994. Seasonal patterns and remote spectral estimation of canopy chemistry across the Oregon Transect. Ecological Applications **4**:280-298.

McGuire, A. D., J. M. Melillo, D. W. Kicklighter, Y. Pan, X. Xiao, J. Helfrich, B. M. III, C. J. Vorosmarty, and A. L. Schloss. 1997. Equilibrium responses of global net primary production and carbon storage to doubled atmospheric carbon dioxide: Sensitivity to changes in vegetation nitrogen concentration. Global Biogeochemical Cycles **11**:173-189.

Mooney, H. A., P. J. Ferrar, and R. O. Slatyer. 1978. Photosynthetic capacity and carbon allocation patterns in diverse growth forms of *Eucalyptus*. Oecologia **36**:103-111.

Ohmann, J. L., and M. J. Gregory. 2002. Predictive mapping of forest composition and structure with direct gradient analysis and nearest-neighbor imputation in coastal Oregon, U.S.A. Canadian Journal of Forest Research **32**:724-741.

Ollinger, S. V., J. D. Aber, and C. A. Federer. 1998. Estimating regional forest productivity and water yield using an ecosystem model linked to a GIS. Landscape Ecology **13**:323-334.

Oren, R., D. S. Ellsworth, K. H. Johnsen, N. Phillips, B. E. Ewers, C. Maier, K. V. R. Schäfer, H. McCarthy, G. Hendrey, S. G. McNulty, and G. G. Katul. 2001. Soil fertility limits carbon sequestration by forest ecosystems in a CO_2-enriched atmosphere. Nature **411**:469-472.

Parton, W. J., J. W. B. Stewart, and C. V. Cole. 1987. Analysis of factors controlling soil organic matter levels in Great Plains grasslands. Soil Science Society of America Journal **51**:1173-1179.

Phillips, D. L., and D. G. Marks. 1996. Spatial uncertainty analysis: propagation of interpolation errors in spatially distributed models. Ecological Modelling **91**:213-229.

Pierce, L. L., and S. W. Running. 1994. Regional-scale relationships of leaf area index to specific leaf area and leaf nitrogen content. Ecological Applications **4**:313:321.

Poorter, H. 1989. Interspecific variation in relation to growth rate: on ecological causes and physiological consequences. *in* H. Lambers, M. L. Cambridge, H. Konings, and T. L. Pons, editors. Causes and consequences of variation in growth rate and productivity of higher plants. SPB Academic Publishing, The Hague.

Poorter, H., and J. R. Evans. 1998. Photosynthetic nitrogen-use efficiency of species that differ inherently in specific leaf area. Oecologia **116**:26-37.

Powers, R. F., and P. E. Reynolds. 1999. Ten-year responses of ponderosa pine plantations to repeated vegetation and nutrient control along an environmental gradient. Canadian Journal of Forest Research **29**:1027-1038.

Raftery, A. E., G. H. Givens, and J. E. Zeh. 1995. Inference from a deterministic population dynamics model for bowhead whales. Journal of the American Statistical Association **90**:402-416.

Reich, P. B., M. D. Abrams, D. S. Ellsworth, E. L. Kruger, and T. J. Tabone. 1990. Fire affects ecophysiology and community dynamics of central Wisconsin oak forest regeneration. Ecology **71**:2179-2190.

Reich, P. B., T. Koike, S. T. Gower, and A. W. Schoettle. 1995. Causes and consequences of variation in conifer leaf life-span. Pages 225-254 *in* W. K. Smith and T. Hinckley, editors. Ecophysiology of coniferous forests. Academic Press, San Diego.

Reich, P. B., M. B. Walters, and D. S. Ellsworth. 1992. Leaf life-span in relation to leaf, plant, and stand characteristics among diverse ecosystems. Ecological Monographs **62**:365-392.

Reich, P. B., M. B. Walters, and D. S. Ellsworth. 1997. From tropics to tundra: Global convergence in plant functioning. Proceedings of the National Academy of Sciences USA **94**:13730-13734.

Rosati, A., K. R. Day, and T. M. DeJong. 2000. Distribution of leaf mass per unit area and leaf nitrogen concentration determine partitioning of leaf nitrogen within tree canopies. Tree Physiology **20**:271-276.

Running, S. W., and J. C. Coughlan. 1988. A general model of forest ecosystem processes for regional applications. I. Hydologic balance, canopy gas exchange and primary production processes. Ecological Modelling **42**:125-154.

Running, S. W., and E. R. J. Hunt. 1993. Generalization of a forest ecosystem process model for other biomes, BIOME-BGC, and an application for global-scale models. Pages 388 *in* C. B. Field and J. R. Ehleringer, editors. Scaling Ecophysiological Processes: Leaf to Globe. Academic Press, San Diego.

Schimel, D. 1998. The carbon equation. Nature **393**:208-209.

Schimel, D. S., W. Emanuel, B. Rizzo, T. Smith, F. I. Woodward, H. Fisher, T. G. F. Kittel, R. McKeown, T. Painter, N. Rosenbloom, D. S. Ojima, W. J. Parton, D. W. Kicklighter, A. D. McGuire, J. M. Melillo, Y. Pan, A. Haxeltine, C. Prentice, S. Sitch, K. Hibbard, R. Nemani, L. Pierce, S. Running, J. Borchers, J. Chaney, R. Neilson, and B. H. Braswell. 1997. Continental scale variability in ecosystem processes: Models, data, and the role of disturbance. Ecological Monographs **67**:251-271.

Schlesinger, W. H. 1991. Biogeochemistry: An analysis of global change. Academic Press, Inc., San Diego.

Smith, M.-L., and M. E. Martin. 2001. A plot-based method for rapid estimation of forest canopy chemistry. Canadian Journal of Forest Research **31**:549-555.
Smith, R. B., R. H. Waring, and D. A. Perry. 1981. Interpreting foliar analyses from Douglas-fir as weight per unit of leaf area. Canadian Journal of Forest Research **11**:593-598.

Smithwick, E. A. H., M. E. Harmon, S. M. Remillard, S. A. Acker, and J. F. Franklin. 2002. Potential upper bounds of carbon stores in forests of the Pacific Northwest. Ecological Applications **12**:1303-1317.

St. Clair, J. B. 1994. Genetic variation in tree structure and its relation to size in Douglas-fir. II. Crown form, branch characters, and foliage characters. Canadian Journal of Forest Research **24**:1236-1247.

Thornton, P. 1998. Regional ecosystem simulation: combining surface- and satellite-based observations to study linkages between terrestrial energy and mass budgets. PhD Dissertation. University of Montana.

Thornton, P., H. Hasenauer, and M. A. White. 2000. Simultaneous estimation of daily solar radiation and humidity from observed temperature and precipitation: an application over complex terrain in Austria. Agricultural and Forest Meteorology **104**:255-271.

Thornton, P., and S. W. Running. 1999. An improved algorithm for estimating incident daily solar radiation from measurements of temperature, humidity, and precipitation. Agricultural and Forest Meteorology **93**:211-228.

Thornton, P., S. W. Running, and M. A. White. 1997. Generating surfaces of daily meteorological variables over large regions of complex terrain. Journal of Hydrology **190**:214-251.

Thornton, P. E., B. E. Law, H. L. Gholz, K. L. Clark, E. Falge, D. S. Ellsworth, A. H. Goldstein, R. K. Monson, D. Hollinger, M. Falk, J. Chen, and J. P. Sparks. 2002. Modeling and measuring the effects of disturbance history and climate on carbon and water budgets in evergreen needleleaf forests. Agricultural and Forest Meteorology **113**:185-222.

Thorson, T. D., S. A. Bryce, D. A. Lammers, A. J. Woods, J. M. Omernik, J. Kagan, D. E. Pater, and J. A. Comstock. 2003. Ecoregions of Oregon (color poster with map, descriptive text, summary tables, and photographs). *in*. U.S. Geological Survey, Reston, Virginia.

Tucker, G. F., and W. H. Emmingham. 1977. Morphological changes in leaves of residual Western Hemlock after clear and shelterwood cutting. Forest Science **23**:195-203.

Turner, D. P., W. B. Cohen, and R. E. Kennedy. 2000. Alternative spatial resolutions and estimation of carbon flux over a managed forest landscape in Western Oregon. Landscape Ecology **15**:441-452.

Turner, J., and P. R. Olson. 1976. Nitrogen relations in a Douglas-fir plantation. Annals of Botany **40**:1185-1193.

van den Driessche, R. 1974. Prediction of mineral nutrient status of trees by foliar analysis. The Botanical Review **40**:347-394.

VEMAP Members. 1995. Vegetation/ecosystem modeling and analysis project: Comparing biogeography and biogeochemistry models in a continental-scale study of terrestrial ecosystem responses to climate change and CO_2 doubling. Global Biogeochemical Cycles **9**:407-437.

Walker, G. W., and N. S. MacLeod. 1991. Geologic map of Oregon. *in*. U.S. Geological Survey, Reston, VA.

Walters, M. B., and P. B. Reich. 1999. Low-light carbon balance and shade tolerance in the seedlings of woody plants: do winter deciduous and broad-leaved evergreen species differ? New Phytologist **143**:143-154.

Waring, R. H., W. H. Emmingham, H. L. Gholz, and C. C. Grier. 1978. Variation in maximum leaf area of coniferous forests in Oregon and its ecological significance. Forest Science **24**:131-139.

Waring, R. H., and J. F. Franklin. 1979. Evergreen coniferous forests of the pacific northwest. Science **204**:1380-1386.

Waring, R. H., and S. W. Running. 1998. Forest ecosystems: analysis at multiple scales, 2 edition. Academic Press, San Diego.

White, J. D., S. W. Running, and P. Thornton. 1998. Assessing simulation ecosystem processes for climate variability research at Glacier National Park, USA. Ecological Applications **8**:805-823.

White, M. A., P. E. Thornton, S. W. Running, and R. R. Nemani. 2000. Parameterization and sensitivity analysis of the BIOME-BGC terrestrial ecosystem model: net primary production controls. Earth Interactions **4-003**.

Williams, M., E. B. Rastetter, G. R. Shaver, J. E. Hobbie, E. Carpino, and B. L. Kwiatkowski. 2001. Primary production of an arctic watershed: an uncertainty analysis. Ecological Applications **11**:1800-1816.

Williams, M., Y. E. Shimabukuro, D. A. Herbert, S. P. Lacruz, C. Renno, and E. B. Rastetter. 2002. Heterogeneity of soils and vegetation in an eastern Amazonian rain forest: implications for scaling up biomass and production. Ecosystems **5**:692-704.

Wright, I. J., P. B. Reich, and M. Westoby. 2001. Strategy shifts in leaf physiology, structure and nutrient content between species of high- and low-rainfall and high- and low-nutrient habitats. Functional Ecology **15**:423-434.

Wright, I. J., M. Westoby, and P. B. Reich. 2002. Convergence towards higher leaf mass per area in dry and nutrient-poor habitats has different consequences for leaf life span. Journal of Ecology **90**:534-543.

Yin, X. 1993. Variation in foliar nitrogen concentration by forest type and climatic gradients in North America. Canadian Journal of Forest Research **23**:1587-1602.

Zinke, P. J., and A. G. Stangenberger. 1979. Ponderosa pine and Douglas-fir foliage analyses arrayed in probability distributions. Pages 221-225 *in* Forest Fertilization Conference. British Columbia Ministry of Forests, Union, Washington.